Swiss Federal Office of Energy SFOE Energy Research and Cleantech

HOTCAT4STEAM

Integrated Steam Generation for Solid Oxide Electrolysis via Downstream Catalytic Fuel Synthesis



The core of Research Platform Power-to-X at OST in Rapperswil, where experiments for project HotCat4Steam are conducted. The Solid Oxide Electrolyser built by EPFL is visible on the left hand side.







Date: 23rd November 2023

Location: Rapperswil and Sion

Publisher:

Swiss Federal Office of Energy SFOE Energy Research and Cleantech CH-3003 Bern www.bfe.admin.ch

Co-financing:

OST – Ostschweizer Fachhochschule, IET Institut für Energietechnik, Oberseestrasse 10, 8640 Rapperswil-Jona, www.ost.ch/iet

EPFL – Valais, École Polytechnique Fédérale de Lausanne – Valais, Rue de l'Industrie 17, 1950 Sion, www.epfl.ch/labs/gem

Interessengemeinschaft Power-to-X (IG-PtX), c/o St.Galler Stadtwerke, Vadianstrasse 8, 9001 St.Gallen, www.ig-ptx.ch, members see Appendix 1A.2 page 109

Gaznat, Av. Général-Guisan 28, 1800 Vevey, www.gaznat.ch

Subsidy recipients:

OST – Ostschweizer Fachhochschule, IET Institut für Energietechnik, Oberseestrasse 10, 8640 Rapperswil-Jona, www.ost.ch/iet

EPFL – Valais, École Polytechnique Fédérale de Lausanne – Valais, Rue de l'Industrie 17, 1950 Sion, www.epfl.ch/labs/gem

Authors:

Christoph Steiner, OST, christoph.steiner@ost.ch
Thibault Macherel, EPFL – Valais, thibault.macherel@epfl.ch
Philippe Aubin, EPFL –Valais, philippe.aubin@epfl.ch
Luca Schmidlin, OST, luca.schmidlin@ost.ch
Markus Friedl, OST, markus.friedl@ost.ch
Jan Van herle, EPFL -Valais, jan.vanherle@epfl.ch
Dr. Luiz Reichenbach de Sousa, formerly at OST

SFOE project coordinators:

Stefan Oberholzer, stefan.oberholzer@bfe.admin.ch

SFOE contract number: SI/501825-01

The authors bear the entire responsibility for the content of this report and for the conclusions drawn therefrom.



Summary

This report is based on several reports made during the phase of Pentagon, HEPP & HotCat4Steam Project. It has been updated from year to year. This is the final version.

The HotCat4Steam project aimed at developing a steam generator and steam conditioner and integrate both in a power-to-gas plant fitted with a Solid Oxide Electrolyser (SOE). SOE's require steam as feed and allow the production of renewable hydrogen with very high efficiency. The waste heat from a downstream exothermal catalytic synthesis of methane is used in this project to generate the steam. The main challenge is to generate the steam flow and at the same time fulfil the strict requirements of an SOE. This goal was achieved during this project on the "Research Platform Power-to-X" of OST.

The "Research Platform Power-to-X" is a power-to-methane plant comprising a PEM electro-lyser and has been successfully commissioned in 2019. Its functionality was demonstrated, and a number of intermediate project goals could be reached by the end of that year, including generating 3.5 kg/h of steam with temperatures around 240 °C and with pressure fluctuations below 20 mbar as required to feed the high-temperature electrolyser. The Solid Oxide Electrolyser (SOE) has been commissioned and has been tested and successfully validated in autumn of 2022. The coupling of the SOE and the methanation plant has been successfully validated in spring 2023.

Main findings

- The steam generation system selected for the installation consisting of a capillary steam generator, an expansion vessel and the heat transfer medium sub-system is able to capture the heat from the polytropic methanation reactor and generate steam at the required quality for an SOE system.
- This system allows for simpler design of the over-all installation as no high-pressure equipment is required for the steam section. Furthermore, it offers flexibility in operation as an external heat source or sink is easily to integrate in the circuit, making the operation of the SOE independent to a certain heat extraction from the methanation: both systems can run at different production rates, provided an additional heat sink, source or storage is integrated in the system.
- A polytropic methanation reactor is designed by OST and built by a Swiss contractor. It
 comprises of two catalytic active zones and an intermediate injection of CO₂. This configuration allows controlled operation of the methanation reaction at high conversion rates
 without the need for ballast steam to maintain reaction temperatures within the catalyst
 specifications.
- The coupling of the SOE and the upstream steam generation is modified and optimized during the testing phase between autumn 2022 and spring 2023. An automatically PID-regulated pressure control valve can be problematic, if the parameters are not perfectly balanced. A manual valve position shows better results, especially if the other process parameters in the steam generator remain constant.
- Two SOE stacks, an older one already used as a fuel cell (stack #1801) and a modified, unused one (stack #1803) are successfully tested. Unexpectedly, the older stack (#1801) performed slightly better than the pristine stack (#1803). The SOE efficiencies based on



the higher heating value (HHV) of hydrogen is measured to be 113.5 % for the old stack (#1801) and 112 %¹ for the new stack (#1803).

- The takeover of the hydrogen by the H₂ compressor stage shows stable and reliable performance from the beginning. Nevertheless, the start-up procedure is simplified during the tests and the process parameters are optimised in such a way that the reliable transfer is even more possible and leads to an improvement of the process parameters within the SOE stack.
- The thermal energy (total 1.63 kW) for the steam generation by thermal oil are composed of the following parts:
 - 17.2 % harvested from a feedwater-preheater, where the heat source is the SNG-product cooling stage.
 - 49.0 % from the heat released by the methanation reaction, collected by the thermal oil circuit transferring the thermal energy to the evaporation and the superheater.
 - The rest of the thermal energy has to be supplied by the thermal oil unit with its electrical heater.
- The thermal heat management allows collecting 0.80 kW exothermal heat at 250 °C to be transferred to the steam production unit. The water feed to the steam generator is preheated by the SNG-product from the reaction with 0.28 kW useful heat. To produce steam at 240 °C, a total amount 1.63 kW of thermal heat is supplied to the water. 1.08 kW (or 66.3 %) are supplied by the methanation reaction. In the SOE, the steam utilisation rate is 70.6 %.
- Direct water-cooled methanation generates stable steam production at low flowrate (20 g/min). At a higher flowrate (35 g/min), a damping volume is necessary to ensure the stability of the produced steam. Moreover, thermosyphon operation is tested and validated on the direct water-cooled methanator, cancelling the energy need for a recirculation pump and increasing the overall efficiency of the methanator.
- The overall efficiency (SNG-output versus energy-expenditures) shows significant improved numbers compared to the SNG produced with hydrogen from a PEM-electrolyser. Depending on the system boundaries, the numbers from the system with SOE are between 22 %-points and 93 %-points higher. The absolute number in overall efficiency ranges from 18.6 % to 54.9 %.

4/109

¹ Hydrogen outlet over electrical input to the SOE stack without the amount of natural gas used to keep the system hot.



Content

Sumr	mary	3
Abbre	reviations	7
1.	Introduction	8
1.1.	High Temperature Electrolysis (HTE)	8
1.2.	HTE's Role in the Future Energy System	
2.	Project HotCat4Steam	9
2.1.	Purpose of the project	9
2.2.	Timeline	
2.3.	HotCat4Steam vis-à-vis other Projects	10
3.	Experiments	12
3.1.	Research Platform Power-to-X at OST	12
3.2.	WP1: Methanation	14
	3.2.1. Polytropic methanation reactor at OST plant	14
	3.2.2. Methanation reactor at EPFL laboratory	
3.3.	WP2: Heat management and steam generation	
	3.3.1. Heat management at Power-to-X Research Platform	
	3.3.2. Steam generation at Power-to-X Research Platform	
3.4.	WP3 and WP4: Solid oxide electrolysis, BoP components and system balan	
5.4.	3.4.1. Pressurized Single Cell Setup	
	3.4.2. The SOE Unit	
	3.4.3. Integration of the SOE Unit in the Research Platform Power-to-X	35
3.5.	WP5: Control	40
	3.5.1. Control of the SOE unit	
	3.5.2. Control of the methanation plant	
	3.5.3. Control of the Coupling: "SOE into the Methanation Plant"	
4.	Results and Discussions	48
4.1.	WP1: Methanation	48
	4.1.1. Operation of the Polytropic Methanation Reactor at OST plant	
	4.1.2. Evaporating water-cooled methanation reactor at EPFL laboratory	
	4.1.3. Simulation of Methanation	
4.2.	WP2: Steam generation	
	4.2.1. Operation of the capillary steam generator at OST plant	
	4.2.2. Stabilization of the steam production at EPFL laboratory	
4.3.	WP3, WP4 and WP5: Operation and control of the SOE	
	4.3.1. Pressurized single cell setup	
	4.3.2. SOE unit: Test with the bypass	
	4.3.3. SOE unit: Test with the stack #1801	



	4.3.4. SOE unit: Test with the stack #1803	89					
4.4.	SOE-Methanation Coupling: Results	94					
	4.4.1. Coupling procedures	94					
	4.4.2. Results of the SOE-Methanation system						
	4.4.3. Results of the PEM–Methanation system	98					
	4.4.4. Overall efficiency and comparison of the Methanation Plant	101					
	4.4.5. Fields for Further Improvements	102					
5.	Dissemination and Outlook	104					
5.1.	Dissemination	104					
5.2.	Outlook	105					
6.	Conclusions						
Appe	endix	107					
A.1	Literature	107					
A.2	Members of IG-PtX:						
A.3	Schematic Communication Flow of the Research Platform's PLC "DeltaV"						



Abbreviations

AEL: Alkaline Electrolyser or alkaline

electrolysis for electrolyzing liq-

uid water

BoP: Balance of Plant

BPC: Back pressure controller

CFD: Computational Fluid Dynamics

CHW: Chilling water

ColdBoP: Cold Balance of Plant for instal-

lations at low temperatures

DC: Direct Current

DAC: Direct Air Capture, capturing of

carbon dioxide CO₂ from the at-

mosphere.

DMW: demineralised water

EFCF: European Fuel Cell Forum

FG: Forming gas

GEM: Group of Energy Materials at

EPFL

HAZOP: Hazard and Operability is a pro-

cedure for safety assessment.

HEX: Heat exchanger

HHV: Higher Heating Value

HMI: Human-Machine Interface

HotBoP: Hot Balance of Plant for instal-

lations at high temperatures

HTC: Heat transfer coefficient

HTE: High-Temperature Electrolysis

IV: Correlation between Current (I)

and Voltage (V). This is measured to characterize an SOE

stack.

LHV: Lower Heating Value MFM: Mass flow meter

NG: Natural gas or methane. NL/min: Normal litre per minute.

OCV: Open Circuit Voltage.
OPC: Open Platform Communi

OPC: Open Platform Communication.
P&ID: Piping and instrumentation dia-

gram.

PA: Process air.

PEM: Electrolyser for liquid water

based on a proton exchange

membrane.

PFR: Plug flow reactor.

PLC: Programmable logic controller

SNG: Synthetic natural gas, meaning

synthetic methane.

SOC: Solid Oxide Cell.

SOE: Solid Oxide Electrolysis and

Solid Oxide Electrolyser.

SOEC: Solid Oxide Electrolyser Cell.

SOFC: Solid Oxide Fuel Cell.

SPCL: Safety Programmable Logic

Controller.

TRL: Technology Readiness Level

TO: Thermal Oil.

VI: Virtual Instrument, a program

for measurement and control

written in LabVIEW.



1. Introduction

1.1. High Temperature Electrolysis (HTE)

High-Temperature Electrolysis ("HTE", also called "steam electrolysis") is an electrochemical technology allowing to electrolyze water in its gaseous form (steam) at high temperatures. The electrolysis is performed in cells consisting of electrodes and an electrolyte made of solid oxides and ceramics. The cells are referred to as solid oxide electrolyser cells (SOEC) and the electrolyser as well as the electrolysis as "solid oxide electrolyser" or "solid oxide electrolysis" (both SOE). The cell is similar to a solid oxide fuel cell (SOFC) but operating not in fuel cell mode but in electrolyser mode.

A very important part of SOE operation is the balance of plant (BoP). It feeds the cells with the required gases at the required conditions, receives the output gases from the cells, exchanges heat and allows startup procedure as well as shut down and standby operation. The balance of plant of an HTE is often divided into HotBoP and ColdBoP depending on the temperatures involved.

SOE is more efficient than conventional electrolysis of liquid water one reason being that part of the energy input is in the form of heat, most of it as latent heat, i.e. the evaporation enthalpy of water. In this project HotCat4Steam we aim at experimentally demonstrating that the heat input can be taken from a downstream catalytic exothermal process. The latter are required in Power-to-X plants, when hydrogen is converted to other energy carriers such as hydrocarbons (of which the simplest is methane), methanol or fuels from Fischer-Tropsch processes. In the context of Power-to-X it is important to add that SOE also allows co-electrolysis of H₂O and CO₂ to syngas.

SOE are about to reach technology readiness level (TRL) 9. They are available with an electric power input up to 100 kW_e with the first plants in the range of 1 MW².

In this project, a stack technology from the manufacturer Solydera is used, an Italian – Swiss company. More and more SOFC manufacturers enter also into HTE, since the stack technology is the same, only the system differs in the BoP. The transition from SOFC manufacturer to HTE manufacturer is thus rather natural.

1.2. HTE's Role in the Future Energy System

Since this project has started, the role of Power-to-X has been recognised in Switzerland's Energy Perspectives 2050+ for all variants of scenario "Zero" and is included in Europe's energy strategy especially for the production for fuels for ships and airplanes. Therefore, the goals of increasing the efficiency of Power-to-X is important. The main cost and the main environmental impact of operating an electrolyser are determined by the electricity, hence every gain in net efficiency (of SOE versus electrolysis of liquid water) is a gain in the operating cost and environmental impact. Electrolysis of liquid water reaches efficiencies of 70 % (based on HHV) at best for hydrogen generation. Steam electrolysis reaches efficiencies of 95 % or better (based on HHV) and is mandatorily connected with a heat source (~150-200°C) that is either available upstream or integrated downstream with the SOE. An electrolyser for liquid water (PEM or AEL) is operated only 2000 to 3000 hours/year. An SOE can be run continuously,

² Project "MULTIPHY" with Sunfire, https://www.iwr.de/news/weltweit-erster-multi-mw-hochtemperaturelektrolyseur-fuer-gruenen-wasserstoff-news36641



thanks to its reversible mode (changing from being an electrolyser to being a fuel cell), hence the investment cost is much better used. Higher efficiency of SOE over PEM and AEL is expected to have an effect in the long run: if a same result can be obtained with three wind turbines instead of four or five, or with 1 km² of PV panels instead of 1.5 km², it is bound to make a difference.

Since we use thermal oil to generate the steam with the low pressure fluctuations required by the SOEC, other heat sources such as waste heat (waste incineration, cement, chemical and other industries) or solar heat can be used when applying the results of HotCat4Steam in the energy system. The main requirement is steam generation at 150 to 200 °C. In addition, direct steam generation is also tested, which is the path proposed also by Topsoe. [11]

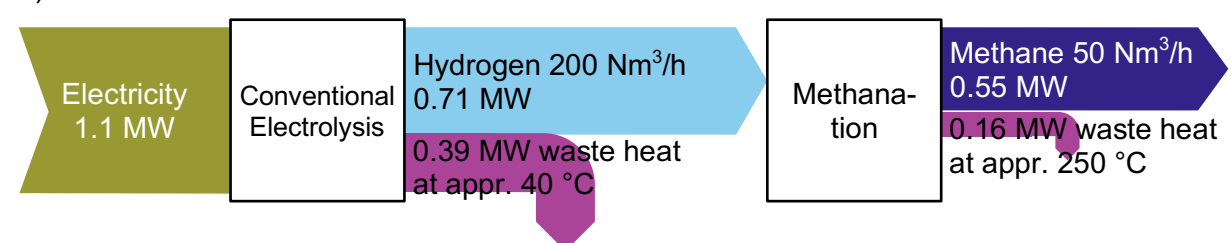
2. Project HotCat4Steam

2.1. Purpose of the project

The main purpose of this project is to experimentally demonstrate the increased electrical efficiency of a Power-to-X process with a HTE. The gain in efficiency is 1) due to the higher efficiency of HTE in comparison to conventional electrolysers and 2) due to the use of waste heat from the catalytic process downstream of the HTE to generate the steam as input for the HTE. Figure 1 shows a Power-to-Methane process as example for Power-to-X in the MW-scale, whose efficiency $(\dot{m}_{CH4} \cdot HHV)/(electric power)$ is increased from 50 % with a conventional electrolyser to 70 % with an HTE. In contrast to other projects with similar aspirations, this project uses thermal oil for the heat management system and wants to prove the effect experimentally and not just theoretically.



a) Conventional Power-to-Methane Process:



b) Power-to-Methane Process with HTE:

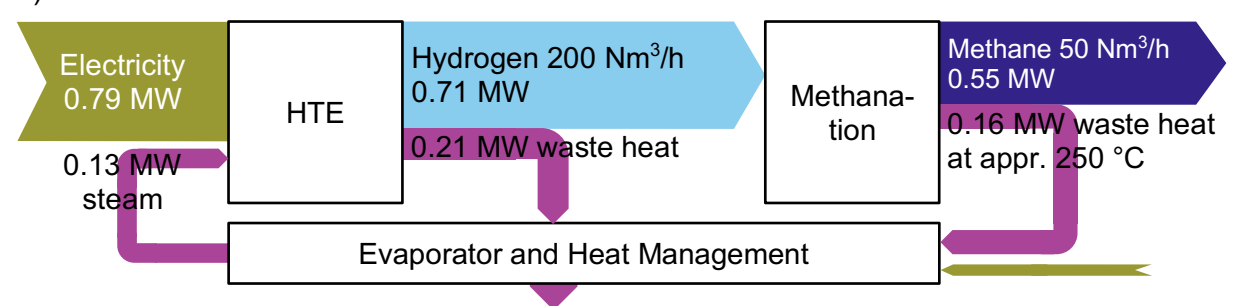


Figure 1: Comparison of Power-to-Methane process with conventional electrolyser a) and HTE b) in the MW range, showing an increase in efficiency from 50 % in a) to 70 %. Chemical energy flows based on HHV. Efficiency is defined as $(\dot{m}_{CH4} \cdot \text{HHV})/(\text{electric power})$.

2.2. Timeline

The project started in November 2018. The project has turned out to be much more complex requiring more efforts than anticipated. Part of the delays can be explained by the pandemic. Work has continued throughout the year of 2021. The project was extended to enable the project team to reach the goals of the project. Late 2022, after extensive efforts and collaboration between the two research groups, the plant combining HTE, methanation and heat management, has finally been operated safely and successfully over several hours during test campaigns of two weeks. In early 2023, a new stack has been installed in the SOE unit and the entire plant has been operated for a final week of test in march 2023. Data evaluation and report writing was conducted during summer 2023.

2.3. HotCat4Steam vis-à-vis other Projects

When the application for this project was written in 2018, other projects with similar aspirations were listed in the application (Table 2). The projects, where SOE were coupled with downstream catalytic processes, are listed in this report in Table 1 again complemented with other projects, where waste heat from an external process is used. The table clearly shows that the research questions addressed in HotCat4Steam remain of high relevance and help to solve an important piece to bring SOE to the market.

10/109

³ Source: Friedl, M., Schmidlin, L., Steiner, Ch. and Ruoss, F., "Forschungsplattform für Power-to-Gas", Aqua and Gas, No. 3, 1st March 2022, translated to English

	Project	Time	Location	Partners	Electr.	Power	Heat Source	Heat transfer	Gas Production	Efficiency	Remarks
	EUDP	2013 -	Foulum	Haldor-Top-	SOE (8 x	50kW _e	Adiabatic	Steam gener-	CH ₄ : 10m ³ /h (in-	79.8% calcu-	Methanator and steam
		2017	(DK)	soe	75 cells)		methanator	ator	cluding inlet bio-	lated (ннv)	generator not ther-
		0040	Daniel	0 5 10-	005 (00	45114	0	D. III.	CH ₄)	700/	mally coupled
	HEL-	2013 -	Dresden	Sunfire, KIT	SOE (90	15kW _e	Series methana-	Boiling water,	CH ₄ : 5.4 m ³ /h	76% calculated	3.5 kWe electrical
Ę	METH	2018	(D)		cells), 15		tor, 30 bar, 300°C	250°C (pres-	(target full size)	(HHV)	heater for steam to
Application					barg, 800°C			surised)			SOE inlet, direct cou-
<u>:</u>	GrlnHy	2016 -	Colzaitter	Sunfire	SOE	80 – 180kW _e	Steel plant	steam	H ₂ : 20-45 m ³ /h	75% (нну)	pling issues
dd	Gilliny	2018 -	Salzgitter (D)	Sumire	SUE	OU - TOUKVVe	Steer plant	steam	П2. 20 -4 5 III ⁻ /II	75% (HHV)	Steam generation from waste heat not
		2010	(D)								included
of the	ADEL	2011 -	EU-part-	HTceramix	SOE (cells,	0.25 kW _e	Electric heaters	none	H ₂ :	(thermoneutral)	Materials research
	, LDLL	2013	ner test	TTTOOTATTIX	short	0.20 KVVe	Licotiio iiodtoio	110110	1 12.	(unormonoutal)	> 10 kh operation
e 2		20.0	labs		stack)						To tar operation
Project from Table	SOPHIA	2014 -	Cologne	HTceramix,	SOE 25	3kW _e	Upstream CSP	Molten salt	CH ₄ : 0.3m ³ /h	65% (_{HHV})	Pressure differential
_		2017	(D)	EPFL, DLR	cells 15bar				(50% load)	, ,	<50mbar, final demo
l ö			,		700°C				,		stack heating failed
1 t	PENTA-		Rap-	EPFL, OST	SOE not	5kW _e	Polytropic metha-	Thermal oil	CH_4 : > 0.25 m^3/h	Calculated to	Real thermal coupling
)je	GON	2019	perswil		integrated		nator, multi-point		(planned)	be 19.8%	of methanator with
15							injection			points more ef-	SOE
_	HEPP	Since	Rap-	EPFL, OST	PEM, SOE		Different	Thermal oil		ficient than with	
		2017	perswil			SOE: 5kW _e	methanators			PEM (HHV	
	HotCat4	Since	Rap-	EPFL, OST	SOE	5 kW _e	EPFL lab-	Thermal oil,	CH ₄ :		Direct steam genera-
	Steam	2018	perswil				methanator, OST-	steam	7 L/min (EPFL)		tion at >12 bar
	F (0040	0.1	DI D	005	4.05.134/	methanator	-1	> 0.4 m ³ /h		0.1.11
	Future Fuels	- 2019	Cologne	DLR	SOE	1.65 kW _e	Solar steam gen-	steam			Schiller et al. (2019)
	GrInHy	2019 -	(D)	Sunfire.	SOE	720 kW _e	erator steel plant	steam	H ₂ : 200Nm ³ /h	84% (LHV)	
Sts	2.0	2019 -	Salzgitter (D)	,	SUE	720 KVVe	steer plant	steam	П2. ZUUNIII-/II	99% (HHV)	
)je	2.0	2022	(D)	Salzgitter						9970 (HHV)	
bro	DDOME	0004	D (1)	AG	005	05 114/		N 4 - 1(1(11 451.71		Intternal Heaven Communication
New projects	PROME-	2021 -	Roma (I)	ENEA, FBK,	SOE	25 kW _e	solar thermal col-	Molten salt,	H ₂ : 15 kg/d		https://prometeo-pro-
ž	TEO	2024		EPFL, IM- DEA			lectors	PCM			ject.eu
	C2FUEL	2019 -	Dunkirk	Elcogen	SOE	Lab scale			H ₂ : 1 Nm ³ /h		Lehtinen and Noponen
		2023	(F)		700°C				-		(2021)

Table 1: HTE projects using waste heat for steam generation. Excerpt from Table 2 of the Application updated with more recent projects.

3. Experiments

3.1. Research Platform Power-to-X at OST

The basic layout of the Research Platform Power-to-X at OST is shown in Figure 2 below with all partner organizations in Figure 3.

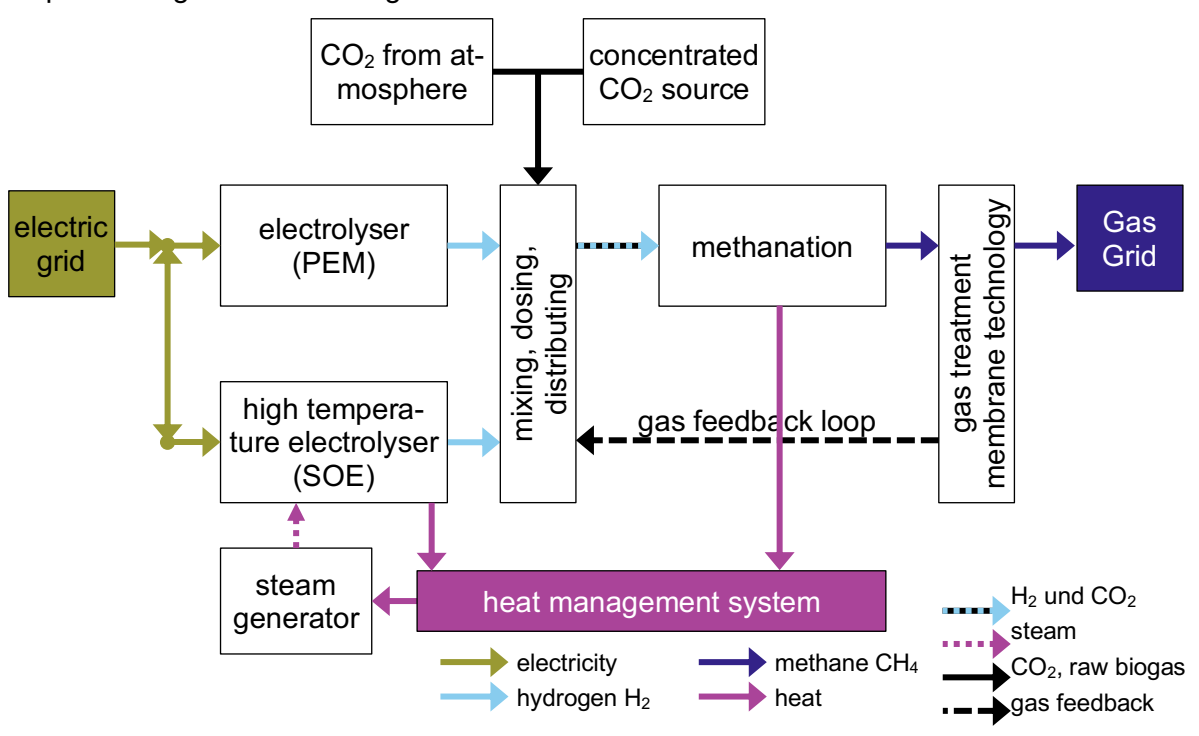


Figure 2: Basic layout of the test plant in Rapperswil showing the components relevant for project HotCat4Steam, [10] Fig. 3 excerpted and translated



Figure 3: Partners contributing to the research platform at OST in Rapperswil.



The key units for the present project are the polytropic methanation reactor, the heat recovery system (by thermal oil) and the steam generator. These are indicated in Figure 4 showing the process flow diagram of the Research Platform Power-to-X. The steam expansion vessel is not explicitly shown in the previous figure but is one of the key features developed in the frame of the present project. The most important components are also indicted in the picture of Figure 5. The components are briefly described in the following subsections.

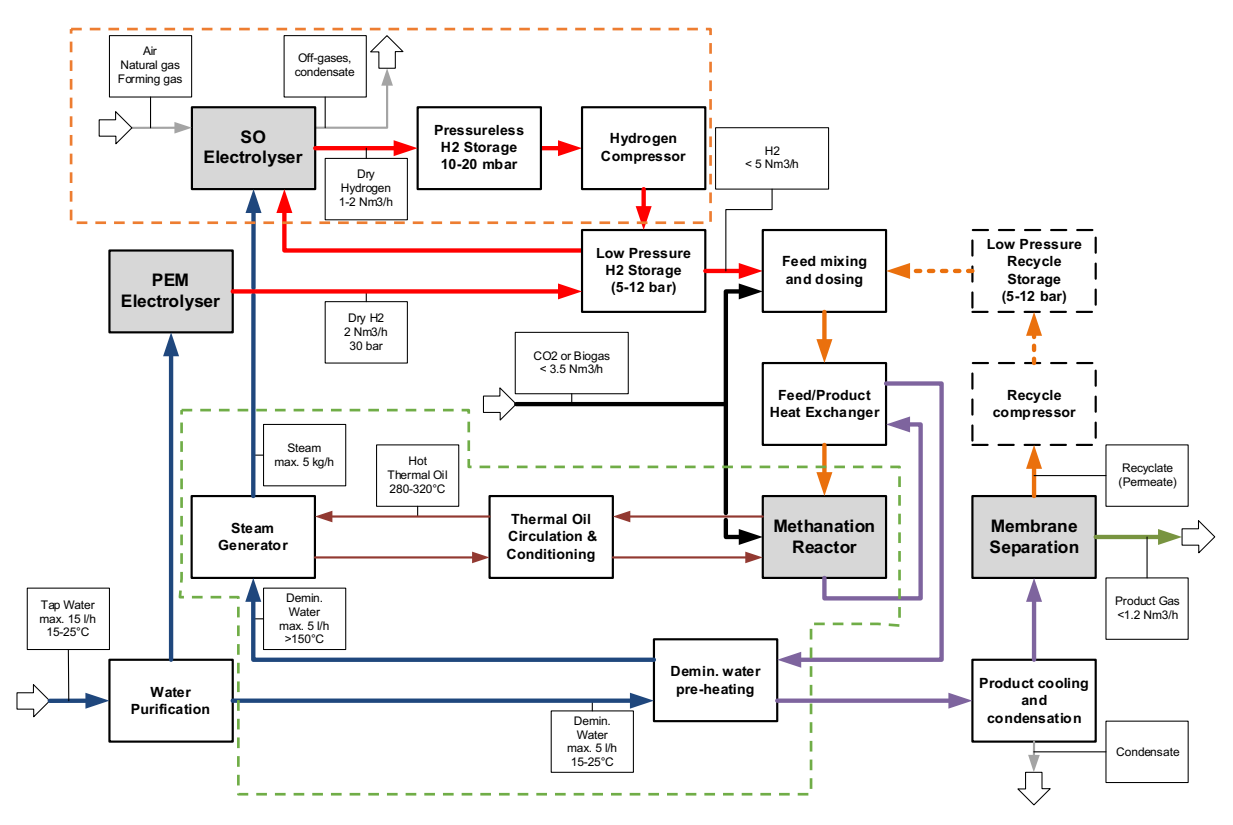


Figure 4: Process flow diagram of the Research Platform Power-to-X. Green dashed box: HotCat4Steam Key section, designed, built and successfully operated by OST. Orange dashed box: SOE section

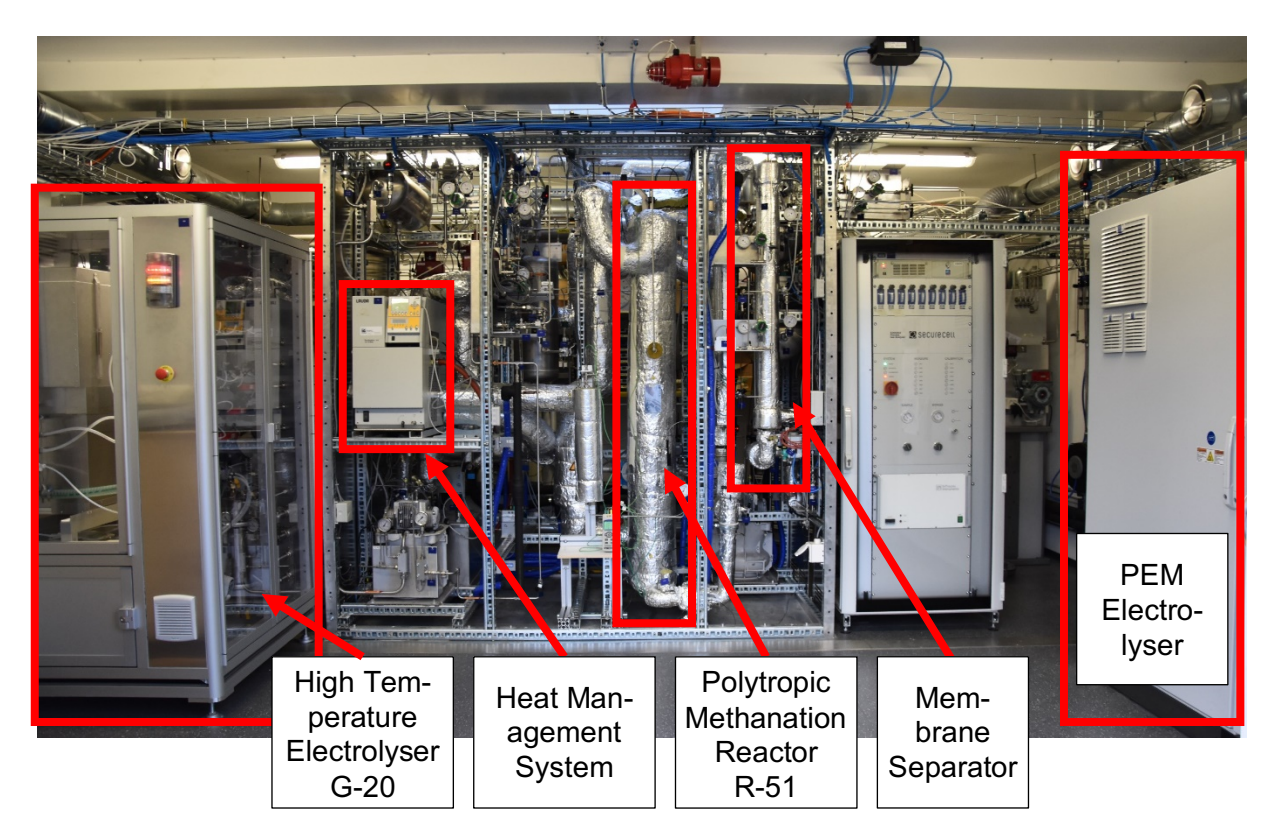


Figure 5: Inside view of Research Platform Power-to-X at OST in Rapperswil with the key components indicated.

3.2. WP1: Methanation

3.2.1.Polytropic methanation reactor at OST plant

This unit is a jacketed pipe with appr. 40 mm inner diameter. The outside jacket has an inner diameter of approximately 60 mm. The dimensions were chosen based on the experience of OST with methanation reactors and as a compromise between available materials and the predictions from a simulation study performed at OST where heat transfer and reaction were studied. These simulations, in which geometry, flowrates, gas composition among others were studied, showed that the selected design allows to extract more than the expected 1-2 kW of heat from the methanation reaction with a thermal fluid system and not exceed the maximum operating temperatures of thermal fluid (350 C), reactor wall materials (400 °C) or catalyst pellets (ca. 650 C). Figure 6 shows an example of the results produced by this simulation study.



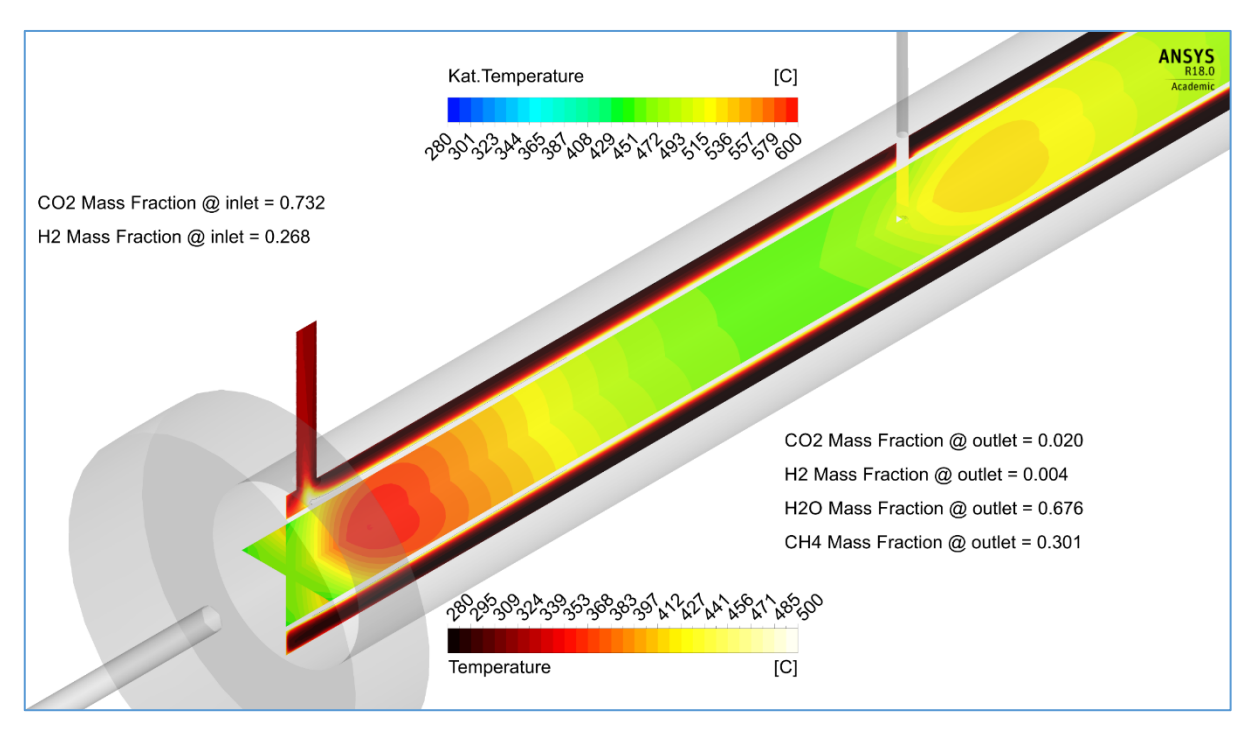


Figure 6: Example of OST reactor simulation results showing temperature field inside of a tubular fixed bed reactor.

The simulation models consists of two zones:

- □ Zone of the heat transfer medium (jacket) and where heat is either absorbed or transferred to the second zone;
- Zone where the educts flow (inner tube) and react in the presence of the catalyst according to the equations below:

$$CO + 3H_2 \Rightarrow CH_4 + H_2O$$

 $CO_2 + H_2 \Rightarrow CO + H_2O$
 $CO_2 + 4H_2 \Rightarrow CH_4 + 2H_2O$

Reaction kinetics for these equations were modelled following the scheme proposed by Schlereth [20]. Modified coefficients were employed to fit results obtained by OST in previous experiments with the same catalyst to be used in the test rig. Mass transfer inside the reaction area was modelled considering convection and diffusion. Energy and mass conservation equations were solved simultaneously for both zones, whereas heat transfer in the catalyst considered the cylindrical geometry of the catalyst pellets. To simplify calculations a pseudo-3D model was used, in which a slice comprising of three degrees of the symmetrical and cylindrical reactor was modelled. The simulations considered only steady-state conditions for the system.

To improve heat transfer, the jacket contains a guiding rod that forces the heat transfer fluid to flow in a defined pattern around the tube rather than straight along its axis. This enhances flow speed and heat transfer. Compensators take care of the thermal expansion of the unit. The whole unit is approximately 1800 mm long and the actual reaction chamber has a usable length of approximately 1600 mm, where catalyst may be inserted. The reaction chamber is divided in two reaction zones. A small pipe located at approximately 1/3 from the reactor inlet allows for introduction of CO_2 at this level. Figure 7 shows the methanation reactor during factory acceptance tests.



Figure 7: Polytropic Methanation Reactor R-51 during factory acceptance test for pressure.

The concept of splitting the injection of CO_2 and so the reaction zone was introduced to allow for control of the reaction without the introduction of ballast steam. Ballast steam is often applied in practice. Raising steam however requires energy as well as condensing the excess water in the product gases. This would thus reduce from the onset the achievable efficiency of the system.

A bed of inert beads separates the two reaction zones. These beads are also used to fill the top and bottom of the reactor. A temperature sensor is fitted in the centre of the inner tube of the reactor, allowing measuring the temperature of the reactor at 10 discrete points within it. The position of the temperature measurement points have been chosen as shown schematically in Figure 8 considering the expected temperature profile in the catalyst beds (also shown from the aforementioned simulations) to allow measurement of the 'hot spot'.



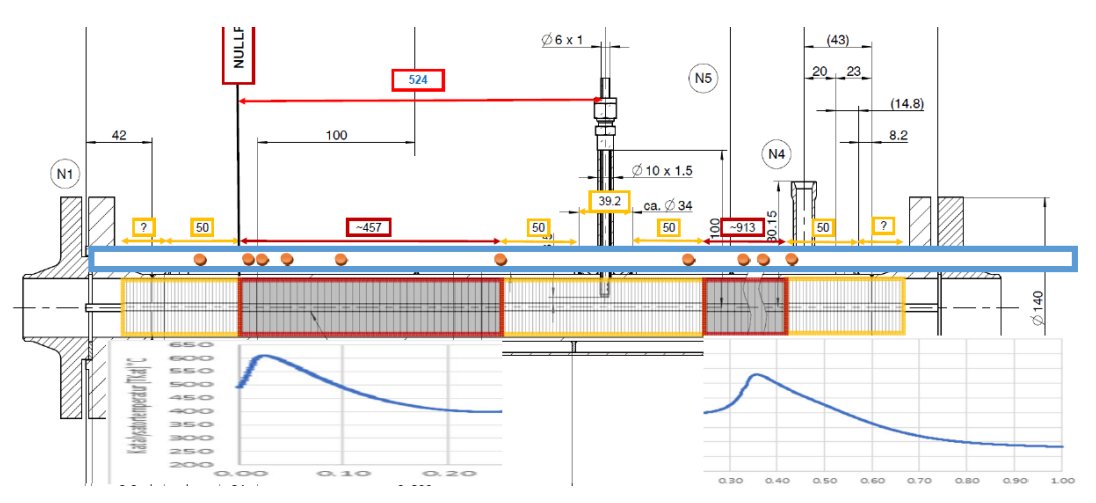


Figure 8: Schematic drawing showing the indicative position of the temperature sensors inside the polytropic reactor (orange dots), as well as simulated temperature profiles in the axis of the unit. Gas flow is from left to right.

3.2.2. Methanation reactor at EPFL laboratory

The tasks related to WP1 are both the comparison of CO and CO₂ methanation and the simulation of EPFL's methanation reactor (Figure 9). The methanation reactor was designed to be coupled with an SOE with a stream of hydrogen of approximately 5 kW_{HHV} to 8.5 kW_{HHV}. Nickel based pellets were used to ensure reaction at low temperatures of 200°C. The cooling liquid consists of evaporating water for its direct use in the SOE. Figures 1, 2 and 3 present the reactor, the PID of the experimental setup and the experimental setup in Sion, respectively.

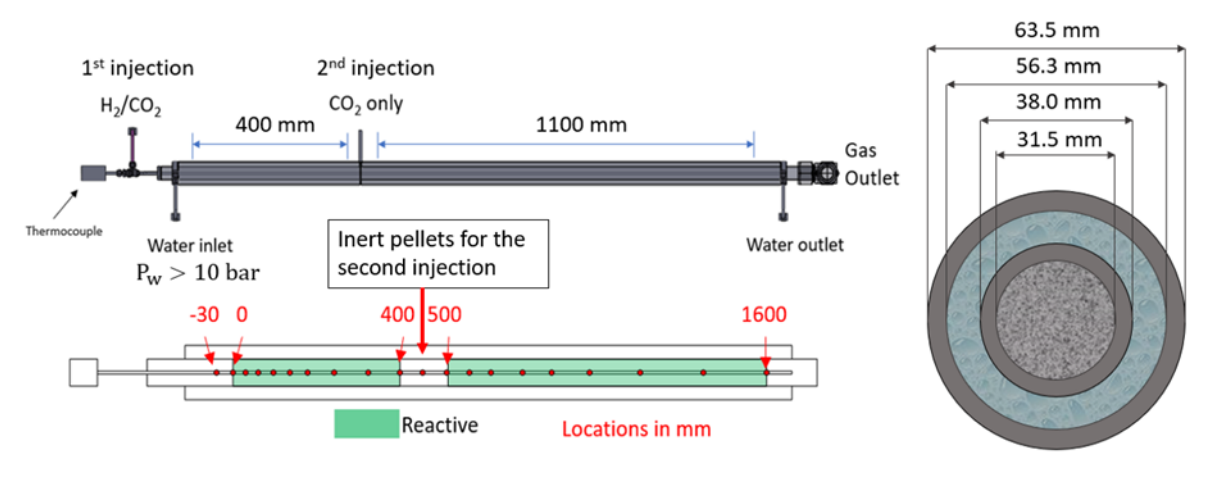


Figure 9: Reactor CAD with cross-section and the locations of the temperature measurements, reprinted with permission from [1].

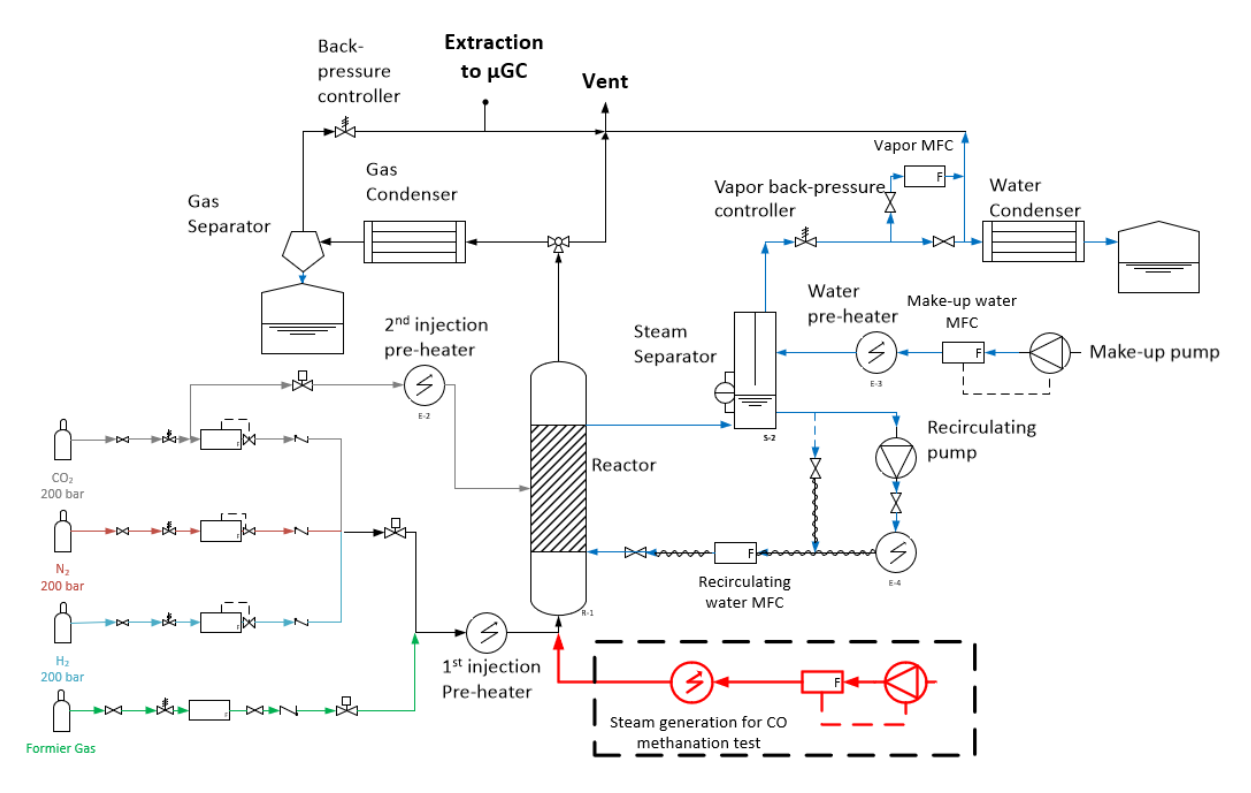


Figure 10: PID of the experimental methanator setup in EPFL's laboratory, reprinted with permission from [2].

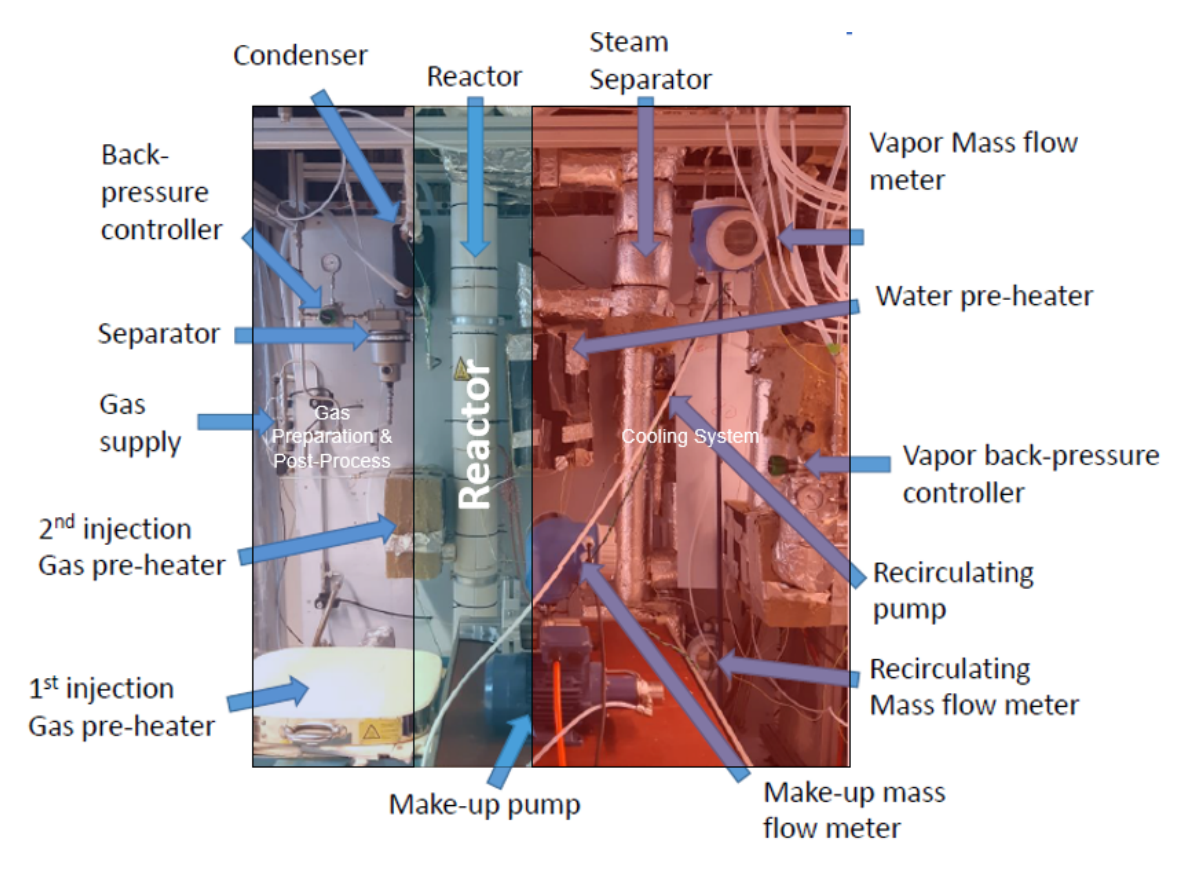


Figure 11: Experimental methanator setup in EPFL's laboratory, reprinted with permission from [1]. 18/109



A series of EL-flow from Bronkhorst are used to control the flwo rates of the various gases (H₂, CO₂, CO and N₂). The gases are first pre-heated before being sent into the reactor. In the case of syngas methanation (H₂, CO₂, CO), steam is mixed with the hot gases prior to the injection to limit carbon deposition inside the reactor. At the outlet of the reaction, the generated water in the gas mixture is condensed before being separated.

The cooling system consists of direct partial evaporation of water. The pressure is used to control the minimum temperature inside the reactor. A surplus of water is sent into the reactor to stabilise the evaporation process. Consequently, vapor-liquid separation at the outlet of the cooling system is required followed by the recirculation of the liquid mixed with make-up water.

3.3. WP2: Heat management and steam generation

3.3.1. Heat management at Power-to-X Research Platform

The heat management system consists of a laboratory thermostat model Integral XT 4 HW by the company Lauda, a set of 3-way mixing valves, piping and instruments. Table 2 shows the key features of the thermostat and Figure 12 shows the P&ID of the complete section.

Parameter	Value
Operating Temperature	30 - 320 °C
Heating power	3.2 kW
Max. thermal fluid flow	45 I/min
Cooling capacity	16 kW
Heat transfer fluid use	
Type: Ultra 350 (Marlotherm)	
Max. operating Temperature	350 °C

Table 2: Key process parameters of thermostat (Source: Lauda GmbH)

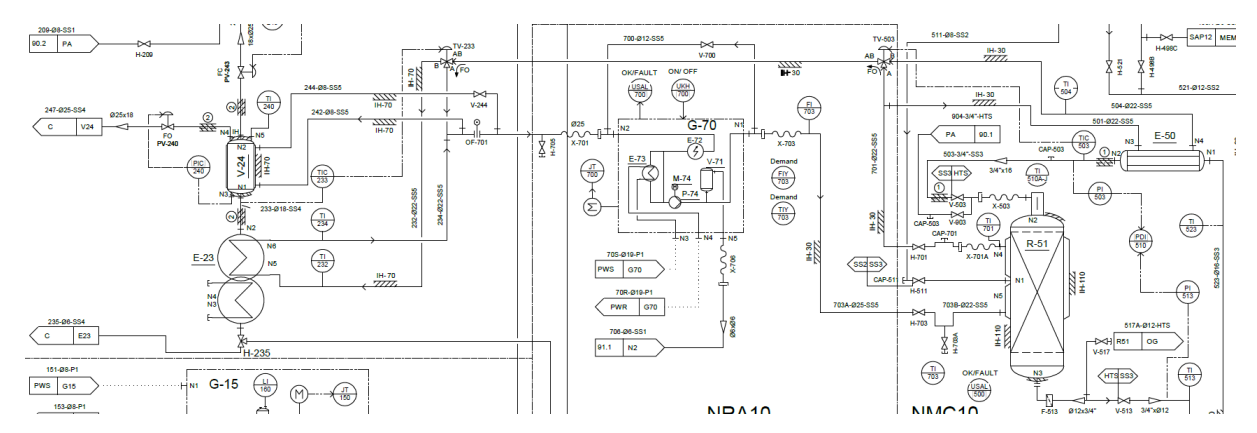


Figure 12 Extract from the Research Platform Power-to-X P&ID showing the heat transfer system (Source: OST)

The thermostat offers the possibility of compensating for heat losses as well as for dissipating heat if required, simulating the flexibility of latter large-scale operations. The temperature of heat transfer fluid at the outlet of the unit is set by the test rig's over-arching process control system as well as its flow rate. An Endress+Hauser Promass F-300 Coriolis-type mass flow-meter measures heat transfer fluid flow. A Pt-100 transducer close to the outlet of the thermostat measures temperature.

The heat transfer fluid flows into and out of the jacket of the reactor. A proportional 3-way valve divides the heat transfer fluid flow at the outlet. The hot heat transfer fluid exiting the reactor's jacket is sent to either a heat exchanger where feed gas to the reactor is heated or directly to the steam generator. Both heat transfer fluid streams are then mixed and sent to another proportional 3-way valve, with which the amount of heat transfer fluid going to the evaporator can be modulated. This design allows controlling the heat used to raise steam in the evaporator. The amount of heat transfer fluid going to the jacket of the expansion vessel is fixed, set by a needle valve on that sub-circuit.

3.3.2.Steam generation at Power-to-X Research Platform

This unit is a so-called capillary total evaporator. The principle of operation is described in the literature [9] and other teams working on SOE have successfully tested this type of steam generator [19]. However, these tests involved steam generators that are electrically heated. Tests at OST with a unit of similar design, provided by the Institute of Chemical Process Engineering [28] and heated by heat transfer fluid have shown that this unit is able to fulfil the stringent pressure fluctuations requirement of the SOE (below 20 mbar). At that stage, however, the maximum throughput at acceptable pressure fluctuation was limited and below the required flow for the SOE unit.

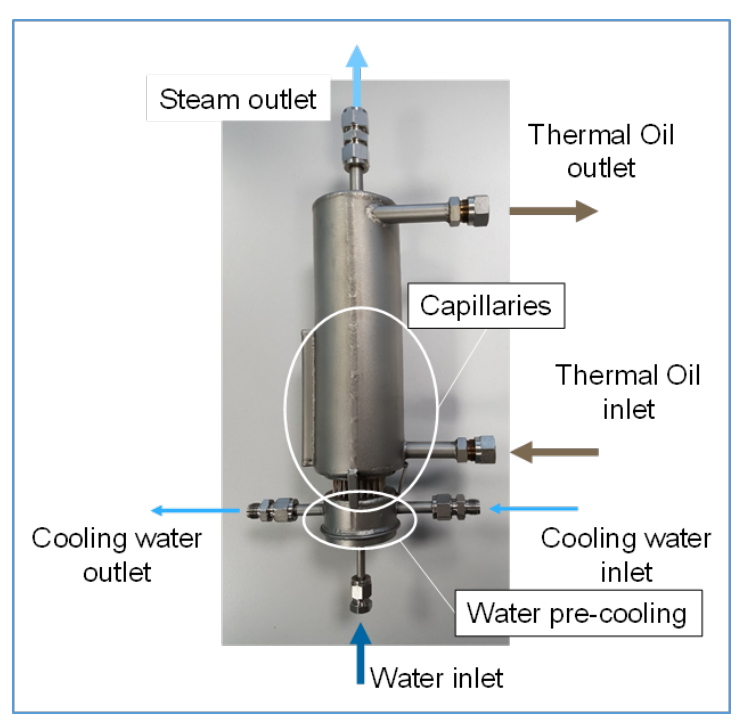


Figure 13: Detailed view of steam generator of the HotCat4Steam project with material flows.

OST decided to modify the design of the complete steam generation section to include a vessel (Tag-Nr. V-24) offering buffer volume and dampen the fluctuations. The vessel design further includes a TO jacket that ensures the produced steam is always superheated. The new design described above is tested and the results are presented and briefly discussed later in this report. A CAD rendering of the final assembly is shown in Figure 15.



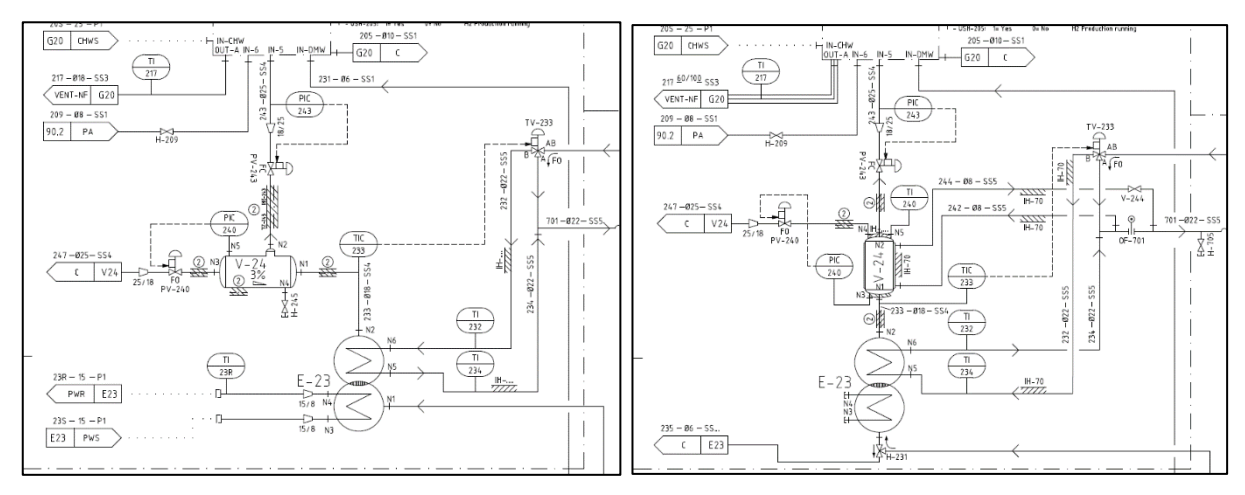


Figure 14: Steam generation section: original design (left) and modified (right).

Demineralised water is produced in the plant in a dedicated unit. This water is fed by a micro annular gear pump controlled by a Coriolis-type flow rate flowmeter. This type of pump in combination with a Coriolis flowmeter was selected as it allows for precise and fluctuation-free feeding of the water at reasonably high (up to 10 barg possible) pressures. The forwarded water is then directed to a preheat-exchanger where part of the heat of the product gases exiting the methanation reactor can be recovered. Temperature sensors in the water flow located before and after the heat exchanger allow calculating the thermal energy gained over the latter unit.

The preheated water enters the "pulsation free" total evaporator (E23, steam generator), which has a temperature transducer at its exit. This already superheated steam enters an expansion vessel (V-24), located right after and above the steam generator, where any remaining pulsations are equalized, and the steam further superheated by the thermal oil. Thanks to two installed pressure control needle valves, the steam can be sent either to vent or to the SOE. The pressure can be controlled by a setpoint equal to the admission pressure to the SOE and a pressure measurement downstream.

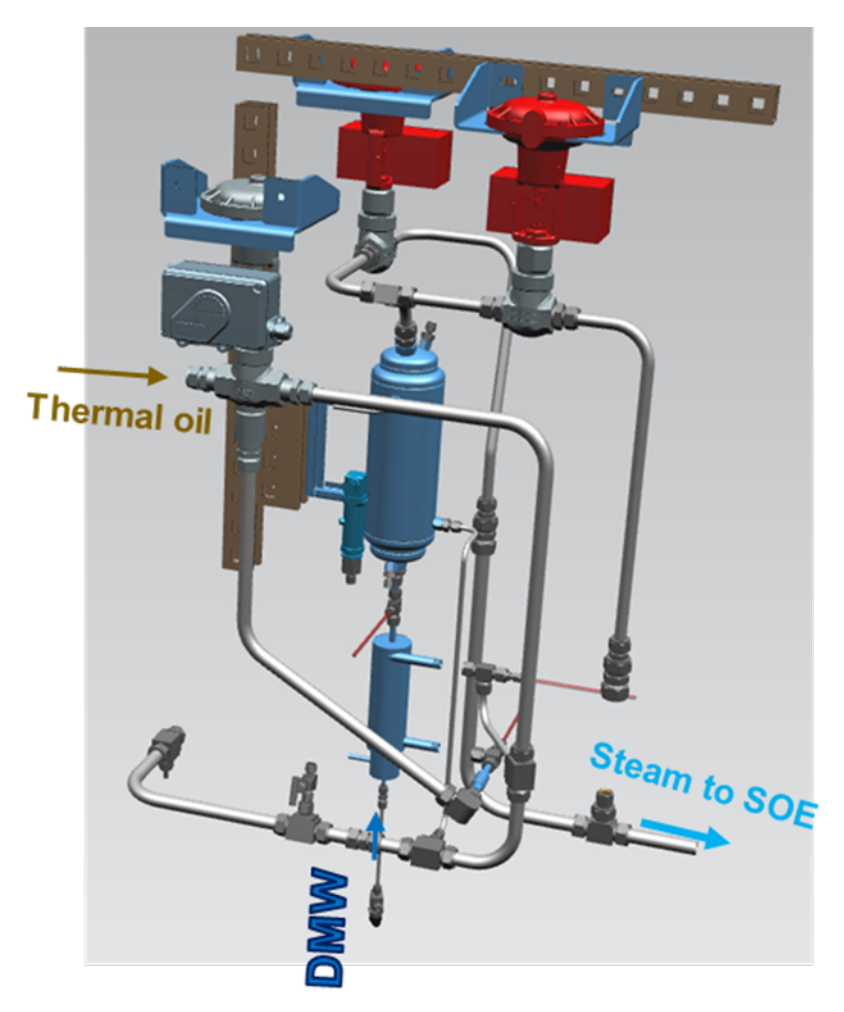


Figure 15: CAD-Rendering of Steam generating section.



3.3.3.Steam generation at EPFL laboratory

Experiments have been performed on the stability of steam production at EPFL laboratory, in Sion. The concern for steam pulsation at the inlet of the SOE is linked to two aspects: (1) maximum flow pulsation in the SOE stack, and (2) measurement of the quantity of steam entering the stack. The pulsation management is related to the reactor design and operation as well as the system level dampening method. Therefore, solving for lower pulsation at the inlet of the SOE requires to optimize the reactor design and operation, and design a dampening system.

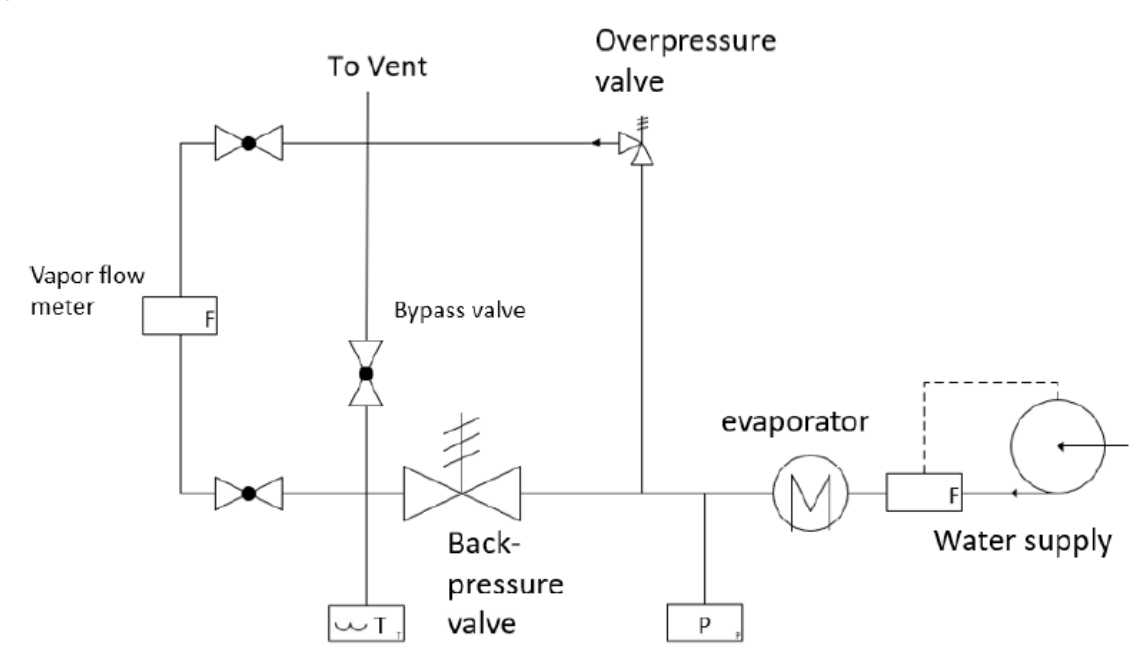


Figure 16: P&ID of the installation for the calibration of the mass flow meter.

To measure and validate the steam stability generated by the reactor, a steam mass flow meter (MFM) was installed and calibrated. Figure 16 shows the P&ID of the temporary mass flow meter installation. The MFM is coupled to a commercial evaporator for two purposes: Calibrate the MFM and record the steam stabilization with the evaporator for future comparison with the steam produced by the methanation reactor.

The MFM was calibrated in 2021. Figure 17 presents the calibrated steam measurement compared with the liquid water injected into the commercial evaporator, at two different mass flows. The average flow is accurate enough in both situations (< 1.0 % of error).

The MFM is therefore used to compare the steam stabilization between the reactor and the commercial evaporator. Its performance is presented in chapter 4.2. Based on the results, the need of a dampening device to decrease those fluctuations is analysed.

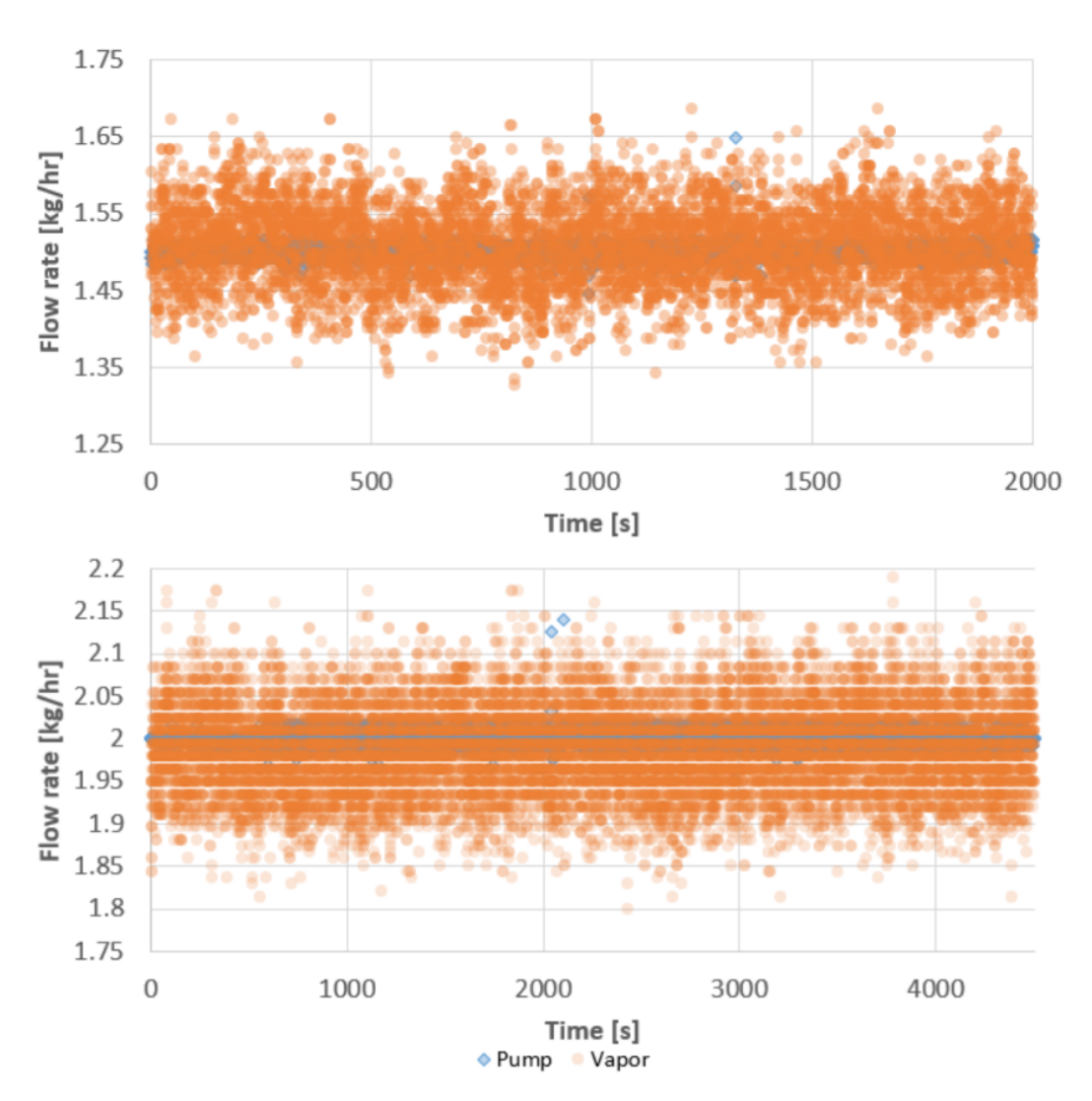


Figure 17: Steam measurement at the outlet of a commercial evaporator compared to the liquid water injected.

Cooling operation at EPFL

The parametric study during CO_2 methanation was completed using active cooling of the reactor using a pump. This was done for a few reasons: (1) maintaining the flow rate of recirculation mostly constant, (2) ensuring sufficient water recirculation for the range of reactant flowrate, and (3) attempt at stabilizing the evaporation process for the range of reactant flowrate. However, the use of a recirculating pump limits the cooling water pressure due to their limit in temperature. An alternative operation was used, reaching a higher recirculating temperature beneficial to the conversion rate. It cannot be discussed in detail in this report for reasons of confidentiality.

At the EPFL laboratory, the height of the ventilation hood is approximately 2 m which limits the height at which the separator is installed, and thus, limiting the maximum flowrate of steam that can be recirculated. For the safe operation of the reactor, the analysis presented below is performed only using 24 NL/min of H_2 inlet flow into the reactor. The vapor fraction must still be limited to avoid the critical heat flux that could result in dry-out or inverse annular flow at the



hot spot of the reactor. In these cases, the heat transfer would drastically diminish at the location of highest heat generation. If the heating area were to interact thermally with only vapor, the cooling system would act as an insulation which would cause the hot spot to go out of control. During the parametric study on CO_2 methanation performed on the reactor, the steam generation flow at 24 NL/min H_2 was between 21.67 g/min and 23.34 g/min, mostly depending on the inlet temperature of the reactor. With recirculation of 200 to 220 g/min, the vapor fraction at the outlet was thus below 20 %. In alternative mode, the aim is to limit the vapor fraction under 50 %. In addition, during the various runs performed at various reactant flow rates, the system is the most stable at the lower end of the reactant range. Consequently, operating only at the low end of the reactant flow rate can avoid already identified instabilities that could only be acerbated using lower recirculation.

With a fixed reactant flowrate, and thus, an almost fixed heat generation, the stability of the system as a function of pressure and recirculation flowrate are assessed. The response in vapor flow rate at the outlet of the system is compared to the active cooling case. The mass flow meter is the one presented previously with the 0.5 sec damping to remove noise.

The temperature profile in the packed bed (and the subsequent conversion) can take significantly longer to stabilize compared to the cooling system pressure. Nevertheless, it can be assumed that the change in conversion level is negligible and the stability of the temperature profile at 24 NL/min H₂ regardless of the cooling water pressure allowed the test of the stability using smaller timeframe compared to the conversion analysis presented in the previous work.

3.4.WP3 and WP4: Solid oxide electrolysis, BoP components and system balance

3.4.1.Pressurized Single Cell Setup

The first step in SOE pressurization is to pressurize a single cell. To achieve this, a pressurized setup had to be designed and tested. This setup was designed and built in 2021 and 2022 and is presented here. The current version of the setup consists of sealing the cell using a compressive seal. To do so, the force is transmitted through the electrical heater as shown in Figure 18. During the development of the system the force is applied using a hydraulic press. However, the ultimate solution will be a pneumatic piston controlled using electrical valves. Currently, the installed force sensor only acts as an indication of the applied force. In the final version, it will also be the process variable of the PID for the pneumatic piston control and it will also be part of the safety procedure in the case the piston (or a component along the axis) fails.

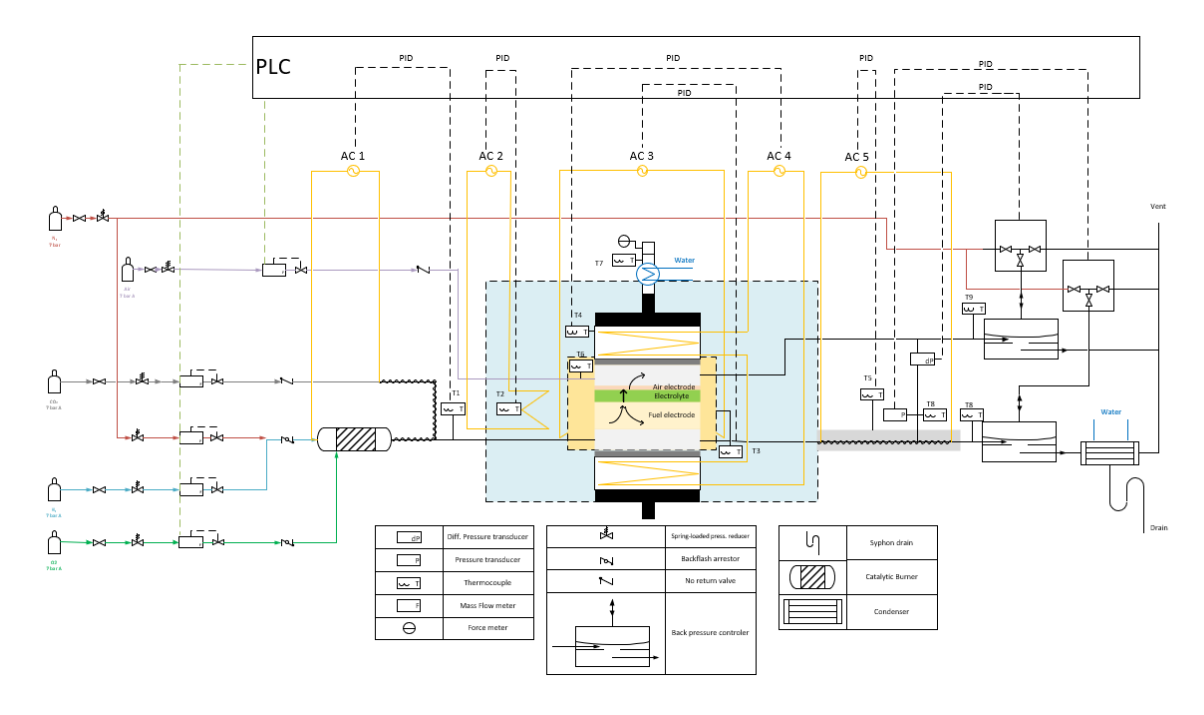


Figure 18: Simplified P&ID for the pressurized test rig

The pressurization is performed using back-pressure controllers. On the air side, the fluid is cooled under 150 °C before entering the back-pressure controller BPC (its temperature limit).

On the fuel side, there are a few alternatives that exist for the pressurization depending on the willingness to condense before or after the back-pressure controller. For simplicity and reliability, the back-pressure controller is selected to ensure temperatures up to between 450 °C and 550 °C. This allows the outlet flow to be sent in the back-pressure controller directly.

The two back-pressure controllers are controlled through electrical valves using the line pressure on the fuel side and the differential pressure between the fuel and air lines as the process variables of the PID for the Back Pressure Controllers of the fuel and air, respectively.



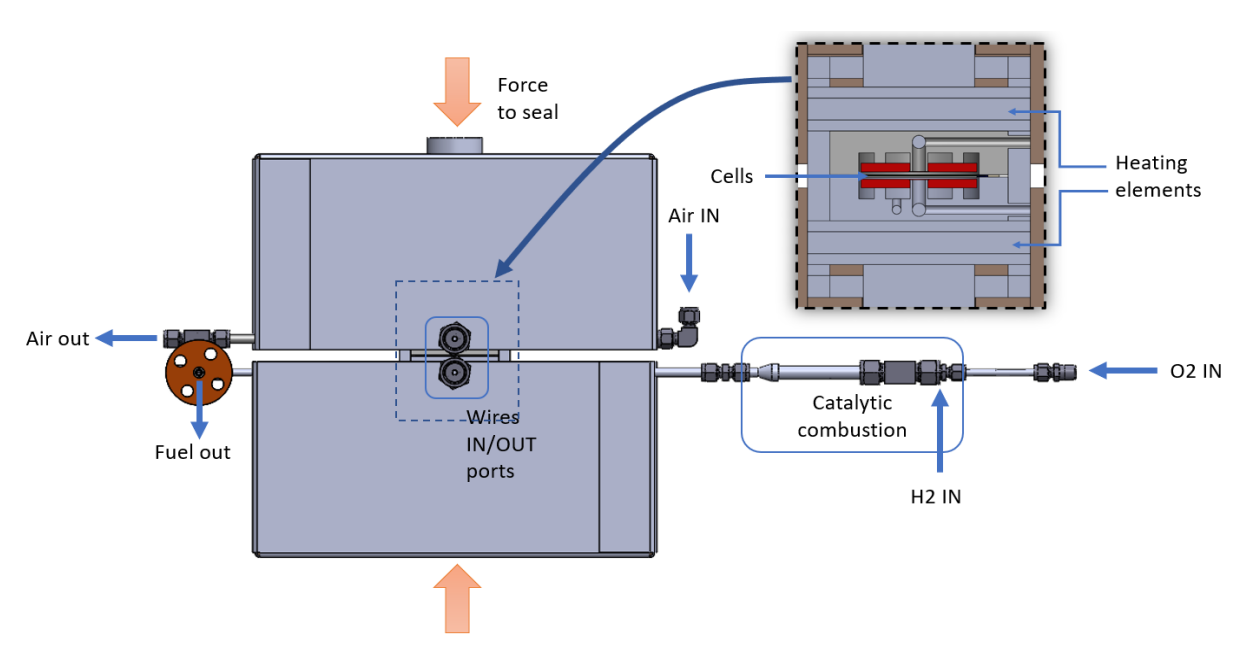


Figure 19: Oven and cell mounting for the pressurized cell rig.



Figure 20: Pressurized single-cell setup

Catalytic burner development

The development of a catalytic burner for steam production is needed for pressurized single cells testing. The current evaporator used in these tests is not designed for pressurized evaporation; many parts would break if pressurized. In addition, the steam produced during catalytic combustion is more stable than during evaporation, further justifying the development of a

catalytic burner. Figure 21 shows the schematic of the catalytic burner installed on a traditional single cell setup.



Figure 21: Catalytic Burner in traditional single cell setup

The current version of the catalytic burner consists of 8 cm of rolled Pt black doped nickel mesh inside a 10 mm outer diameter tube followed by another 8 cm of nickel mesh without doping. The doping consisted of using a brush to cover the mesh with a mixture of Pt black and a carbon-based binder. This sub-optimal technique only doped the mesh with a few mg of Pt, but sufficient for the quantity of hydrogen to be combusted. Even at ambient temperature, the catalytic activity of Platinum should be sufficient for the almost complete combustion of the hydrogen.

Some preliminary tests were conducted and the results are presented in Figure 22. Long-term tests are required to validate that the catalytic burner does not affect the performance. This was the case of the first version of the catalytic burner whose binder had sulfur and fluoride. In the first case, Figure (A), the resistance of the cell became such that the exothermicity occurring beyond the thermoneutral heated up the cell and improved the performance. However, the second test was only tested for 10 hours in which limited change occurred, but a long-term test is required to ensure the new catalytic burner does not impact the cell performance.



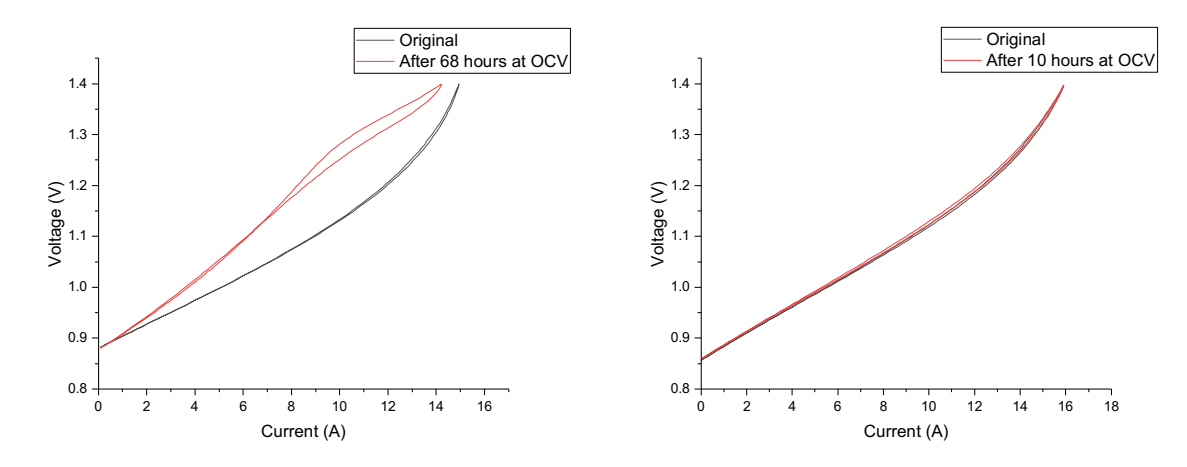


Figure 22: IV curves using the two catalytic burners developed: (a) using PVA binder and (b) using a C-H based only binder

3.4.2.The SOE Unit

This part of the report presents the SOE unit built by EPFL and integrated in the Research Platform Power-to-X at OST in 2020-2021. The SOE unit consists of a Balance of plant unit (BoP unit) and a control rack. The heart of the BoP is composed by a HotBox, containing the heating network responsible for bringing the stack to the requested temperature, and a Stack-Box, which contains the stack itself (Figure 26). The HotBox, the heating network and the Stackbox are based on the Bluegen system from SolydEra. As the BlueGen is designed for fuel cell operation only, it is modified for electrolysis operation. In practice, this requires adding a steam-fuel heat exchanger to heat up the steam(-H₂) SOE inlet using the hot H₂(-steam) SOE outlet, which needs to be integrated as extra-component into the HotBox. Moreover, a specific condenser is designed and built in order to remove the remaining steam from the hydrogen produced and meet the requirement of dryness for the gas to be used by the hydrogen compressor and the methanator. Finally, a new gas distribution plate is designed to supply the stack with the requested gas. All those modifications require to redesign the HotBox and the StackBox.



Figure 23: The SoE-BoP and the control rack prepared by EPFL, before being moved to the Research Platform Power-to-X at OST.

The SOE-BoP is supplied by five gas/liquid lines: air, stack fuel, burner fuel, steam and demineralised water (DMW) lines (see Figure 24 taken from the drawing in Figure 31). The air is used to heat the hotbox and the stackbox by preheating the incoming air thanks to a burner and an air-air heat exchanger. It is also used to sweep the produced oxygen from the anode during the electrolysis. The stack fuel line supplies the stack with hydrogen, forming gas (FG) or nitrogen. It is mixed with steam and heated thanks to the fuel-fuel heat exchanger before entering the stack. The burner fuel line provides natural gas to the burner to heat the air and bring the whole SOE-BoP to the requested temperature. It is used during HEATING mode, HOTSAFE mode and HOTSTANDBY mode as presented on Table 3 but should be turned off during production mode (ELECTROLYSIS) at nominal conditions as the stack should provide the additional energy to heat the air. Finally, the DMW line brings DMW into the HotBox, which is turned into steam by passing through the air-air heat exchanger. Afterwards, this steam is mixed with the CH₄ supplied to the burner to prevent carbon deposition in the line. Without it, the carbon would quickly obstruct the burner fuel line, until blocking it completely.

Before entering the burner, the mixture of CH₄ and steam passes through a reformer that converts it into a mixture of H₂ and CO. This reformate is burnt when it is in contact with the air coming out from the stack. The reformer is a part of the original Bluegen design of the HotBox made by SolydEra. With the configuration used for this project, it is not useful but it has been kept in order to simplify the construction of the SOE unit.



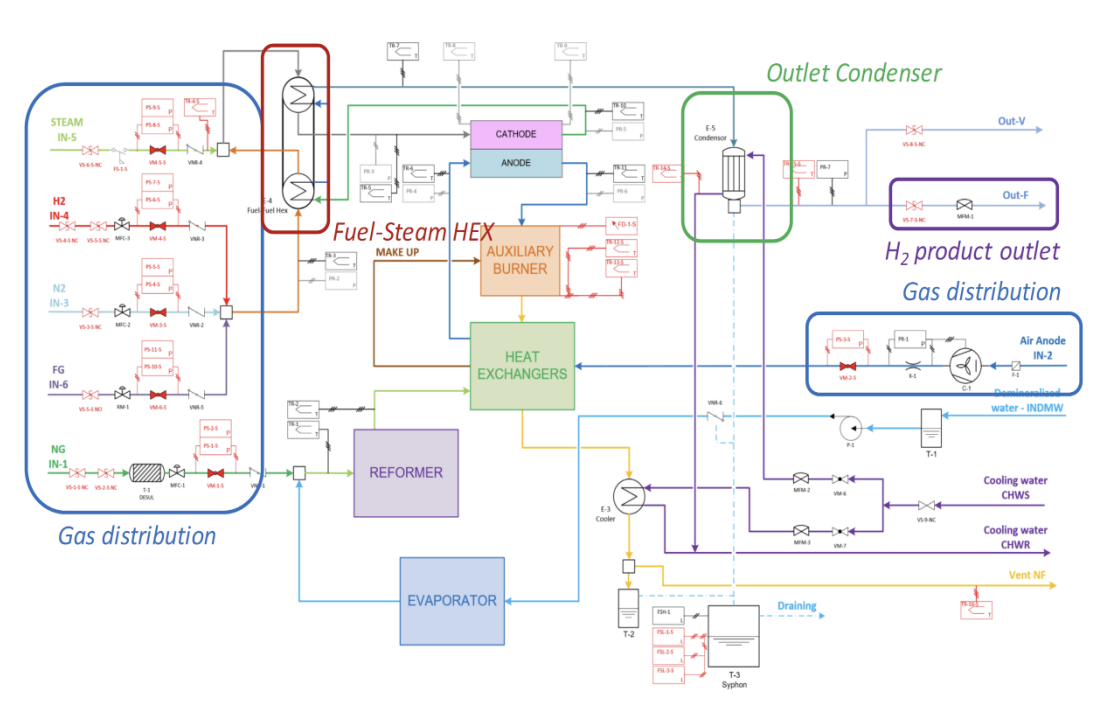


Figure 24: P&ID of the SOE-BoP taken from the drawing in Figure 31.

	1. Start-up	2. Hot Safe	3. Hot Standby	4.Production	5.Shut-down
IN-1: NG burner feed	er feed ON, adjusted ON, adj		ON, adjust.	OFF	OFF
IN-2: Air feed	ON	ON	ON	ON	ON
IN-3: N ₂ /H ₂ feed	ON	ON	OFF	OFF	ON
IN-4: H ₂ feed	OFF	OFF	ON	ON	OFF
IN-5: Steam feed	OFF	OFF	ON	ON	OFF
SOE current	OFF	OFF	OFF	ON	OFF
OUT-F (fuel outlet)	N ₂ /H ₂ recyc	N ₂ /H ₂ recyc	H ₂ to vent	H ₂ to Meth.	N ₂ /H ₂ recyc
OUT-A (air off-gas vent)	Fluegas	Fluegas	Fluegas	O ₂ -rich air	Air

Table 3: SOE operating modes and corresponding inlet/outlet flows

The new steam-fuel heat exchanger is designed using known and approved manufacturing and shaping techniques. The main constraints are to meet the heat exchange and temperature needs while respecting the limited space available next to the existing BoP. The design of the exchanger has gone through multiples iterations and simulations before being validated, built and integrated to the existing BoP. The simulation is performed with nominal conditions as well as part-load conditions, to ensure the minimal requested temperature over a broad range of flows and power. The purpose of the CFD simulations was to:

- 1. Determine the outlet temperature of the incoming gases.
- 2. Simulate and analyze the steam-hydrogen mixture.
- 3. Calculate and optimize the pressure drops according to the operating points.

The exchanger is composed of 17 parallel channels. One channel allows the preheating of cold inlet hydrogen. The steam-hydrogen mixture is produced at the inlet of the second channel, after the H₂ preheating. All other channels allow the superheating of the steam-hydrogen mixture before the SOE stack. The preheating is carried out in co-current with the outgoing gases, superheating in counter-current flow. A picture of the mounting is not shown for confidentiality reasons.

The condenser is a welded assembly. All the welds are done by the EPFL workshop. The completed condenser is shown in Figure 25. The connections with the SOE system are via welded Swagelok connectors. It is mounted on the BoP and validated.



Figure 25: Condenser to dry the produced hydrogen (left: CAD part, right: the condenser mounted on the BoP)

The insulation is entirely redesigned to accommodate the existing BoP, the new gas distribution plate and the additional heat exchanger. The insulation around the BoP, the hot box as well as the insulation around the stack box, is realized with the aim to:

- 1. Thermally isolate the stack and the entire BoP.
- Offer protection against fire.
- 3. Contain all electrical connections, especially the power DC supply to the stack.
- 4. Allow and contain potential measurements of different cells (clusters).

The insulating envelopes are designed from folded sheet metal, to contain all insulating parts and maintain all parts together.

The BoP unit also contains an entire gas distribution (inlet and outlet) panel designed to fit with the OST infrastructure. The closet containing the HotBox and the StackBox is designed to respect safety requirements. It is fully ventilated to avoid flammable gas accumulation and is equipped with hydrogen detectors. A junction box is installed at the back of the BoP for all the electrical connections (instrumentation, power, control, ...) The box is constantly overpressurized to avoid any accumulation of gas inside it.



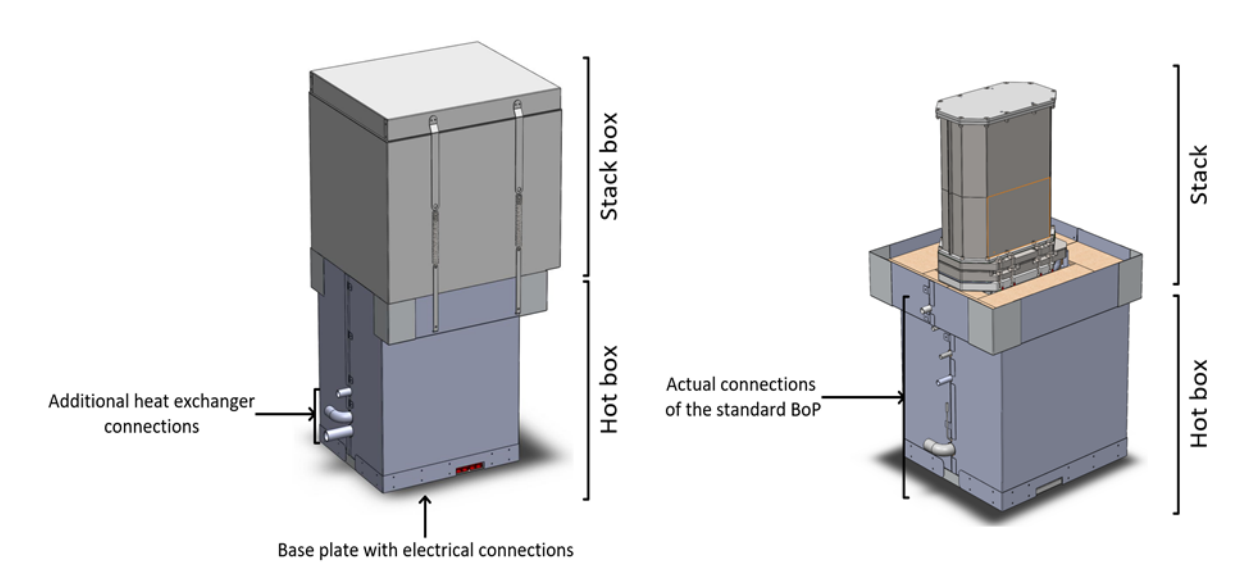


Figure 26: The modified Stackbox and the Hotbox

The SOE unit was transferred and connected to the OST plant in early 2020, as shown in Figure 5. More details about the integration of the SOE unit with the rest of the plant are presented in the next chapter. However, at that moment the SOE unit was not yet ready to operate properly. In 2020 and 2021, it still needed numerous improvements, debugging and finalizations before being ready to start. Here is a non-exhaustive list of what has been achieved at the hardware level during those two years:

- Installation of the steam line and the heating ropes
- Ordering and replacement of Shinko controllers, which were not adapted to the signals received.
- Test and calibrate of each element (MFC, MFM, pressure gauges, pressure switches, DMW pump, air blower, thermocouples, cooling system, ...)
- Sealing of the junction box and test of the pressurization
- Ordering and replacement of Jumo controller and the diodes used for the air blower
- Test of the condenser and the condensation box
- Programming and connection of the PR4116

- ..

The covid situation and the numerous incomplete and unfinished elements discovered on the SOE unit led to constant delays. Moreover, having the SOE in Rapperswil made it difficult for the EPFL team to perform rapid and efficient work due to the long necessary travel and organization.

In 2021, a bypass is mounted in the stackbox as shown on Figure 27. It is composed by two tubes that transport the air and the fuel from the inlet to the outlet of the BoP. It is used to simulate the presence of the stack and allows to test and validate the entire SOE-BoP unit without risking to damage a stack.

The test with the bypass, performed in early 2022, allowed to characterize the behaviour of the burner up to a temperature of 830 °C, as well as the temperature profile of the overall SOE-BoP. Thanks to those results, a heating methodology of the BoP was developed, determining the amount of air, methane and forming gas flows necessary to start the heating SOE-BoP and keep it at a constant rate until the requested temperature.

Additionally, a burner control methodology has been designed, based on the results of the bypass test. More details about it will be presented in the results and discussion chapter.



Figure 27: The bypass installed inside the StackBox in 2021

In mid-2022, stack #1801 from SolydEra was mounted in the SOE-BoP system as shown on Figure 28. The mounting of the stack required a modification of four parts inside the BoP which had the wrong dimensions and were preventing the stack installation. Therefore, the BoP has been emptied of insulation sand, the faulty parts have been removed and replaced by newly machined ones. Later the stack has been successfully installed without damage and the BoP has been refilled with insulation sand. Due to those faulty parts, the installation took more time than expected and delayed the testing week to September 2022 instead of August.

Finally, in January 2023, stack #1801 has been replaced by stack #1803 to perform the final experiments of the project.







Figure 28: Mounting of the stack #1801 in 2022.

3.4.3.Integration of the SOE Unit in the Research Platform Power-to-X

The SOE unit is integrated into the Research Platform Power-to-X by means of both signals (control and information) as well as by means of physical connections/supply and take-off of gases and other media. This integration is summarized in Figure 29, an extract of the plant's P&ID. Figure 30 shows the back panel of the SOE unit with some of the physical connections of a part of these media.

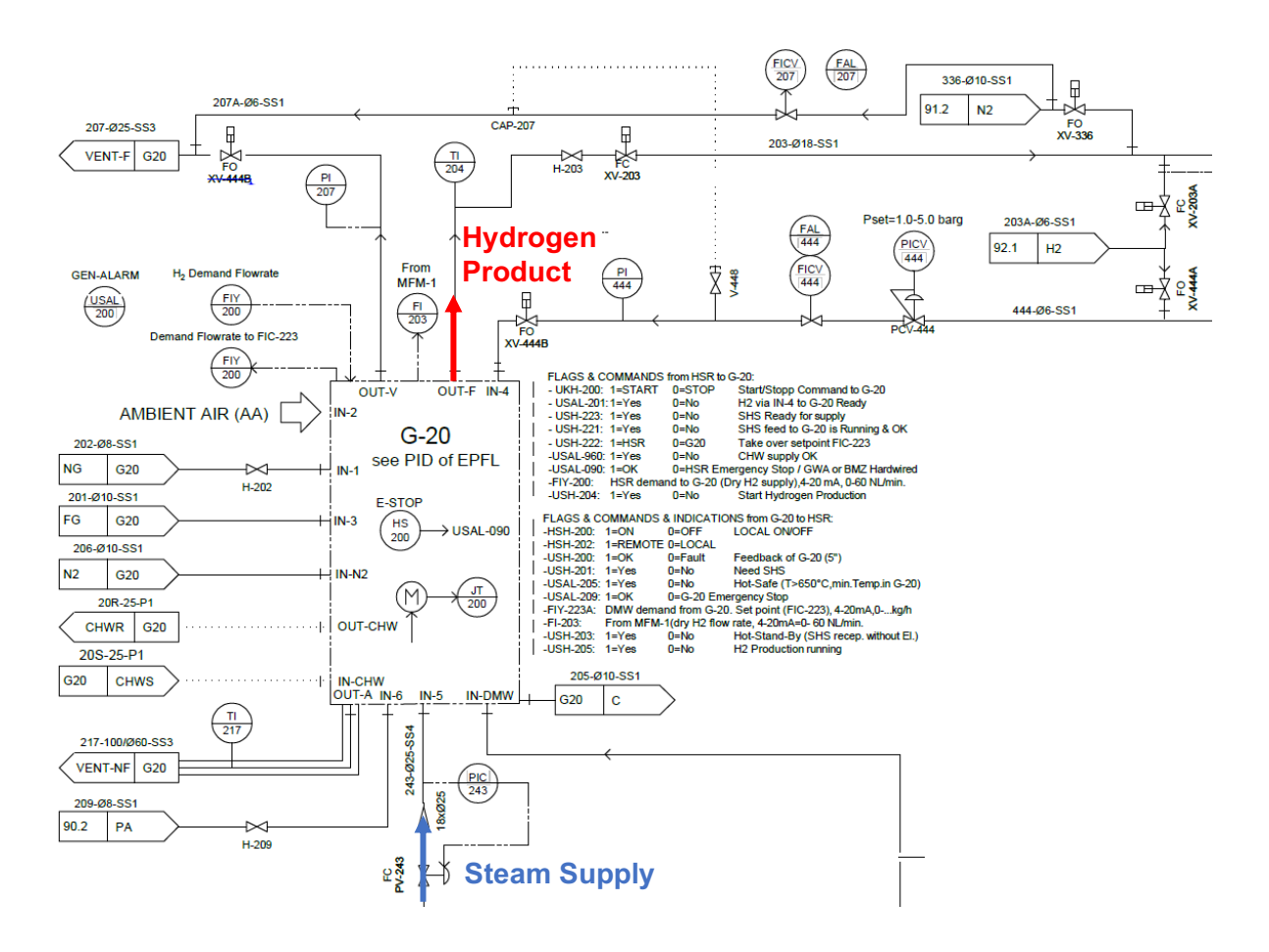


Figure 29: Extract from the P&ID showing the SOE-Unit (G-20). For details on the SOE Unit see Figure 31.





Figure 30: View of the physical connections (media) to the SOE unit (G-20) during assembly.

The SOE unit is provided with several gases and cooling water from the Research Platform Power-to-X. Table 4 below shows a list of these media with the key characteristics of supply. Further to the feed with steam the unit requires feeding with 'make-up' hydrogen, forming gas $(5 \% H_2 / 95 \% N_2$, abbreviated FG), natural gas (NG) and process air (PA).

Parameter	Value
Steam Feed	
Flowrate	1.2 – 5.0 kg/h
Temperature	120 - 300 °C
Pressure	30 - 100 mbarg
Acceptable pressure fluctuations	20 mbar
Oxygen content	< 1 ppm
Hydrogen Product	
Flowrate	0.12 – 0.33 kg/h
Temperature	5 - 10 °C

Table 4: Key process parameters of the SOE unit (G-20)

Make-up hydrogen is mixed with the steam inside the SOE unit, to protect the electrode material from oxidizing in pure steam. The hydrogen/steam mixture is fed to a heat exchanger, which captures the energy from the hydrogen produced at the cathode. Make-up hydrogen is supplied from either bottles or from V-44, with the latter being the preferred option. The feeding

rate of make-up hydrogen is set and monitored locally (FICV-44). Forming gas is required to keep the unit in its hot state and prevent the electrode material from oxidizing. G-20 also required feeding with DMW from unit G-15, as explained in chapter 3.4.2.

When the unit G-20 produces hydrogen, the outlet gas is cooled, and its residual water is condensed before it is sent to the methanator test rig. G-20 is connected to the chilled water supply for this cooling/condensing step. Finally, G-20 has a dedicated hot exhaust line, though which product hydrogen uncondensed and uncooled can be sent to the vent line in case of need. G-20 has an outlet for the condensate separated from the product hydrogen.

The signals exchanged between G-20 and the test rig's process control system are shown in Table 5. The unit has its own dedicated power supply and control cabinet named 'FLEX-TB'.

A number of pressure and temperature sensors is placed at the in- and outlets of G-20. In particular, PIC-234 monitors and controls the pressure of the steam at the inlet of G-20 via the pressure control valve PV-243. PI-203 and PI-207 monitor the pressure at the product outlet of G-20. TI-204 monitors the temperature at the main outlet of G-20 and has a safety function, shutting down XV-203 and opening XV-207 in case of a temperature rise at the outlet, caused by disturbances inside of G-20. This set-up protects the downstream of G-20 from high temperatures.

Signal	Description	Signal Type		
Flags & Commands from the Research Platform to G-20				
UKH-200	Start/Stop Command to G-20	Digital		
USAK-201	Make-up H2 Ready	Digital		
USH-223	SHS ready for supply Digital			
USH-221	SHS feed to G-20 Running & Ok	Digital		
USH-222	Take over setpoint FIC-223	Digital		
USAL-960	CHW Supply OK	Digital		
USAL-090	HSR Emergency Stop /GWA or BMZ Hardwired	Digital		
FIY-200	HSR Demand to G-20 (dry H2 Supply)	420mA		
USAH-204	Start hydrogen production	Digital		
Flags, Comn	Flags, Commands & Indicators from G-20 to the Research Platform			
HSH-200	Local ON/OFF	Digital		
HSH-202	Remote/Local	Digital		
USH-200	Feedback of G-20 (OK/Fault)	Digital		
USH-201	Need SHS	Digital		
USAL-205	HOTSAFE mode indicator	Digital		
USAL-209	G-20 Emergency Stop	Digital		
FIY-223A	DMW Demand from G-20	420mA		
FI-203	H2 Product flowrate	420mA		
USH-203	Hot Stand-by (SHS reception without electrolysis	Digital		
USH-205	H2 Production running	Digital		

Table 5: Signals from/to SOE Unit G-20



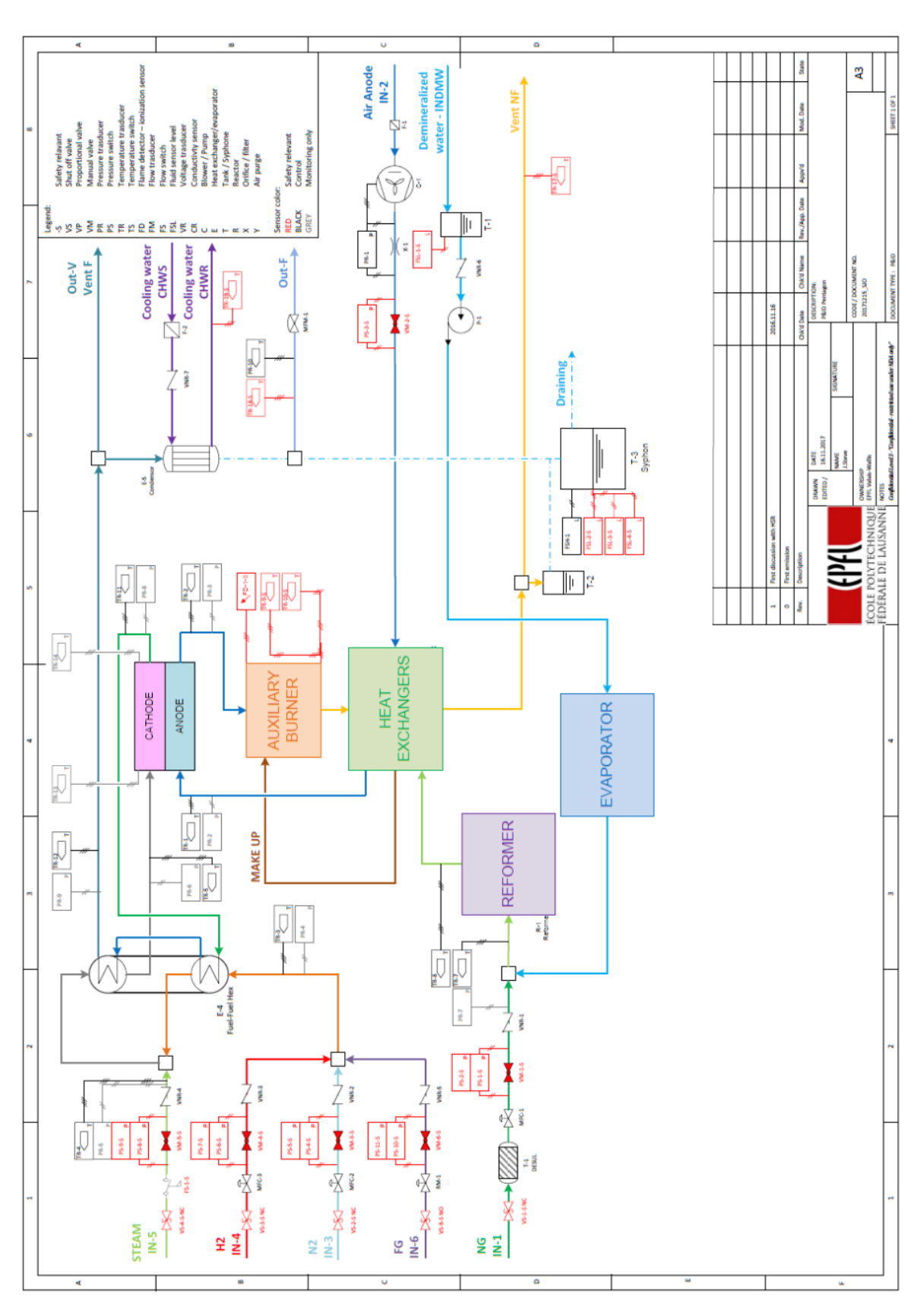


Figure 31: P&ID of the SOE Unit G-20

3.5. WP5: Control

3.5.1.Control of the SOE unit

The entire SOE BoP is controlled through the SOE control rack. The rack contains all the electrical elements requested for safety (diode, relays, ...), power supply, data acquisition and PLC elements. The control rack is based on the usual architecture used for controlling test-benches at the GEM laboratory in Sion. As for the BoP, the rack was modified and adapted to run a full stack in ELECTROLYSIS mode.

The control system of the SOE unit is divided in three parts (i) LabView, (ii) Open Platform Communication server (OPC server), and (iii) PLC. They are shortly described below. Figure 32 shows the structure of the components involved in communication between LabVIEW and the PLC.

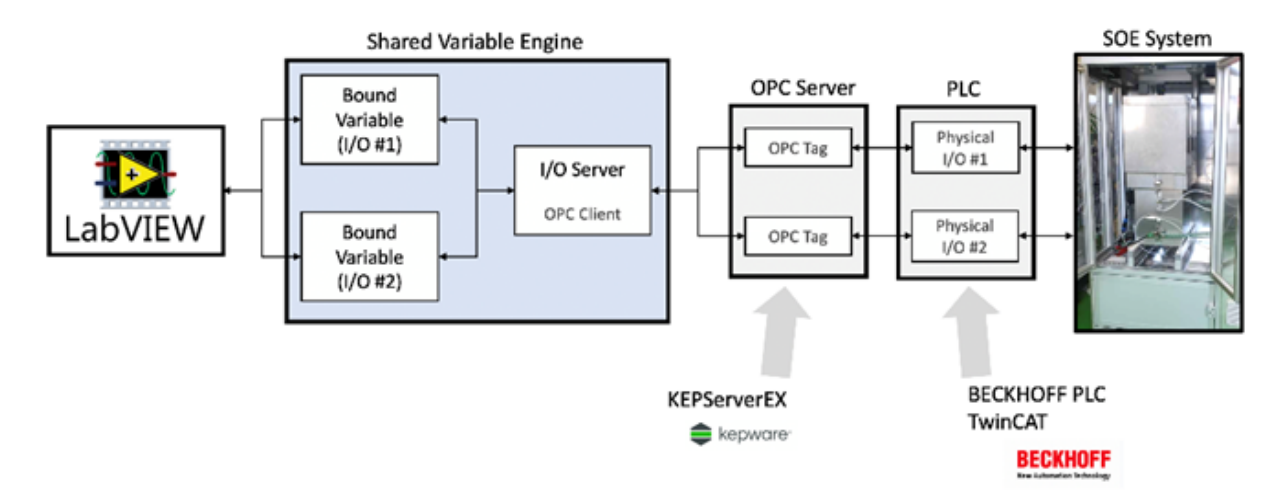


Figure 32: Communication of Labview with the PLC via OPC

The LabVIEW data logging and supervisory control defines shared variables. The shared variables are used to access and pass data among several VIs in a LabVIEW project or across a network. A shared variable can represent a value or an I/O point. With the data logging and supervisory control module, it is possible to log data automatically, add alarming, scaling, and security to the shared variable, and set the shared variable via a program. The data logging supervisory control module provides OPC client I/O servers for communicating with any server implementing the OPC server interface. This allows LabVIEW to communicate with any PLC that is interacting with an OPC server. The OPC client I/O server will list all available OPC servers that are installed and running on a local or network computer.

Labview is also used as a platform for Human-Machine Interface (HMI). It is a user interface to connect the user to the actual system, here the SOE. The LabVIEW HMI allows the user to control the following devices:

- 1. Agilent 34970A: to obtain temperature and pressure measurements quickly, exports the data and allows viewing real-time measurements.
- 2. Bronkhorst and Red-y: mass flow meters and controllers to ensure reliable control of gases that are input and output into the SOE system.
- 3. EA-PSI 9500 Power Supply: to control the current input into the SOE stack.



- 4. KNF Pump SYMDOS 10: controls the amount of water input into the evaporator for steam reforming / generation.
- 5. Shinko DCL33A Controller: for measuring, controlling and maintaining the temperature of different parts, through electric heaters, of the SOE system.

To allow visualizing all variables of the SOE system such as measurements as well as the operation of the listed devices, alarms and modifying the operating conditions, multiple interface tabs are available. To not overload this report, only one tab is presented in Figure 33.

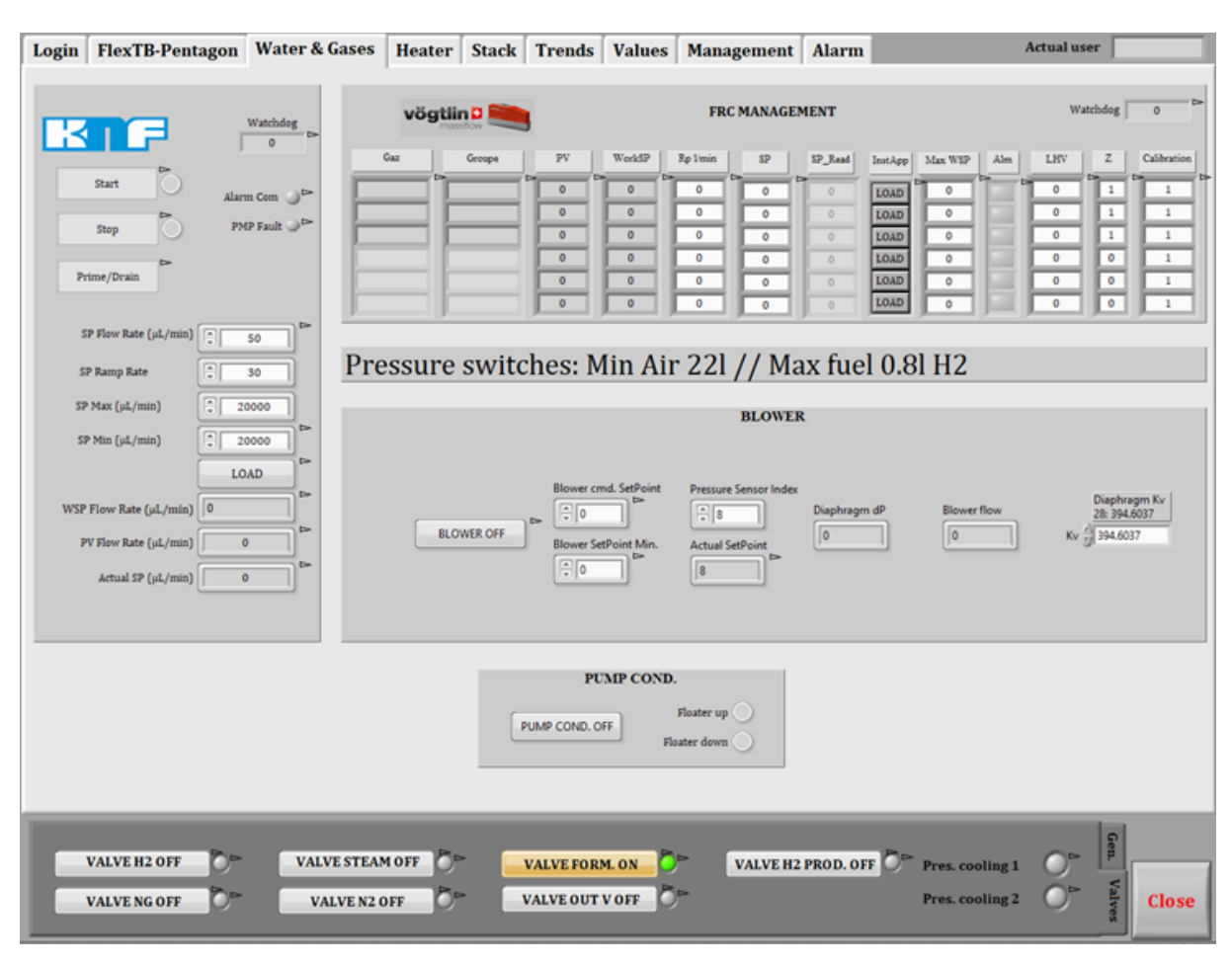


Figure 33: Water & gases Tab on Labview.

OPC is implemented in server-client pairs. The OPC server is a software program that converts the hardware communication protocol used by a PLC into the OPC protocol. The OPC server used, KEPServerEX, permits fast and reliable real-time data exchange and sets safe communication between the PLC control software (Beckhoff TwinCat) and the LabVIEW user interface. It allows the monitoring of the state of the shared variables.

LabVIEW can communicate with any PLC in a variety of ways. OPC defines the standard for communicating real-time plant data between control devices and HMIs. OPC servers are available for virtually all PLCs and programmable automation controllers. KepSERVER is used in order to ensure that the data will be safely sent to the PLC and vice-versa. The interface prevents the SOE system from stopping in case of a malfunction of LabVIEW.

Variables that exchange data between the PLC and the HMI have been created in KepS-ERVER. On this interface, it is possible to assess the quality of the variables as well as its type and value. KepSERVER must be operating in its normal way to guarantee that the communication is not lost. Malfunction of this interface may prevent the user from operating the SOE system from the HMI.

The PLC programming concerns the task of designing and implementing control application. A PLC program consists of a set of instructions that represents the logic to be implemented for specific industrial real-time applications. Once this program is downloaded to the PLC placed in Run mode, the PLC continuously works according to the program. The programming of the PLC controller of the SOE system was performed in order to ensure the following:

- Valves closure in case of any activation of any critical alarm.
- Shutdown of the power supply device in case of malfunction.
- Ensure that forming gas is feeding the system in case of an emergency stop.
- Prevent the user from closing the outlet valves while the inlets are open.
- Safe shutdown of the system in case of emergency.

Here is a non-exhaustive list of issues that must lead to an emergency shutdown:

- Depressurization of the junction box.
- Overtemperature of the burner.
- Disappearance of the burner flame.
- Overtemperature of the air chimney at the outlet of the system.
- Steam temperature out of the acceptable bonds (risk of condensate).
- Failure of the cooling circuit.
- Water level in the condensation box.
- Air, H₂, Steam or Forming gas failure.
- **–** ...

The normal function of this interface is pivotal. It controls the safety protocols implemented to avoid accidents and misuse. Malfunction of this interface prevents the entire system from working. Figure 34 depicts the general block diagram of the TwinCAT PLC programming.



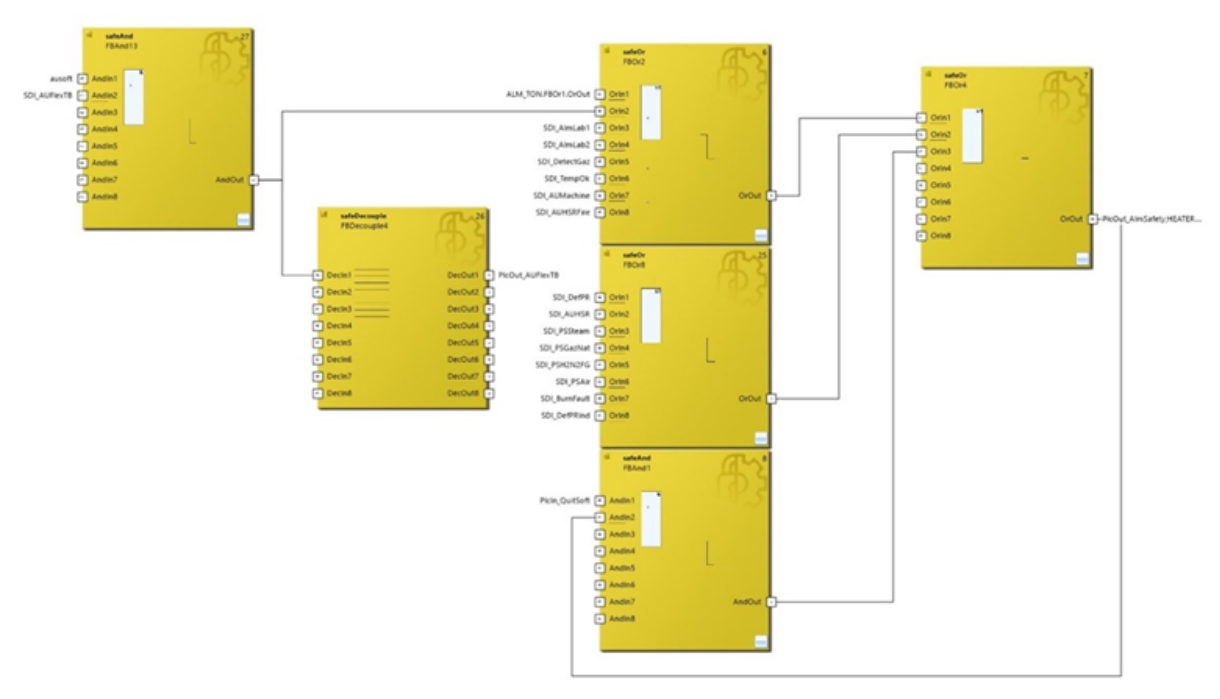


Figure 34: Safety protocols implemented in PLC.

The control of the burner flame is a critical safety aspect of the system. The burner must be secured by a continuous control of the flame presence. If the flame is not detected during startup or if it disappears while the system is in HEATING mode, HOTSAFE mode or HOTSTANDBY mode, the PLC must carry out a series of actions. The burner control methodology is built as the structure presented on Figure 35.

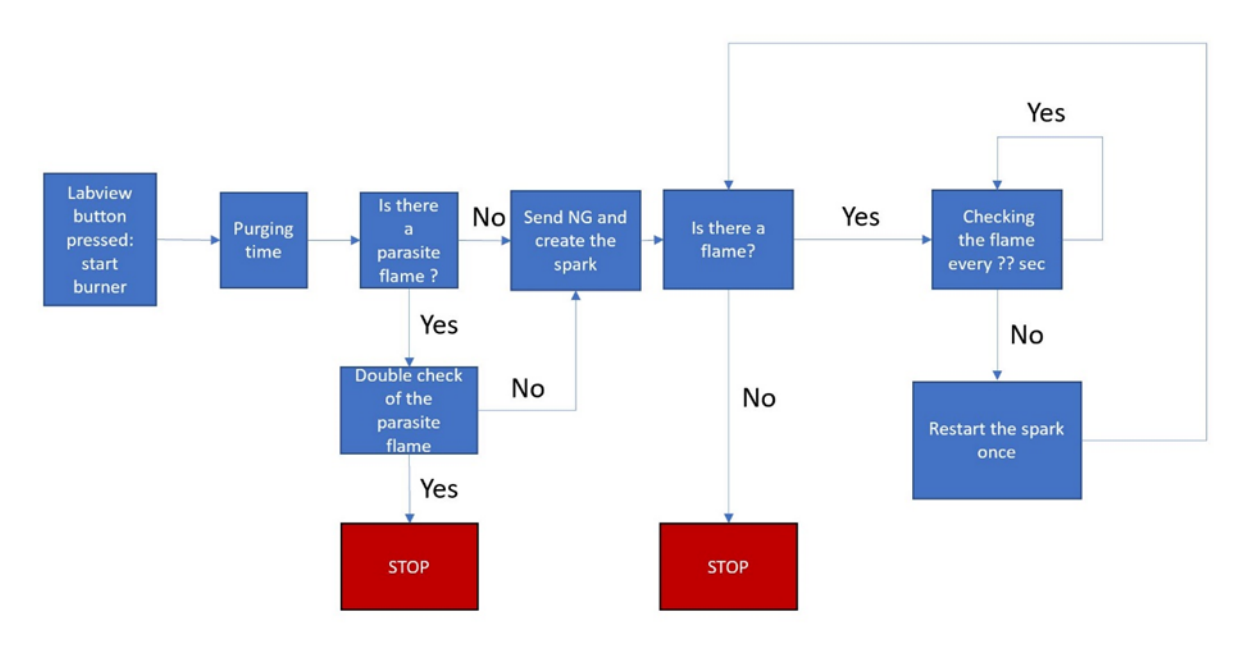


Figure 35: Simplified representation of the burner control methodology.

The detection of the flame is made by analysing the evolution of two temperature measurements placed before and after the burner. Based on the change of those temperatures with time, the creation or the disappearance of the flame is detected. The threshold values determining the appearance or disappearance are critical and must be smartly chosen to avoid unnecessary shutdown or the missing of real burner issues. During the bypass test made in April 2022, a full characterization of the burner has been performed, with multiple "flame starting" and "flame killing". The evolution of the temperatures has been recorded and plotted to determine the right threshold values. Based on these findings, a complete code is implemented in the PLC in order to continuously control the flame presence. More details are presented in the results section.

3.5.2. Control of the methanation plant

The intended industrial character of the demonstration plant has a decisive influence on the choice of the process control system for the methanation plant. The project partner Emerson is specialised in large-scale chemical plants, which is the reason to select their systems and solutions for the control system in this project. The DELTA-V system with its possibility of variable I/O interfaces through the so-called "CHARMs" seemed particularly attractive for this project, as these can be exchanged through other types of I/O cards.

 $\hfill \Box$ A schematic overview of Research Platform's PLC is shown in the Figure in appendix 1A.3.

□ PLC description

The logic of the PLC is programmed in the DeltaV Explorer. This is where the inputs of the charms are picked, the plant areas are determined, logical sequences are programmed, and interlocks and permissions are defined. In addition, the integration of further communication channels (Modbus TCP/RTU) as well as the settings of the data storage in the so-called "continuous historian" of the DeltaV system are carried out.

The HMI is set up in the "Operator Picture" software. The historian software is based on Visual Basic and, with the appropriate knowledge, there are no limits to the visual display of data and system statuses. However, the basic functions of Operator Picture are not always trivial.

Thanks to the block design of DeltaV, the standard blocks are already equipped with interlock as well as alarm and information elements. These are already handled in the industrial standard by the alarm monitoring integrated in DeltaV and the operator is informed according to the prioritisations. The interlocks were implemented somewhat more specifically than the software provides. The logic behind the interlocks is therefore more difficult to interpret at first glance and is documented by our plant engineer in an external list. These interlocks can be delayed, deactivated, or activated depending on the system status.

☐ Communication with other systems

Communication with external devices is generally implemented via the industry standard Modbus. There are several different types of Modbus. Unfortunately, not all devices are on the same standard, which makes various conversion devices necessary. Chiller G-96, Dewpoint sensors as well as the gas warning system run on Modbus RTU (serial cable), while the power meters and PEM electrolyser G-10 communicate via Modbus TCP (RJ45 cable).

In addition, prototypes of gas composition measuring devices from MEMS AG are installed on the plant. This prototype is only equipped with a CAN bus, which is why an additional



converter from the two different bus systems CAN and Modbus is necessary. This communication is not always stable, either on the prototype of the measuring device itself or on the additional conversion.

As already described in section 3.5.1 and Table 5, there is also a communication with the Flex TB. This is not carried out via a bus system, but each individual command or request as well as status respond is connected via a separate wire. Status signals are implemented as digital IO and setpoints and actual values as 4 mA to 20 mA analogue signals. More information about the Controlling of the coupling will be given in section 3.5.3 on page 46.

Data acquisition

Basically, all signals that exist within the PLC can be written to a professional database called "Continuous Historian" up to a maximum number of 512 signals (depending on the selected licence). The way in which the data of the individual signals is written can be configured individually. For example, a write command can be given when a certain deviation from the previous value has occurred and/or a time-related quantity can be specified as a trigger. This data is written to a database in the most space-saving way possible and archived accordingly. They can also be visualised later in a viewer. All other data that has not been stored in the Historian database is no longer available.

□ Safety

It emerged from the HAZOP analysis that the methanation plant should not be executed autonomously. For this reason, only isolated sections that are not directly related to safety have been incorporated into automatic processes and controllers. This means that the plant must be controlled by an operator. This control turns out to be quite challenging, especially since, as already mentioned, the cause of occurring interlocks cannot be easily identified. In some cases, it takes several attempts to switch from HOTSTANDBY mode to PRODUCTION mode without all the interlocks disturbing the process.

Furthermore, the fact that conditional alarming is hardly ever used is an additional stress factor for the plant operator. At any given time during plant operation, many alarms can pop up with no relevance in the respective phase of plant operation. These false alarms are disturbing the manual operation of the plant, especially as the operator tends to become numb to the alarms and might oversee a real alarm.

The layout is certainly equipped with enough interlocks so that operation is always safe. In case of unsafe operation, there is the possibility of an emergency stop. Emergency stops can be caused, for example, by the concentration of certain gases in the laboratory being higher than the allowable threshold level (hydrogen H₂, methane CH₄, carbon monoxide CO, carbon dioxide CO₂) or the activation of a fire alarm. Furthermore, stop buttons for manual emergency activation are distributed throughout the entire facility.

☐ Control strategy of the Methanation plant

There are two main aspects that are central to the control strategy of the Research Platform's system:

First, it is elementary that the stoichiometric ratio between hydrogen H₂ and carbon dioxide CO₂, which can be adjusted via the alpha value, is maintained. This is also the case when different compositions are added to the feed via an active recycle stream. This regulation is carried out by the control system based on the composition in the recycle (measuring point scanned by the mass spectrometer) and the quantity that is fed back.

It then adjusts the amount of carbon dioxide CO₂ supplied externally (gas cylinders or the DAC). This means that the amount of hydrogen fed into the system remains constant.

The second important parameter is the maintenance of the SNG quality, so that an injection into the natural gas network or the CNG filling station is not disturbed. This depends on good process quality, i.e. that the temperature in the reactor does not get too high and the pressure does not get too low, and also that the pressure difference across the separation membrane is sufficient. All three process parameters are determined by the operator and entered as fixed values. The system then regulates the corresponding process variables independently.

In addition, there are smaller programming's, such as the control and discharge of the condensate, the cooling water supply through the chiller, the hydrogen production of the PEM or also the preheating of the feed or the steam generation.

3.5.3. Control of the Coupling: "SOE into the Methanation Plant"

The coupling methodology of the unit G-20 unit with the methanation plant must be carefully controlled and monitored to avoid conditions that could damage parts of the installation. To do so, different communications signals have been implemented, as presented on Table 5. Those signals are exchanged between EPFL's SOE module and OST's Research Platform to allow a safe and controlled coupling.

The signal exchange methodology is schematized on Figure 36. First, the G-20 must wait for two signals from OST before being heated. The two signals confirm that cooling water is delivered to the G-20 and that EPFL can start the heating. Afterwards, the G-20 is heated. When the temperature reaches 650 °C, it enters the HOTSAFE Mode and sends the related signal to OST. The G-20 has then to wait for steam and H₂, which are delivered by OST. Once EPFL receives the confirmation that OST is ready to deliver both, EPFL starts to consume H2 and asks for the control of the steam delivery. The delivery of steam is made through a pump controlled by OST but EPFL can take the control of it. Once EPFL has taken the control of the pump and OST confirms that steam is well delivered to the G-20, the G-20 unit enters the HOTSTANDBY Mode and sends the related signal to OST. In that moment, the G-20 unit is ready to start the electrolysis, but it must first receive a signal from OST saying how much hydrogen they need. As soon as this information is received, EPFL adapts the steam and supplies hydrogen required to produce the requested amount of gas. Whenever EPFL is ready, the G-20 starts the production of hydrogen and enters the ELECTROLYSIS Mode. The hydrogen is however not yet delivered to OST but sent to the vent. It allows EPFL to carefully ensure that the stack is working properly as well as allowing OST to prepare the methanation plant to receive the produced hydrogen. OST must send a final signal confirming that its research platform is ready to receive the produced hydrogen. Once this signal is received, the hydrogen is sent to the methanation plant, and the coupling is validated. The G-20 will then monitor the amount of H₂ produced and send the value to OST.

Delivering the produced hydrogen from the vent to the methanation plant is the most critical part of the coupling. Based on the first results, this part of the methodology has been modified a couple of times through the different testing weeks in order to reach the most efficient and safe coupling method. More details are presented in the "Results and discussions" chapter.



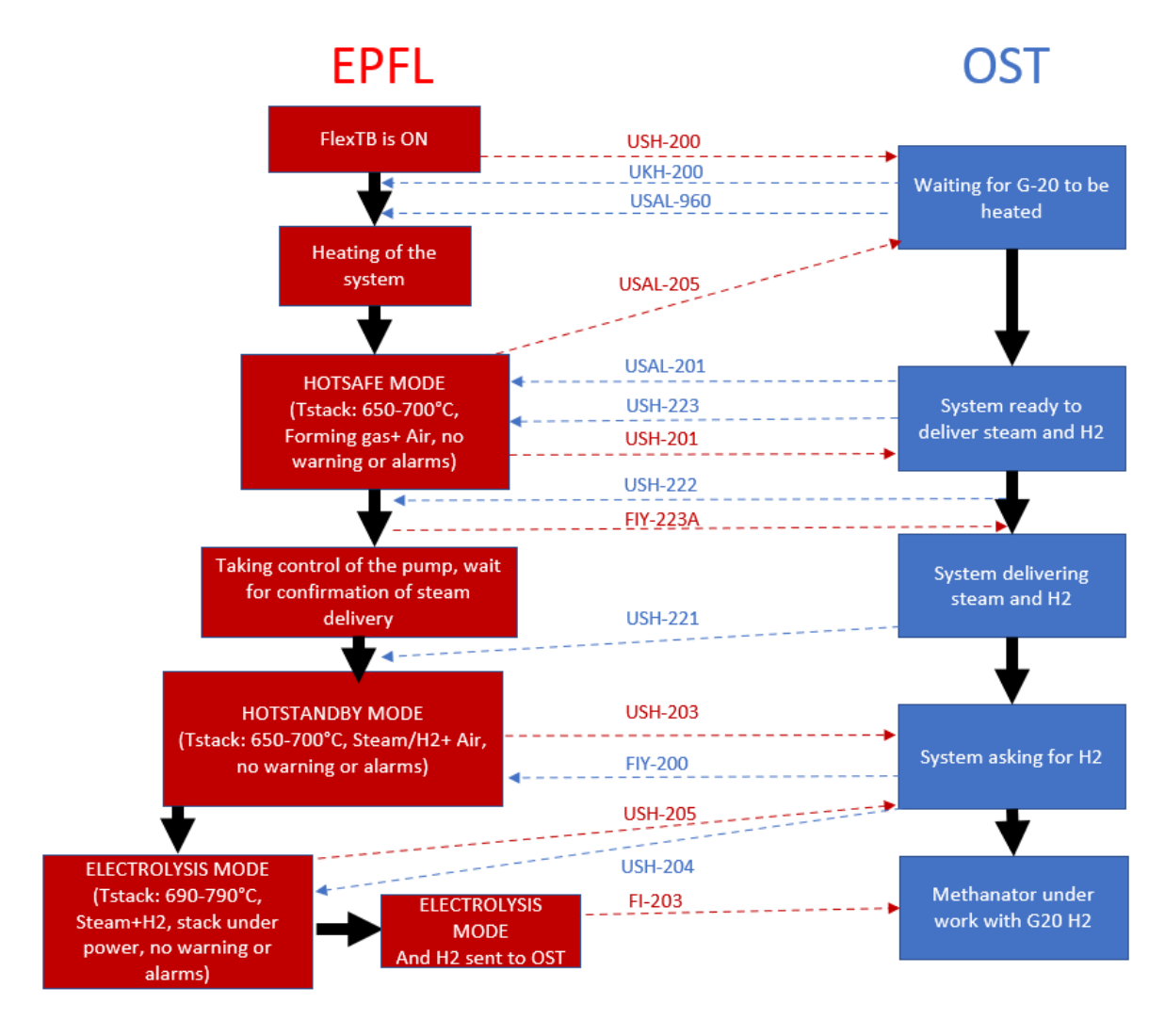


Figure 36: Coupling methodology with signal exchange between EPFL and OST. Red signals are controlled by EPFL, blue signals are controlled by OST. Each signal is described on Table 5.

4. Results and Discussions

4.1. WP1: Methanation

4.1.1. Operation of the Polytropic Methanation Reactor at OST plant

In 2019, the reactor has already been tested at two different H₂ flowrates:

- 1. 0.180 kg/h which is the full load achievable with the PEM electrolyser (e.g. in experiment 20191107)
- 2. 0.300 kg/h, which is close to the full load achievable if both electrolysers were on-line. (e.g. in experiment 20191114)

Data on the second experiment are (mostly) presented because conditions in the reactor were more constant than in the first experiment. In the series of preceding experiments, testing of several sub-systems was performed and large disturbances were introduced in operation (notably system pressure) owing to a too large gas flow being used at the sampling points (see Figure 37). This was corrected in the later experiments by using a much smaller sampling gas flow.

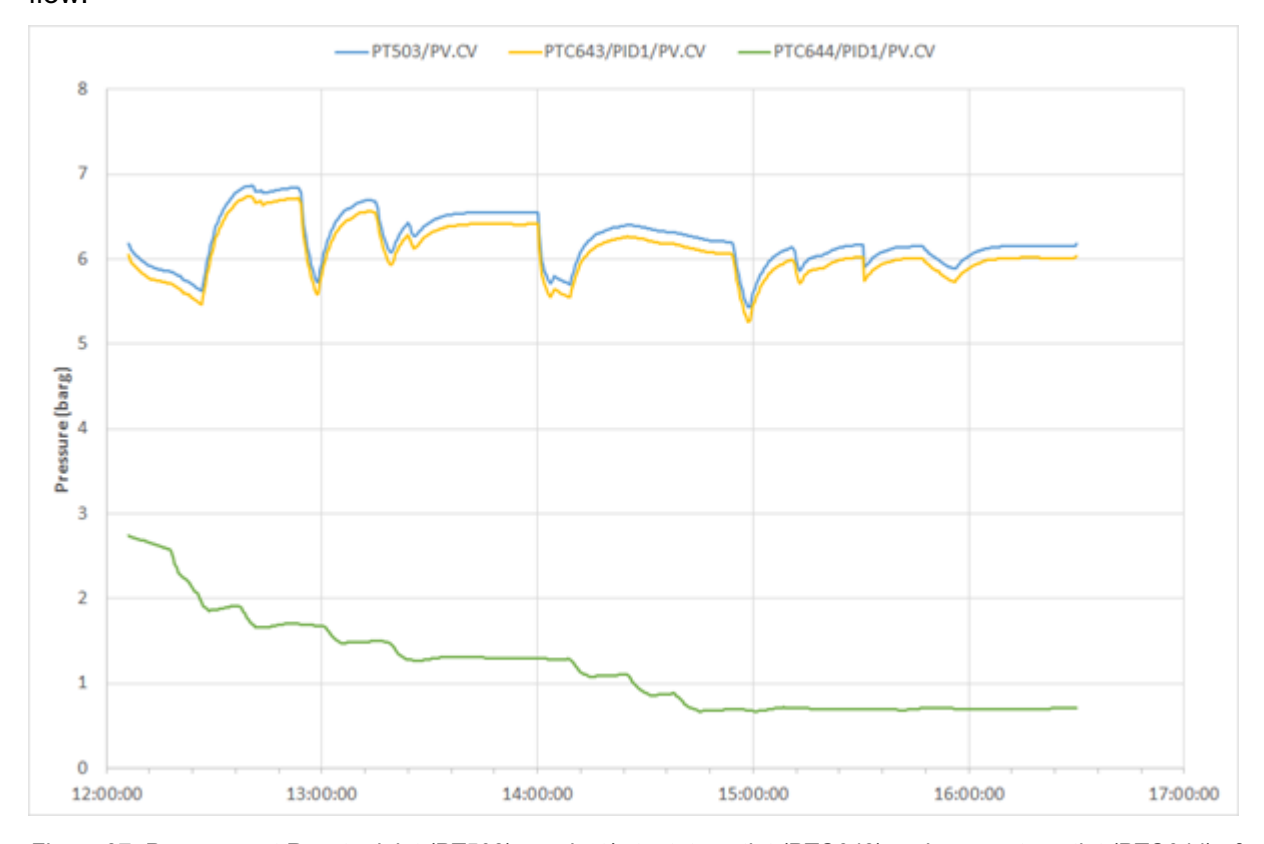


Figure 37: Pressures at Reactor inlet (PT503), product/retentate outlet (PTC643) and permeate outlet (PTC644) of Membrane Separator

Before the SOE unit was installed, the hydrogen exceeding the production rate of the PEM electrolyser is sourced from bottles. The carbon dioxide is sourced from bottles. The total CO₂



flowrate is automatically adjusted based on the total hydrogen being fed to the reactor based on the stoichiometry of the methanation reactor. To avoid the formation of carbon on the catalyst, an excess of hydrogen is used ("Alfa"). The CO_2 flow can be split and fed either mixed with the hydrogen into the first catalyst bed ("top" feed point) or in to a second injection two point located approximately at 1/3 of the total length of the apparatus ("bottom" feed point). Thus, a split ratio ("Beta" = mass flow to top / total CO_2 feed) is used primarily to control the hotspot temperature in the reactor.

From the preliminary experiments in August, we retained that an excess of approximately 2 % (mol/mol) was achievable and a split ratio of approximately 30/70 (top / bottom), keeping the maximum catalyst hotspot temperature below 650 °C in either catalyst bed. For experiment 20191114 Figure 38 shows the feed flowrates and Figure 39 shows the evolution of the temperatures in the reactor (TT510A to TT510J) as well as the pressure at the reactor's entry (PT503) and its exit (PT513).



Figure 38: Gas feed flowrates during experiment 20191114 and values of the parameters Alfa and Beta. FT443: Hydrogen; FT491 and FT511: CO₂.

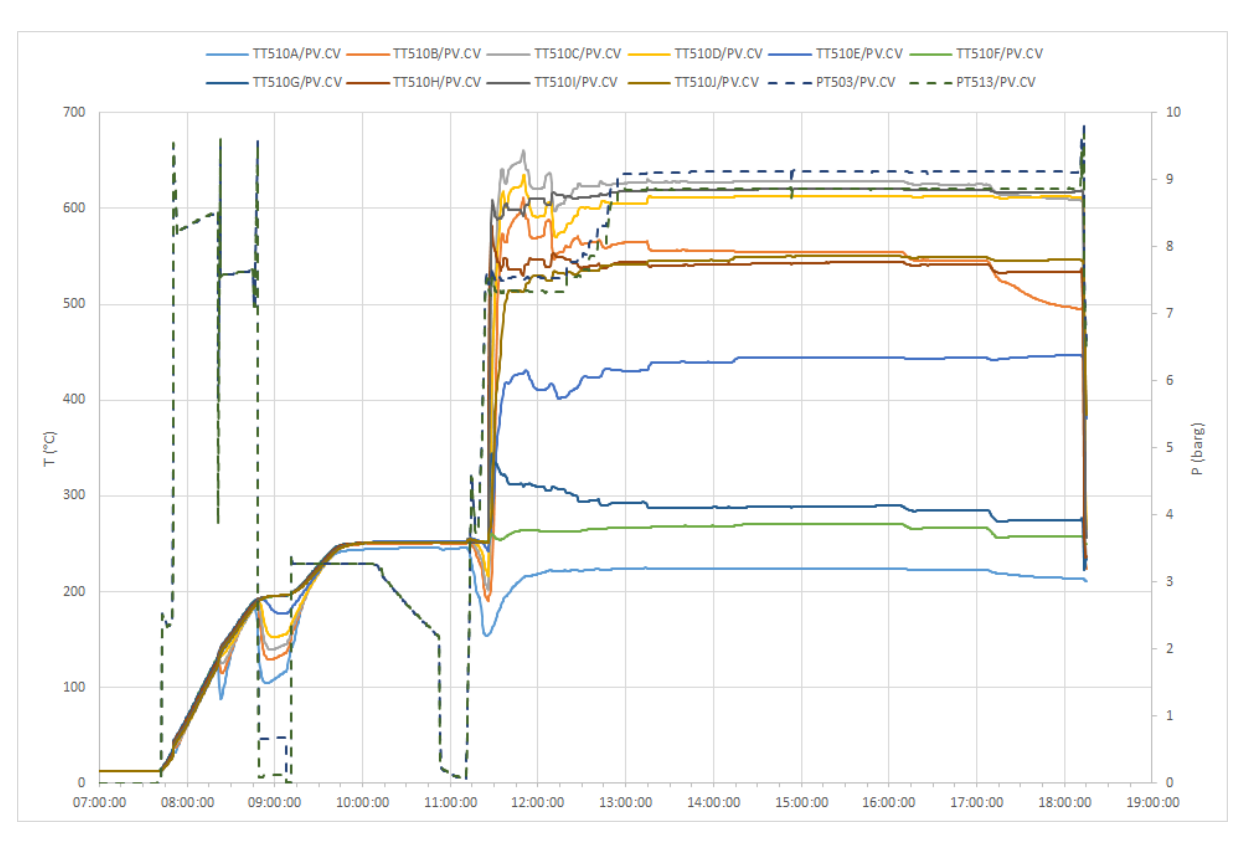


Figure 39: Temperature and pressure evolution during experiment 20191114. Temperatures in the reactor: TT510A to TT510J, pressure at the reactor inlet: PT503, pressure at the reactor exit: PT513.

Figure 38 and Figure 39 show

- The heat-up period of the installation of just under 2 hours, from about 07:45 to 09:45. At 08:45 the reactor was flushed with H₂, resulting in rapid cooling of the catalyst bed and the TO temperature set point was raised to 250 °C. Both actions should have been done earlier, resulting in a less pronounced drop in temperatures between 08:45 and 09:15 and a faster heat-up time.
- the start-up strategy of the reactor: (11:15 to 11:45)
 - o starting from flushing the reactor with pure hydrogen and at low flowrate, a large excess ratio Alfa is set (in this case 80%), along with a 50/50 Split of the CO₂.
 - o The hydrogen flowrate is then successively increased and in parallel, the split ratio is adjusted, allowing more CO₂ to flow towards the bottom injection point.
 - The excess hydrogen is then gradually reduced. All of these modifications are made keeping the max. observed temperature at or below 650 °C.
- As temperatures stabilized around 13:15 the total flowrate of hydrogen is brought to its nominal value. In parallel, the system pressure was gradually set to reach approximately 9 barg at the inlet of the reactor.

After 13:30 no further changes were done on the gas feed to the reactor. Note finally, that from 13:00 onwards the system pressure was kept constant, with the reactor operating with an inlet pressure of 9.12 barg and an outlet pressure of 8.86 barg.





Figure 40: Thermal oil (TO) data and steam generation rate during experiment 20191114.

Figure 40 shows data on the TO circuit. The TO temperatures of this medium at the inlet (TT703) and outlet (TT701) of the reactor's jacket are shown, as well as their difference over the reactor (DT700 = Outlet-Inlet, shown on a 100x scale). The Flowrate of TO (FT703) is also displayed, as well as the power uptake of the thermostat (Power G-70, which covers the energy consumed by both heating and pumping of the TO, plus local control) and finally the steam flowrate (FT223, on a 100x scale).

During heat-up and before the reaction is started, DT700 is negative (-0.5 °C falling to around -0.75 °C) and some 3.7 kW are consumed to heat up the reactor. When the reactor is idle without gas flow (from ca. 10:00 to shortly before 11:00), the temperatures remain constant and a lower power uptake (ca. 2.0 kW to 2.2 kW) is measured. As the reaction is stared (around 11:30), a drastic shift occurs, with the temperature difference becoming positive (between +0.5 °C and 0.75 °C) and the power uptake by the thermostat falling to 650 W.

When steam production is started around 13:30, another change occurs as the thermostat starts compensating some of the energy consumed by the steam generator. The power uptake by G-70 increases and stabilizes at different levels as the steam flow rate is increased.

At 14:15 final changes are made before allowing the system to stabilize: the steam generation rate is raised to a value of 3.5 kg/h and the TO flowrate is drastically reduced. This last change was enacted as the temperature difference of the TO was very small. As a consequence, DT700 raises from ca. 0.5 °C to about 2 °C.

In the experiment discussed so far, the operating parameters of the TO circuit where changed, notably the set point of the TO temperature was first set at 250 °C and changed around 16:15 to 245 °C and finally to 235 °C after 17:00. The objective of these changes was to reduce the

heat contributed by the thermostat, and the corresponding curve shows this was indeed happening: the power consumption falls from an average of 2.82 kW (14:30-16:00) to 2.72 kW (16:30-17:00) and then to 2.55 kW (17:20-18:00). At the same time, the temperature difference over the reactor increases from 1.99°C to 2.07 °C to 2.12 °C for the same three averaging time periods as before.

These averaging periods further represent three steady state situations for the complete system, for which some additional interesting results in terms of the reactor's temperature profiles are shown in Figure 41. This figure also shows similar data for the experiment mentioned earlier with a hydrogen feed rate of 0.18 kg/h. The profiles remain virtually unchanged in experiment 20191114. Only a slightly lower temperature in the region between the catalyst beds (between 400 mm and 600 mm length) and at the reactor outlet can be observed. A difference is observed between these results and those of experiment 20191107, where the hotspot temperatures are slightly higher at the top and lower at the bottom of the reactor. This is a consequence of the slightly different split ratio of 35:65 in the latter experiment. More CO₂ means more conversion of H₂ and so more heat being released. It is interesting to see that an almost doubling of the H₂ flowrate (and thus of the heat being generated in the reactor!) has virtually no impact on the hotspot temperatures.

Finally, the gas composition at sampling point 3 (raw gas from reactor, dried) is shown in Figure 42. The gas composition remained unchanged throughout the experiment. It should be noted though that this data is more discrete in nature as it was collected at different points during the experiment, not continuously.

During the experiment discussed thus far, the reactor showed an excellent chemical conversion rate of 98.0% (based on H_2). The heat released by reaction was calculated to be - 1.755 kW based on the measured gas composition and gas flowrates.

Based on the data from the thermal oil circuit, the heat uptake by this medium was only 1.318 kW. This value should correspond to the previously mentioned heat released by the reaction plus heat losses. This difference is calculated in considering the very small temperature difference of the TO flowing in and out of the reactor. A quick calculation shows that already 0.65 °C difference could explain the observed discrepancy. Consequently, future experiments need to be carried out at lower TO flowrates to increase the temperature gap of this medium and allow for a more precise calculation.

Furthermore, the calculations so far do not include CO₂ lost to condensate, which needs to be taken into account for correct mass and energy balances of the reactor.

A very positive result is the temperature control that could be achieved in the reactor. The observed temperature hotspots could be kept below the maximum allowable catalyst temperature of 700 °C. It is also observed that the temperatures respond to comparably small changes in operation conditions, e.g. the increase of 5 % of the CO₂ flow to the top inlet between the experiments shown so far. This also means, that working with the reactor in a closed recycling loop requires good knowledge of the composition of the recycled gas stream and its flowrate, if an excess of hydrogen in the feed is to be avoided.



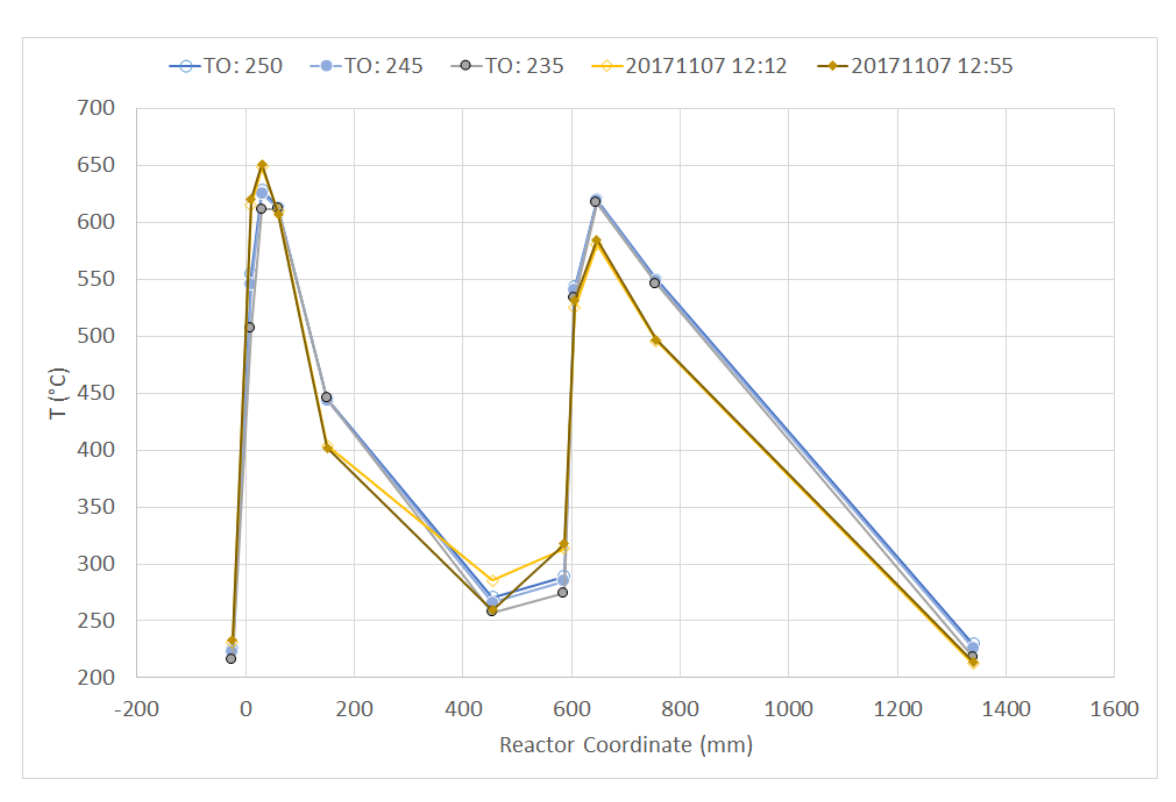


Figure 41: Temperature profiles in the reactor in experiments 20191114 (round symbols, blue/grey at different TO temperature setpoints) and 20191107 (diamonds, yellow/brown, at tow steady state situations in the experiment)

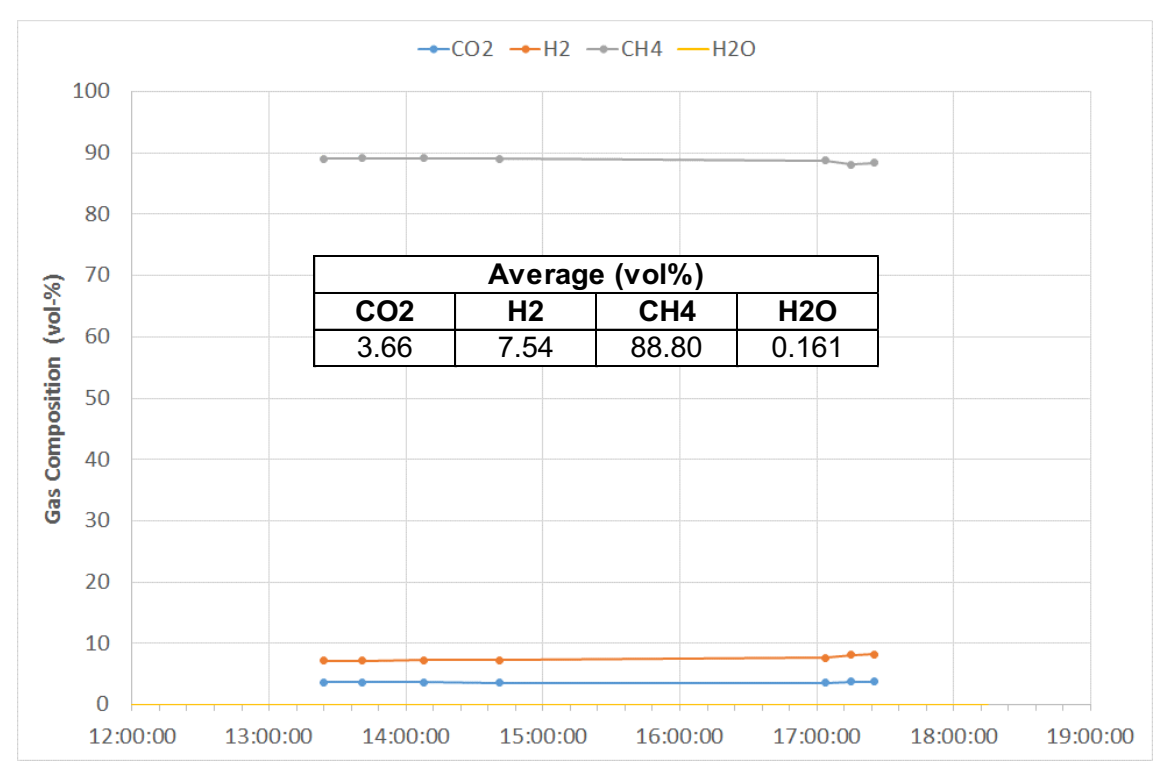


Figure 42: Gas composition in experiment 20191114 at Sampling Point SAP-3

4.1.2. Evaporating water-cooled methanation reactor at EPFL laboratory

A parametric study of CO_2 methanation was conducted. A ratio of 3.85 +/- 0.05 CO_2 per H_2 was maintained while the following variables were varied to identify their effects on the conversion and temperature profile:

- (1) Reactant flow rate
- (2) Reaction pressure
- (3) Cooling system pressure
- (4) CO₂ injected in the second injector instead of the first

(1) - Reactant flow rate

The operation can be extended slightly as done in the following experiment where the flow rate of H_2 was varied from 18 NL/min to 48 NL/min. As presented in Figure 43, an increase in the flow rate of reactant increased the convection and thus required more reaction before the hotspot developed. Regarding the H_2 conversion, at lower flow rates, the trend is dominated by the increased requirement in volume to reach the same conversion. At higher flow rates, the reaction might have been quenched by the second inert region (where the second injection port is used), and thus, as the hot-spot moved towards the outlet, the quench occurred at lower conversion.

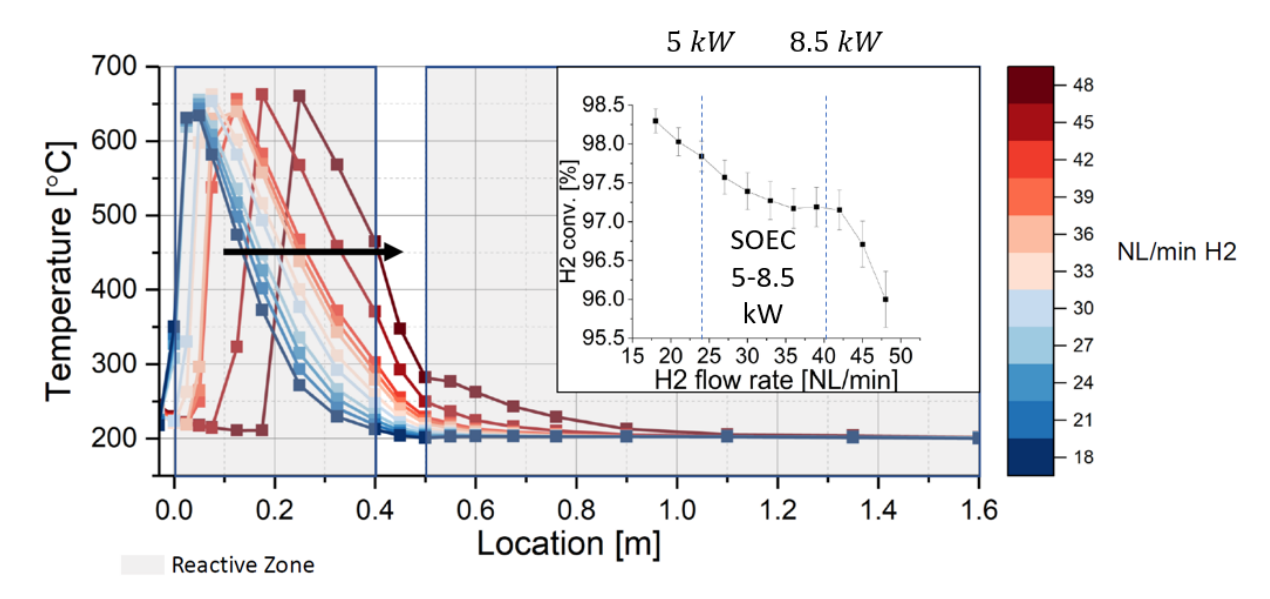


Figure 43: Effect of the reactant flow rate on the temperature profile along the reactor and the hydrogen, reprinted with permission from [1].



(2) - Reaction pressure

Varying the reaction pressure increased the height of the hot-spot by increasing the reaction's kinetics which moved the conversion and temperature at which the rate of reaction and the cooling equates (at the peak) towards higher conversion and higher temperatures. An increase in the conversion was also measured as the kinetics was maintained higher throughout the low temperature "plateau" of the second reaction zone. These effects are shown on Figure 44 for two hydrogen flow rates: 24 NL/min and 36 NL/min.

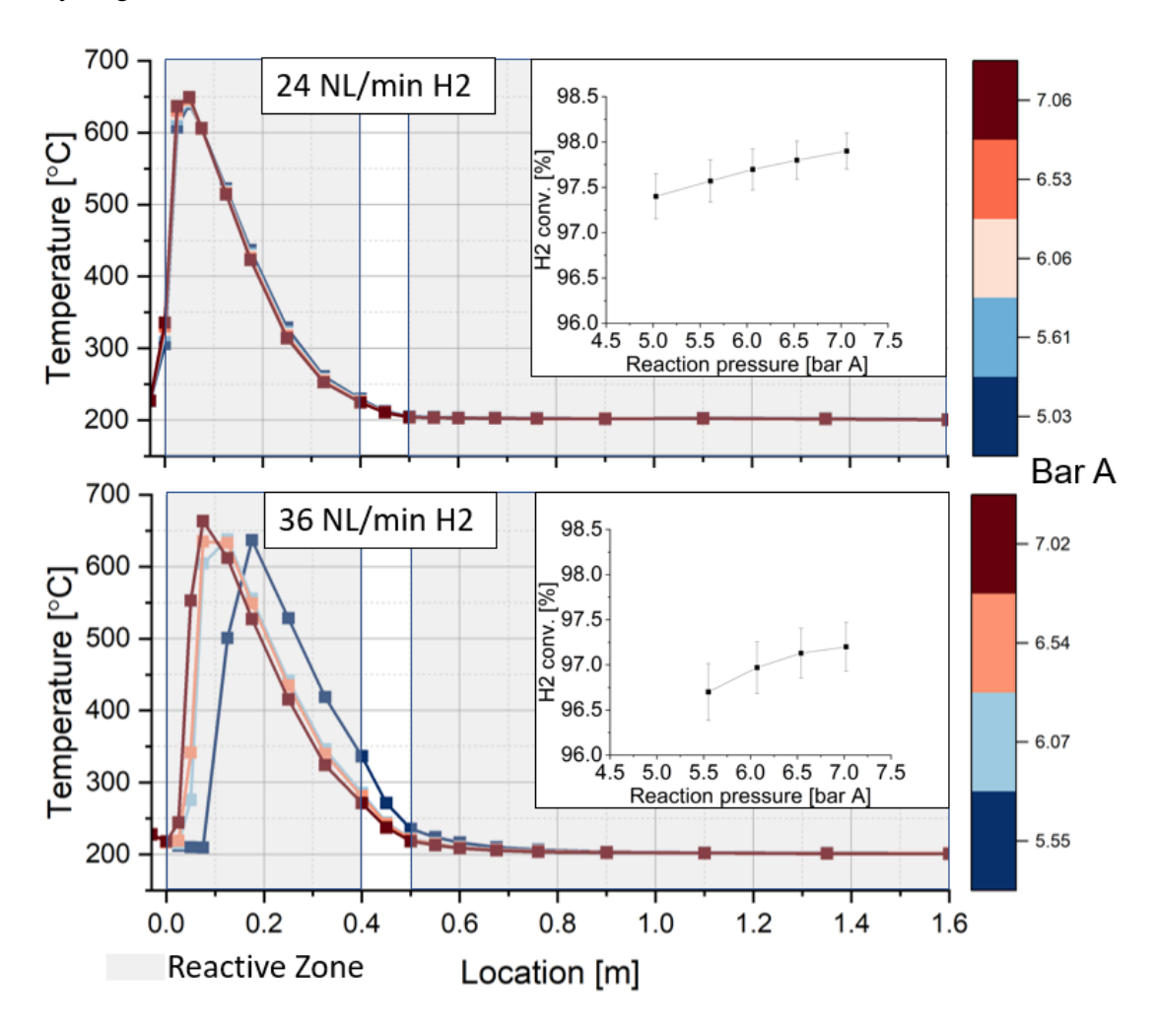


Figure 44: Effect of the reaction pressure on the temperature profile along the reactor and the hydrogen conversion, reprinted with permission from [1].

(3)- Cooling system pressure

The cooling system pressure sets the minimum temperature inside the reactor (at the outlet) through the saturation temperature of the evaporating water. The temperature measurements for 24 NL/min and 36 NL/min presented in Figure 45 indicate an increase in pressure results in a higher temperature of the "plateau" of the second reaction zone. Therefore, the reaction is maintained at a slightly higher level throughout the second zone resulting in a higher conversion at the outlet.

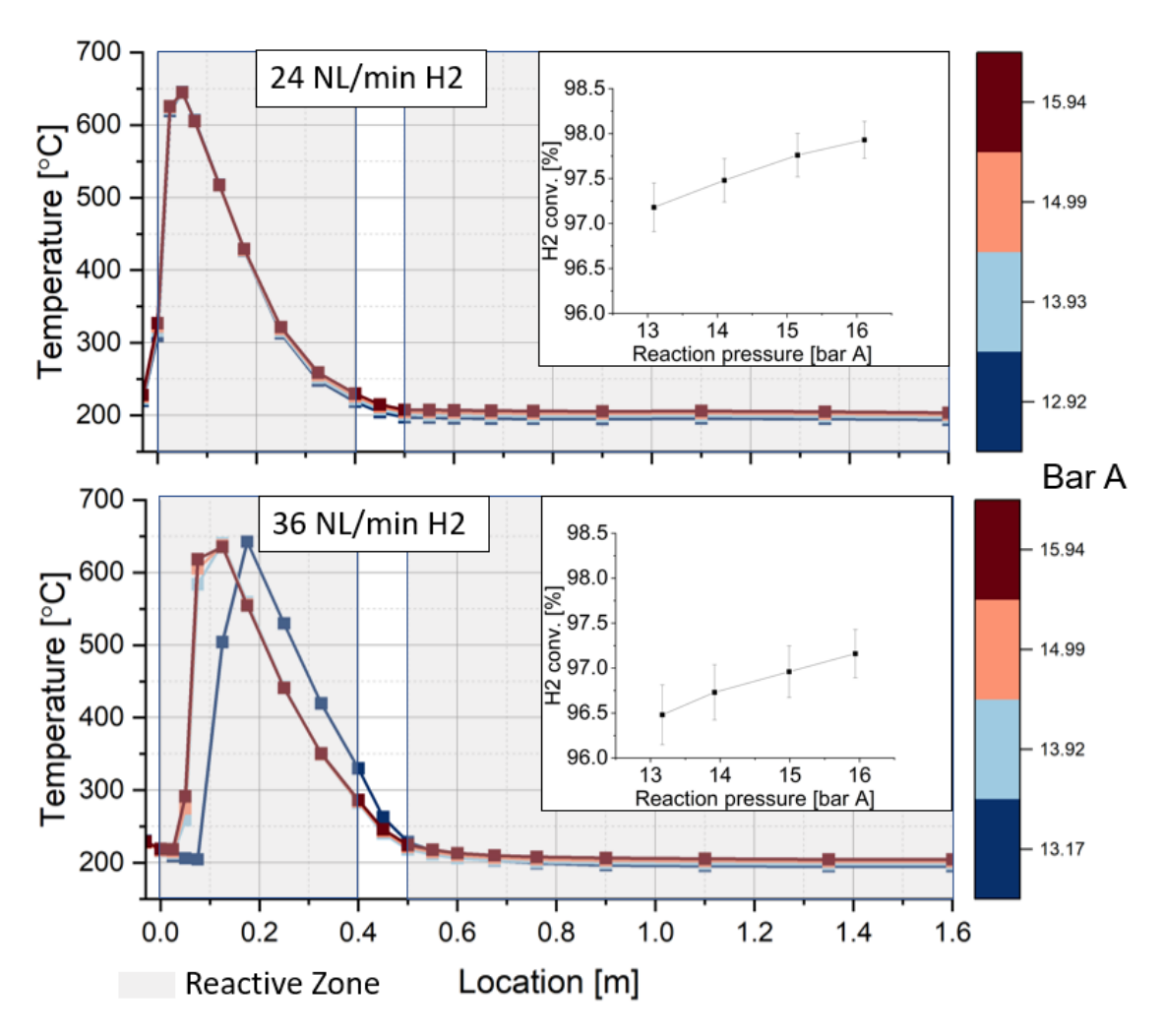


Figure 45: Effect of the cooling system pressure on the temperature profile along the reactor and the hydrogen conversion, reprinted with permission from [1].

(4) - Second Injection

The quantity of CO₂ taken from the first injection to be injected in the second port was varied for two hydrogen flow rates with the results shown on Figure 46. The use of a lower quantity of CO₂ in the first injection should result in a lower first hot-spot which is the case for the 24 NL/min but is not fully captured in the 36 NL/min case due to the distance between temperature measurements. As a greater quantity of CO₂ is injected in the second zone, a second



hot-spot is developed. Due to the larger convection, the second hot-spot is developed at higher quantities of CO₂ injected in the second port for the 36 NL/min case.

The trend in the conversion starts with a decrease in its measurement due to the lower reaction level in the second zone as the temperatures are still low. However, the development of a second hot-spot increases the conversion to its original level. The higher conversion for the 2 NL/min to 3 NL/min CO₂ compared to the 0 NL/min CO₂ might be a result of the varying error of the mass flow meter which alters the CO₂ to H₂ ratio.

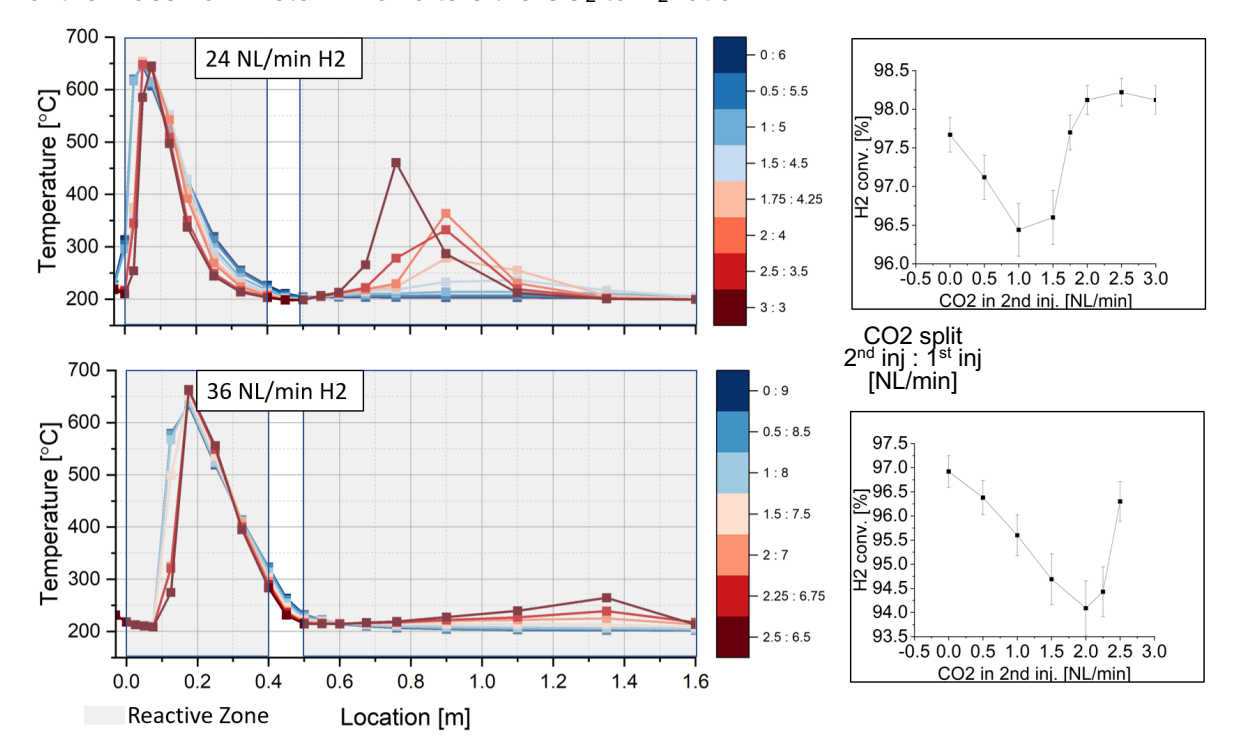


Figure 46: Effect of dividing the CO₂ injected through both ports on the temperature profile along the reactor and the hydrogen conversion, reprinted with permission from [1].

4.1.3. Simulation of Methanation

The description and results of the simulation code are taken from Aubin et al [1].

Model Description

The purpose of the reactor simulation is to capture the general trend of the reactor's state while minimizing the simulation time, and consequently, the level of detail can be selected. Schlereth and Hinrichsen [21] simulated an externally cooled methanation reactor using: (1) a 1D pseudo-homogeneous plug flow reactor (PFR) model, (2) two 2D pseudo-homogeneous models using the α -wall method and the Λ (r) method as presented in Tsotsas [26], and (3) a 1D heterogeneous PFR model. In the comparison between the 1D PFR model and the 2D models, the hot spot in the 1D model was lower than in the 2D models as the PFR uses an average radial temperature. However, in the comparison between the homogeneous and heterogeneous 1D models, the maximum temperature differed significantly depending on the operating conditions. Similarly, Kiewidt and Thoming [14] compared a 1D homogeneous PFR to a 1D heterogeneous PFR model and showed the simulated temperatures and yields do not have a

significant difference between the two models under a GHSV of 6000 h⁻¹. Therefore, the models presented below solve for the temperature profiles and yield using a 1D pseudo-homogeneous PFR model.

Continuity Equations

$$\frac{d\dot{F}_{\rm i}}{dz} = x_{\rm i} \dot{N}_{\rm CO_2}, \qquad {\rm i} = {\rm H_2, CO_2, CH_4, H_2O} \ ,$$

Equation 4:1 - Mass conservation

$$\frac{dP}{dz} = \frac{u(z)^2 \rho_{\rm g}}{d_{\rm p}} \left[\frac{K_1 A_{\rm w}^2}{Re_{\rm d_p}} \left(\frac{(1-\psi_{\rm b})^2}{\psi_{\rm b}^3} \right) + \frac{A_{\rm w}}{B_{\rm w}} \left(\frac{1-\psi_{\rm b}}{\psi_{\rm b}^3} \right) \right],$$

Equation 4:2 – Momentum conservation

$$\dot{m}_{\rm g}C_{\rm p,g}\frac{dT}{dz} = -\Delta H_{\rm R}\dot{N}_{\rm CO_2} + U(T - T_{\rm cw}) ,$$

Equation 4:3 - Energy conservation

where $\dot{F}_{\rm i}$ is the molar flowrate, x is the stochiometric coefficient, $\dot{N}_{\rm CO_2}$ is the extent of the methanation reaction, P is the pressure, u(z) is the superficial velocity, $\rho_{\rm g}$ is the density of the gas, $d_{\rm p}$ is the pellet's surface equivalent sphere diameter, $Re_{\rm d_p}$ is the Reynolds number based on the pellet's diameter $d_{\rm p}$, $\psi_{\rm b}$ is the bed's porosity, K_1 is the pressure drop coefficient, $A_{\rm w}$ and $B_{\rm w}$ are the wall effect correction terms, $\dot{m}_{\rm g}$ is the mass flowrate, $C_{\rm p,g}$ is the gas's specific heat, T is the homogeneous average temperature, $\Delta H_{\rm R}$ is the heat of reaction, U is the overall heat transfer coefficient relative to the average bed temperature, and $T_{\rm cw}$ is the cooling water temperature.

Kinetic Equations

A multitude of kinetic equations have been developed in literature in the form of either power-law and extended power-law, or Langmuir-Hinshelwood and Langmuir-Hinshelwood-Hougen-Watson (LHHW) equations, with the latter being the most accurate representation of the kinetics. The LHHW type model developed by Koschany et al. [15] is used:

$$r_{\text{CO}_2}^{s} = \frac{k_{\text{CO}_2} p_{\text{H}_2}^{0.5} p_{\text{CO}_2}^{0.5} \left[1 - \frac{p_{\text{CH}_4} p_{\text{H}_2}^2 \text{O}}{p_{\text{CO}_2} p_{\text{H}_2}^4} K_{\text{eq,CO}_2} \right]}{\left(1 + K_{\text{OH}} \frac{p_{\text{H}_2} \text{O}}{p_{\text{H}_2}^2} + K_{\text{H}_2}^{0.5} p_{\text{H}_2}^{0.5} + K_{\text{mix}} p_{\text{CO}_2}^{0.5} \right)^2} ,$$

Equation 4:4 - Surface reaction rate

Where

$$k_{\rm CO_2} = A_{\rm CO_2,ref} \exp \left[-\frac{E_{\rm CO_2}}{R} \left(\frac{1}{T_{\rm ref}} - \frac{1}{T} \right) \right] \; , \label{eq:kco_2}$$

Equation 4:5 - Parametrized Arrhenius equation



$$K_{\rm j} = K_{\rm j,ref} \exp\left[-\frac{\Delta H_{\rm j}}{R} \left(\frac{1}{T_{\rm ref}} - \frac{1}{T}\right)\right], \qquad \rm j = OH, H2, mix$$

Equation 4:6 - Parametrized van't Hoff equation

In the above equations, $r_{\text{CO}_2}^{\mathcal{S}}$ is the surface rate of reaction, the p's are the partial pressures of the various species, k_{CO_2} is the reaction rate coefficient, $K_{\text{eq,CO}_2}$ is the equilibrium coefficient, the K's are the adsorption coefficients, $A_{\text{CO}_2,\text{ref}}$ is the kinetic rate pre-exponential coefficient, E_{CO_2} is the activation energy, R is the universal gas constant, T_{ref} is the reference temperature, and ΔH_{j} is the heat of adsorption of each species j listed.

The $K_{\text{eq,CO}_2}$ is computed based on the change in Gibbs enthalpy, which can be modeled from thermodynamic data and approximated by the fitted temperature-dependent formula from [3].

The surface kinetic rate of reaction is transformed into the observed kinetic rate through effectiveness estimated using Thiele modulus, similar to Kiewidt and Thoming [14], with the relationship between the effectiveness and the Thiele modulus taken as the relationship for the sphere as the sphericity of the pellet is close to 1:

$$\eta = \frac{r_{\text{CO}_2}^o}{r_{\text{CO}_2}^s} = \frac{1}{\Phi} \left(\coth(3\Phi) - \frac{1}{3\Phi} \right),$$

Equation 4:7 - Parametrized van't Hoff equation

$$\Phi^2 = l_{\rm p}^2 \frac{r_{\rm CO_2}^s \rho_{\rm cat}}{C_{\rm CO_2} D_{\rm eff, CO_2}} ,$$

Equation 4:8 - Parametrized van't Hoff equation

where η is the effectiveness, $r_{\text{CO}_2}^o$ is the observed reaction rate, Φ is the Thiele modulus, ρ_{cat} is the catalyst density, $\mathcal{C}_{\text{CO}_2}$ is the carbon dioxide concentration, and $D_{\text{eff,CO}_2}$ is the effective diffusion length carbon dioxide. The Thiele modulus is calculated assuming the diffusion of the carbon dioxide is the limiting factor in this process.

The effective diffusivity $D_{\rm eff,CO_2}$ of the gas mixture is calculated using the Bosanquet formula, as proposed in [14]. The characteristics of the pellet pores and porous structure are expressed by the pellet porosity $\varphi_{\rm p}$ and the tortuosity τ . The effective molecular diffusion coefficient $D_{{\rm mix},i}$ is calculated by the Wilke method, where y_i is the molar fraction and D_{ij} is the binary diffusion coefficient. The Knudsen diffusion coefficient $D_{{\rm K},i}$ derived from the kinetic gas theory is dependent on the pore diameter $d_{{\rm pore}}$, the temperature T and the molecular weight M_i .

$$\frac{1}{D_{\text{eff,i}}} = \frac{\tau}{\varphi_{\text{p}}} \left(\frac{1}{D_{\text{mix,i}}} + \frac{1}{D_{\text{K,i}}} \right) ,$$

Equation 4:9 - Bosanquet formula

$$D_{\text{mix,i}} = \frac{1 - y_i}{\sum_i y_i / D_i ij} ,$$

Equation 4:10 - Wilke method

$$D_{K,i} = \frac{d_{pore}}{3} \sqrt{\frac{8RT}{\pi M_i}}.$$

Equation 4:11 - Knudsen diffusion

The empirical equation from Fuller, Schettler, and Giddings [12] is applied to estimate the binary diffusion coefficients:

$$D_{ij} = 0.00103 \frac{T^{1.75} \left(\frac{1}{M_i} + \frac{1}{M_j}\right)^{0.5}}{P\left[(\sum v_i)^{1/3} + (\sum v_j)^{1/3}\right]^2}.$$

Equation 4:12 – Fuller, Schettler and Giddings method of estimating binary diffusion coefficients.

where v is the diffusion volume of each species.

Pressure Drop

The most common equation used for estimating the pressure drop in a packed bed is the Ergun equation [8]. However, throughout the years, many have presented modifications that consider different shapes, characteristic lengths, size distribution, different bed-to-pellet ratios, and wall effects rather than pellets alone [31]–[17]. With respect to the reactor presented in this paper, the diameter-to-pellet ratio of the reactor signifies that the wall effect might have a non-negligible impact. In addition, the pellets used are cylindrical, but the size does not vary significantly. Consequently, an alternative to the Ergun equation was used, the Eisfeld and Schnitzlein [7] method that includes the wall effect and has its coefficients for cylindrical pellets:

$$A_{\rm w} = 1 + \frac{2}{3\left(\frac{d_{\rm p}}{d_{\rm t}}\right)(1 - \psi_b)}$$

Equation 4:13 - First Ergun coefficient.

$$B_{\rm w} = \left[k_1 \left(\frac{d_{\rm p}}{d_{\rm t}} \right)^2 + k_2 \right] ,$$

Equation 4:14 – Second Ergun coefficient.

where $d_{\rm p}$ is the pellet's surface equivalent spherical diameter, $d_{\rm t}$ is the reactor's diameter, and $k_{\rm 1}$ and $k_{\rm 2}$ are the coefficients for the wall effect correction terms.

Heat Transfer

Similar to the pressure drop, alterations to the typical models are used to capture the impact of the cylindrical pellets. The following equation is presented in Kiewidt and Thoming [14] but with the inclusion of the resistances of the wall and cooling system:

$$\frac{1}{U} = \frac{1}{d_t \pi \alpha_{\text{wall}}} + \frac{d_t}{d_t \pi} \frac{c_f}{\Lambda_{\text{bed}}} + R'_{\text{wall}} + \frac{1}{\alpha_{\text{cw}} \pi d_e} ,$$

Equation 4:15 – Overall heat transfer coefficient.



where $\alpha_{\rm wall}$ is the heat transfer coefficient at the contact between the bed and the wall, $c_{\rm f}$ is the Biot based correction factor, $\Lambda_{\rm bed}$ is the overall effective conductivity of the bed, $R'_{\rm wall}$ is the wall thermal resistance, $\alpha_{\rm cw}$ is the heat transfer coefficient of the cooling system and $d_{\rm e}$ is the inner diameter of the evaporator.

The different variables related to the packed bed are calculated as follows [6], [27], [4], [13]:

$$c_{\rm f} = \frac{1}{6}(Bi + 3)(Bi + 4) ,$$

Equation 4:16 - Biot based correction factor.

$$\alpha_{\rm wall} = \frac{\lambda_{\rm g}}{d_{\rm p}} (1.3 + 5(d_{\rm t}/d_{\rm p}) \lambda_{\rm bed}/\lambda_{\rm g} + 0.19 Re_{\rm d_p}^{0.75} Pr_{\rm g}^{0.33}$$
,

Equation 4:17 - Wall contact heat transfer coefficient.

$$\Lambda_{\rm bed} = \lambda_{\rm bed} + Re_{\rm d_p} Pr_{\rm g}/K_{\rm r} ,$$

Equation 4:18 – Overall heat transfer coefficient of the bed.

where Bi is the Biot number, λ_g is the gas conductivity, λ_{bed} is the bed's conductivity with no flow, Pr_g is the gas's Prandtl number, and K_r is the inverted slope parameter.

The values of K_r and $\lambda_{\rm bed}$ bed are calculated by the method presented in Tsotsas [27] with the modifications presented by Bauer [3], and Yagi and Kunii [32] to account for the cylindrical pellets. While identifying the temperature at the centre of the reactor (T_{cen}), the ratio of the bed's heat transfer coefficient with respect to the bulk temperature is compared to the heat transfer coefficient with respect to the center temperature (U_{cen}):

$$T_{cen} = T_{wall} + \frac{U_{cen}}{II} (T - T_{wall}) ,$$

Equation 4:19 - Central temperature.

where U_{cen} is given by Dixon [6]:

$$T_{cen} = T_{wall} + \frac{U_{cen}}{U} (T - T_{wall}) ,$$

Equation 4:20 – Overall heat transfer coefficients related to the central temperature.

For the heat transfer coefficient (HTC) of the cooling system, Dengler and Addoms [5] proposed that the two-phase heat transfer coefficient be estimated by applying a correction to the liquid only heat transfer coefficient:

$$\frac{\alpha_{\rm tp}}{\alpha_{\rm lo}} = 3.5 \left(\frac{1}{X_{\rm tt}}\right)^{0.5} ,$$

Equation 4:21 - Two-phase HTC by Dengler and Addoms [5].

where $\alpha_{\rm tp}$ and $\alpha_{\rm lo}$ are the two-phase heat transfer coefficient and the liquid-only heat transfer coefficient, respectively, and $X_{\rm tt}$ is the turbulent-turbulent Martinelli factor. This correlation was developed with a limited set of data points and can have large errors [21]. Chen [4] proposed

the heat transfer coefficient of the two-phase mixture be a combination of a convective boiling (α_{cb}) and a nucleate boiling (α_{nb}) HTC:

$$lpha_{
m tp} = lpha_{
m nb} + lpha_{
m cb}$$
 ,
 Equation 4:22 – Two-phase HTC by Chen [4].

where the two components are calculated using a suppression factor on the nucleate boiling HTC and an enhancement factor on a liquid-only HTC to account for the phase change that results in an acceleration of the flow and a diminution of nucleation. Even with re-circulation, the quantity of liquid water sent into the evaporator is such that the flow is in the deep laminar region. Kandlikar and Balasubramanian [13] proposed applying a correction of the liquid-only laminar convection, but the comparison was only performed in mini-channels. Due to the lack of models for the specific conditions of the evaporator, this latter is implemented:

$$\alpha_{\rm lo} = 3.66~\lambda_{\rm cw}~/d_{\rm e}~~,$$
 Equation 4:23 – liquid-only heat transfer coefficient,

$$\alpha_{cb} = 1.136 \ Co^{-0.9} (1-x_{v})^{0.8} + 667.2 \ Bo^{0.7} \ (1-x_{v})^{0.8}$$
 ,
 Equation 4:24 – convective boiling component,

$$\alpha_{nb} = 0.6683 \ Co^{-0.2} (1-x_v)^{0.8} + 1058.0 \ Bo^{0.7} \ (1-x_v)^{0.8} \ ,$$
 Equation 4:25 – nucleate boiling component,

$$lpha_{tp} = max\left(lpha_{cb}, lpha_{nb}
ight)$$
 ,
 Equation 4:26 – two-phase HTC from [13],

where λ_{cw} is the conductivity of the cooling water, Co is the convective number and Bo is the bonding number.

The thermal resistance of the bed is significantly larger than the resistance of the evaporating water pre-dryout, and the latter is avoided with the re-circulation process that ensures a vapor fraction under 40 %. In addition, the wall temperature is not measured in the reactor. Consequently, the validation of the two-phase model, through the comparison of the simulation and the experiment, is limited.

Results of Methanation

Table 6 presents the specifications of the bed and pellets used in the reactor simulation, while Table 7 presents the kinetic constants employed, which differ from the original [15] to make the reaction faster at lower T while limiting the conversion estimation and hot spot temperature.

Variables	Values
Tortuosity [τ]	1.75
Pellet porosity [φ _p]	0.55
Pellet conductivity [λ p]	1.3
Pore diameter [d pore]	22.1E-9 m
Pellet density [ρ թ]	2.6E6 kg/ m ³
Bed porosity [φ _b]	0.4

Table 6: Technical specifications of the bed and pellets used for the simulation, modified from [1].



Constant	Koschany et al. [15]	Values*		
K O _{OH,ref}	0.5	1.5		
K _{H20}	0.44	0.44		
K ⁰ _{mix,ref} 0	0.88	0.88		
Д Н он	2.24E4	2.2E4		
Δ H _{H2}	-6.2E3	-6.2E3		
Δ H _{mix,ref}	-1E4	-1E4		
A CO2,ref	3.46E-4	1.95E-4		
E co2	7.75E4	4.5E4		
* Estimated values used in the simulation				

Table 7: The specifications of the reaction models, transcribed reprinted with permission from [1].

Power Sweep

The results on Figure 47 were simulated with reaction gas and cooling water pressures of 6.85 bara and 14.92 bara, respectively. The dashed lines represent the average radial temperature profile while the solid lines are the central temperatures. A greater flowrate shifts the peaks toward the outlet and both the experimental measurement and simulation agree in the existence of the shift, but the shift in the experimental measurement is significantly greater than the simulation. In addition, in the experiment the hot spot at lower flowrates is closer to the inlet indicating a high reaction rate at a lower temperature, but the larger shift of the start of the exponential rise with increasing flowrate indicates otherwise.

The simulation indicates a decrease in the hot spot with increasing flowrates. As mentioned previously, axial conduction can flatten the hot spot the sharper it is, and thus, the experiment cannot fully invalidate the simulated trend. Depending on the actual composition at the start of the second reactive zone, the increase in temperature in the simulation, at that location, might also indicate the actual reaction rates at lower temperatures must be lower than the simulated one. In the experiment, the temperature profiles fall to the same temperature level at the end of the reactor. In the simulation, the ratio of reaction to cooling over the entire second reaction zone is larger than the actual ratio. This results in a higher outlet temperature as the flowrates increase. As for the conversion measurement, the decrease in conversion with increasing flowrates is greater for the simulation than the experiment. In addition, as mentioned previously, the accelerated drop in conversion for the higher flowrates is due to the quenching of the reaction, indicating a greater impact of temperature over composition. The quenching of the reaction did not occur to the same extent in the simulation as the shift of the hot spot towards the outlet was milder. The lack of heterogeneous 2D temperature profiles might explain the aforementioned discrepancies. However, to assess the extent, the actual kinetic model of the pellets is required.

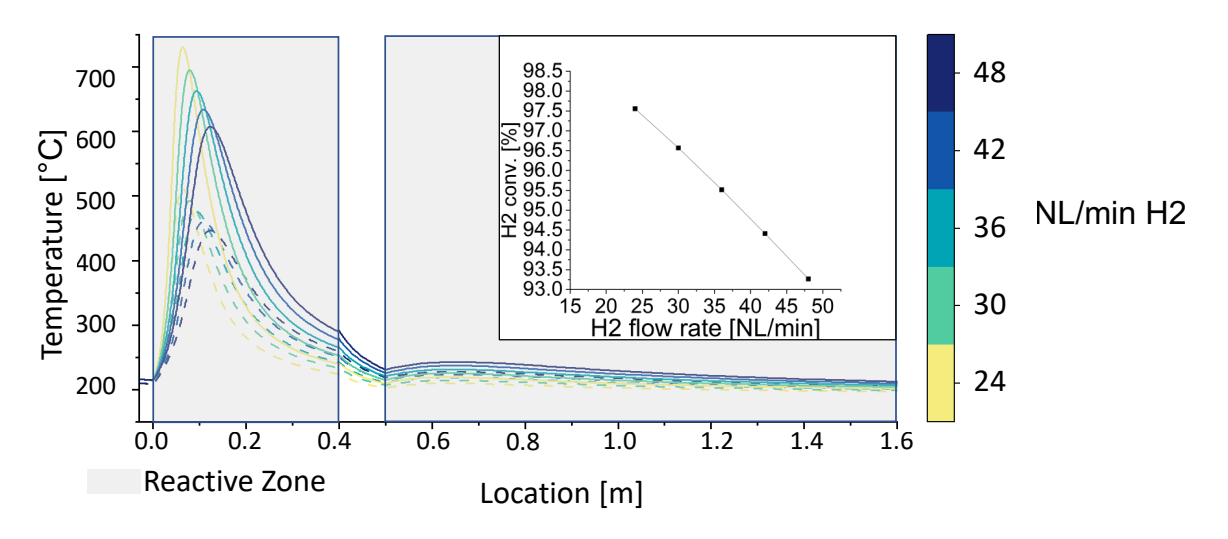


Figure 47: Simulation of the effect of the reactant flow rate: the average temperature (dashed) and the center temperature (solid), reprinted with permission from [1].

Reaction and Cooling-water Pressure

The effects of increasing the reaction pressure (Figure 48 with constant cooling system pressure of 14.92 bara) and the cooling system pressure (Figure 49 with constant reaction pressure of 6.16 bara) are in qualitative agreement between the simulation and the experimental results. The differences in the conversion gained with increasing pressures are within the uncertainties of the experimental results. There are still some discrepancies in the temperature profiles and magnitude of the conversion which can be explained similarly to the power sweep's analysis: not having the exact kinetic model limits the assessment of the accuracy of the various models used.



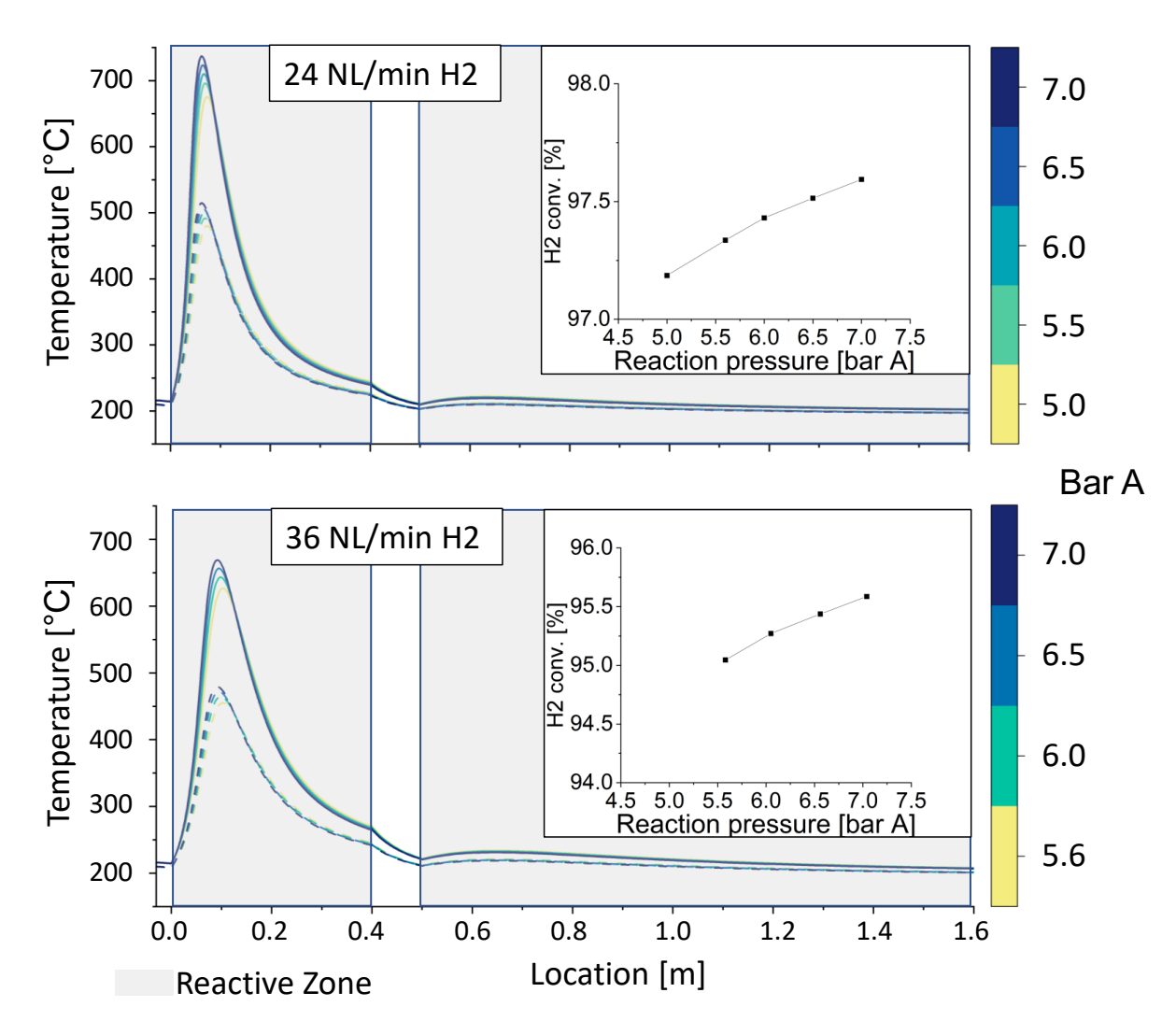


Figure 48: Effect of reaction pressure on the simulation: the average temperature (dashed) and the centre temperature (solid), reprinted with permission from [1].

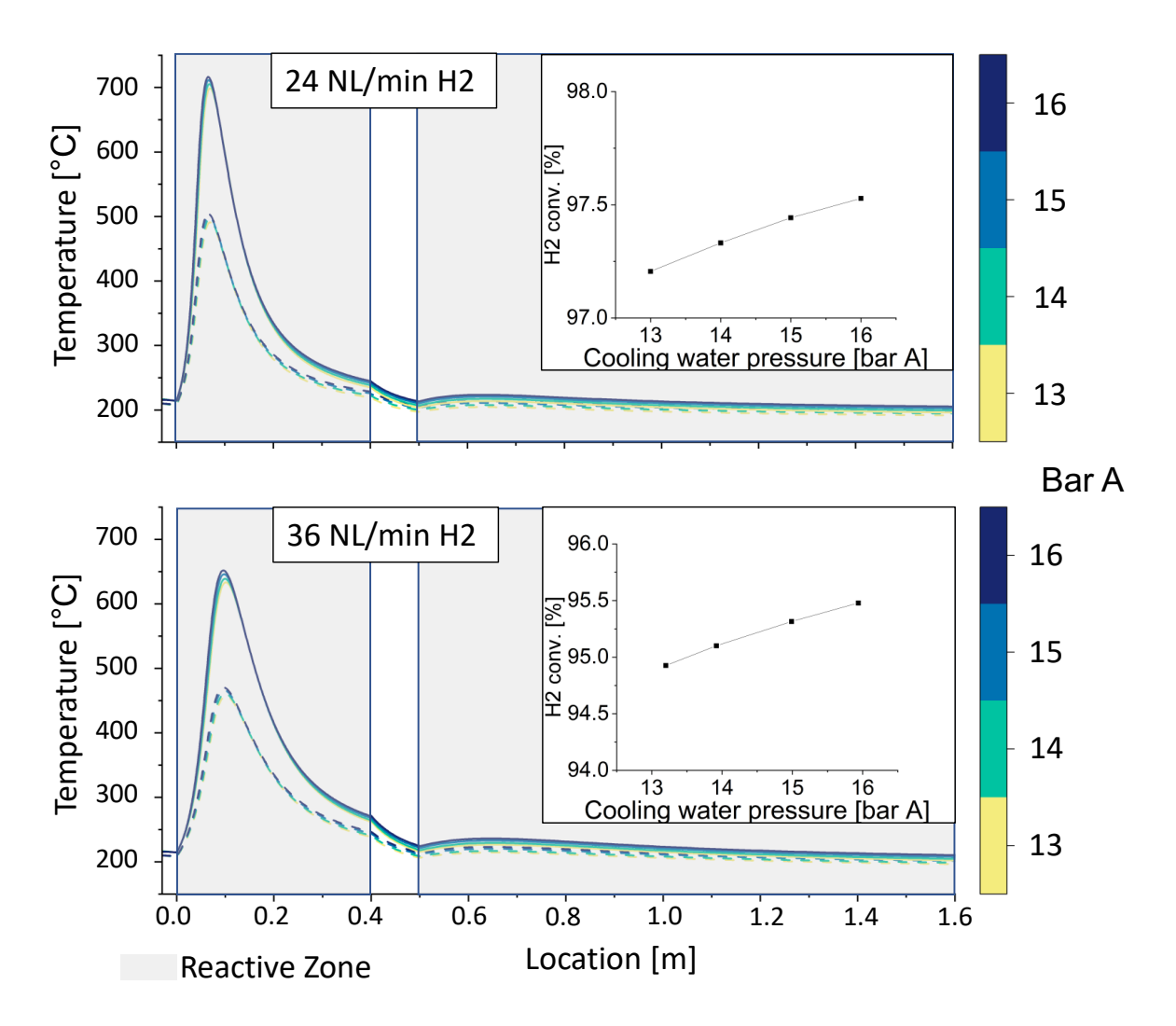


Figure 49: Effect of cooling-water pressure on the simulation: the average temperature (dashed) and the center temperature (solid), reprinted with permission from [1].

Simulation of Syngas methanation

In the case of syngas methanation, the presence of CO at the inlet results in the three reactions listed below occurring the reactor independently of the CO₂ methanation potentially being the summation of the Reverse-Water-Gas-Shift and the CO methanation. The outlet reactor composition is the summation of the favorability of each reaction as a function of temperature and pressure.

$$CO_2(g) + 4H_2(g) \rightarrow CH_4(g) + 2H_2O(g), \Delta H(298 \text{ K}) = -165 \text{ kJ/mol}$$

Reaction 4-1:CO₂ methanation

$$3 H_2(g) \rightarrow CH_4(g) + H_2O(g), \Delta H(298 K) = -206 kJ/mol$$

Reaction 4-2: CO methanation.



$$CO_2(g) + H_2(g) \rightarrow CO(g) + H_2O(g), \Delta H(298 \text{ K}) = 41 \text{ kJ/mol}$$

Reaction 4-3: Reverse water-gas-shift.

Methodology

The system used to perform syngas methanation is the one presented with the 5 kW to 7.5 kW reactor, but with an added evaporator at the inlet. Injecting steam with the reactant is an effective method for avoiding carbon deposition. The manufacturer of the catalyst pellets advised to inject one mole of steam per mole of CO. The temperature profiles along the reactor measured were agglomerated according to the percentage of carbon injected in the form of CO with remainder being CO₂ and the results are presented in Figure 50. In all the cases, the Modular number of 3 was maintained; the stochiometric feed of H₂ to satisfy both overall reactions was injected.

The design of experiment consisted of an orthogonal matrix with two duplicates at the centre and an extra point which defer from the duplicates by a single factor. The results are presented through the hydrogen dry concentration (Figure 51) and methane yield. For direct steam injection, a H₂ dry gas concentration under 5 % is required.

There is no measurement of flow rate at the outlet of the reactor, and the methane yields due to CO methanation and CO₂ methanation vary between points. Consequently, only the carbon to methane yield can be calculated based on the outlet's dry concentration:

$$Yield(\%) = \frac{CH_4^{out}}{CH_4^{out} + CO_2^{out} + CO^{out}}$$

Equation 4:27: Yield calculation

where the various concentrations are the dry concentration measured.

Also, the inlet H/C ratio can also be estimated:

$$H/C @ inlet = \frac{8 C H_4^{out} + 2 H_2^{out}}{C H_4^{out} + C O_2^{out} + C O^{out}}$$

Equation 4:28: Estimation of the H/C effective ratio at the inlet based on the outlet composition.

where the values of 8 and 2 are the stochiometric ratios per H atom for the CO₂ methanation (and CO methanation with 1 H₂O per CO injected).

Results of Syngas Methanation

Temperature Profile

The higher kinetics of CO methanation causes the profiles for all the cases with higher CO percentage to move closer to the inlet while their hot spots are higher. As the outlet temperature is dictated by the cooling water pressure in addition to having similar gas composition at the outlet, all the outlet temperatures are similar regardless of their inlet composition.

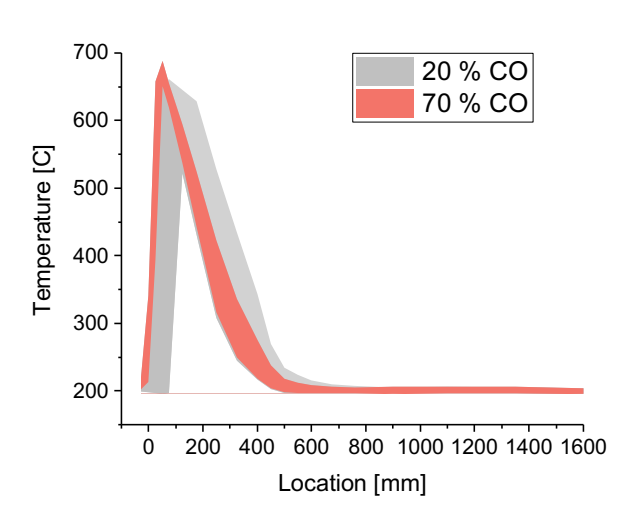


Figure 50: Temperature profiles along the central axis of the reactor for the two groups of syngas concentration, reprinted with permission from [2].

Operating a reactor designed for CO₂ methanation with syngas (or CO) emphasized the concern related to hot spot control. A reactor with a slightly smaller diameter would be favoured for such operation. The increase in flow velocity would push the hot spot towards the outlet while decreasing its magnitude by reducing the bed's thermal resistance. The decrease in the hot spot decreases risk of degradation of the pellets thermally in addition to moving away from the operating region where carbon deposition occurs. This would allow a decrease in the steam injected with the reactant. If less or no steam is injected with the reactant; the steam requirement of the complete system (SOE + methanation) can be decreased. However, removing the steam would cause an increase in reaction according to the Le Châtelier principle and a decrease in convection, resulting in a higher spot located closer to the inlet. Therefore, the diameter would have to be further decreased.

H₂ Concentration and Methane Yield

At the outlet, the CO concentration for all the operating points was below 1 %, indicating that either the CO methanation has higher kinetic or the reverse-water-gas-shift favours the formation of CO₂ through the excess steam. With the ratio of C-H and C-O injected, it can be assumed that carbon formation is negligible.

As it was observed in the case of CO_2 methanation, increases in both the gas pressure and cooling water pressure decreases the H_2 dry gas concentration. Similarly, the decrease in carbon flow rate (and the related decrease in total flowrate) improves the conversion. Nevertheless, when focusing on the effect of the percentage of carbon injected as CO, the effect depends on the total quantity of reactant. A higher hydrogen conversion can be reached for lower CO percentage as CO_2 methanation requires an extra mole of hydrogen. Thus, the resulting H_2 concentration depends on if the increase in kinetic due to CO methanation surpasses the added H_2 . However, the observation indicates an opposite response in H_2 concentration when increasing the CO percentage between lower and higher total carbon flow rate.

At higher flow rates, increasing the CO percentage brought the temperature closer to the inlet, and thus, decrease the potential quench effect of the second injection's inert region. However, Figure 52 presents both the hydrogen concentration and methane yield with color mapping based on the estimated H/C ratio at the inlet. The H₂ concentration is still primarily dictated by



the total flow rate of reactant. However, the relative change in H_2 concentration for each pair of points whose only difference is the total flow rate of reactant is affected by the H/C ratio. The increase in H_2 concentration between the group 1, and group 2 is different than the difference between group 3 and 4 while the change in H/C is opposite between the groups.

In the case of the methane yield, the mapping suggests that the H/C is the primary cause for the trend. At lower CO percentage, an increase in total flow rate caused an increase in H/C and an increase in methane yield. The opposite trend in the methane yield occurs at higher CO percentage. The effect of the CO percentage could be hidden by this more significant effect. Even the equilibrium concentration is affected by the actual H/C/O ratios injected as shown in Figure 53. The cases with the addition or subtraction of 1 % of the injected CO differs in equilibrium H_2 concentration by more than a percent. Therefore, if the ratios H/C/O is not 8/1/2, the outlet concentration can differ significantly.

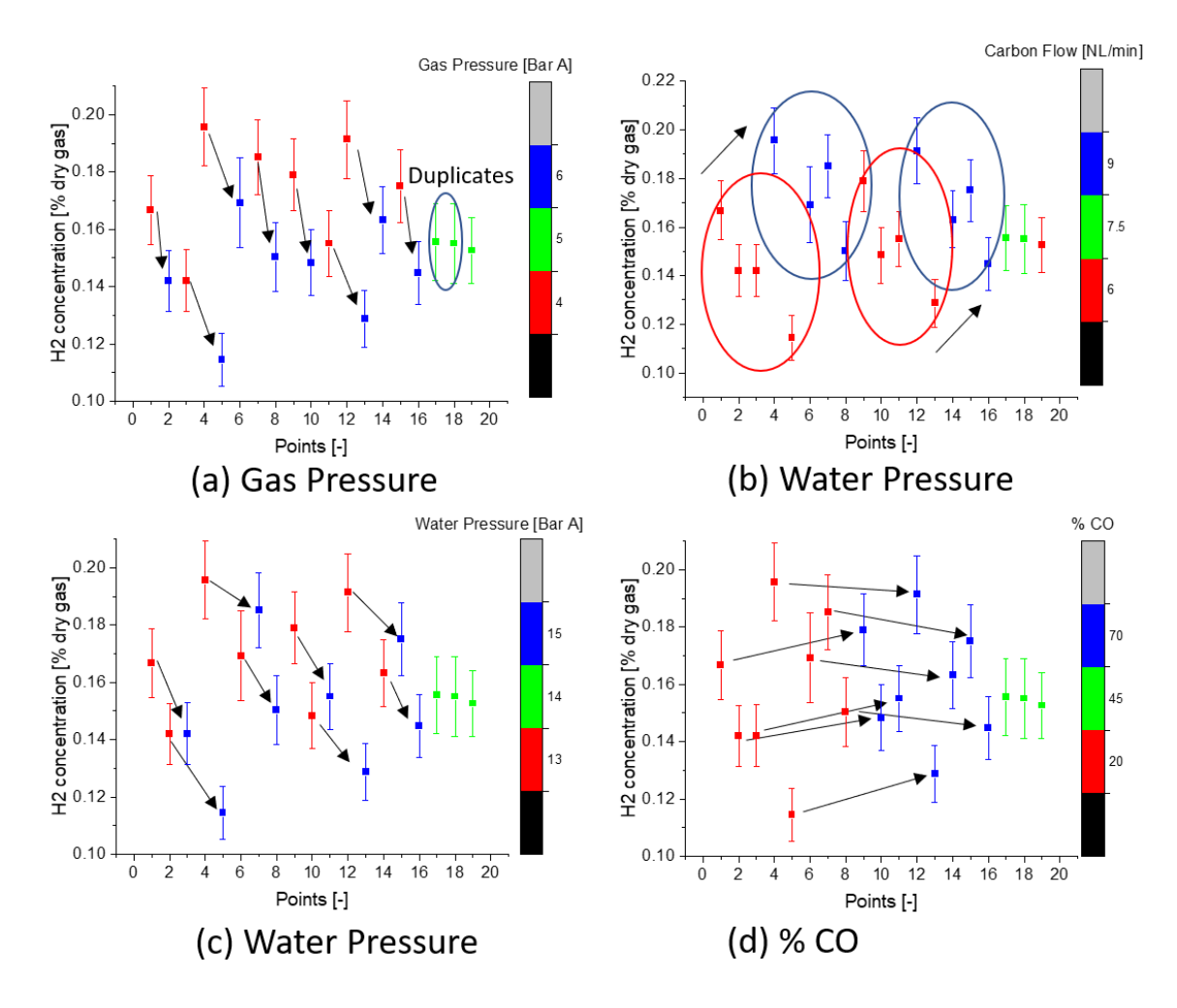


Figure 51: H₂ concentration at the outlet of the reactor for all the operating points, with colour map using the four main control variables, reprinted with permission from [2].

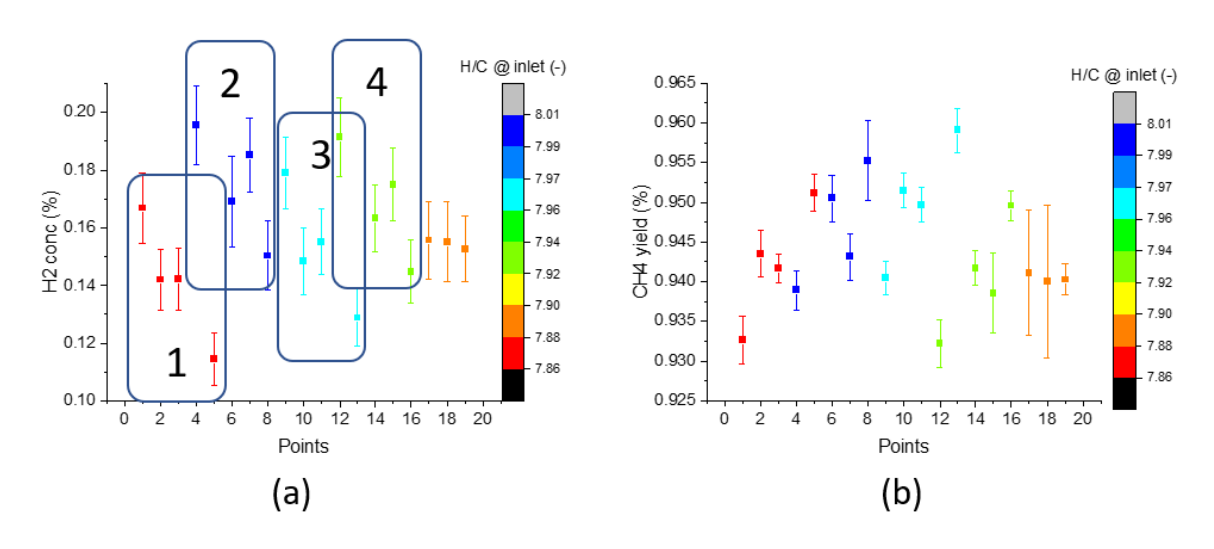


Figure 52: H₂ concentration (A) and methane yield (B) with colour mapping using the estimated H/C ratio at the inlet of the reactor, reprinted with permission from [2].

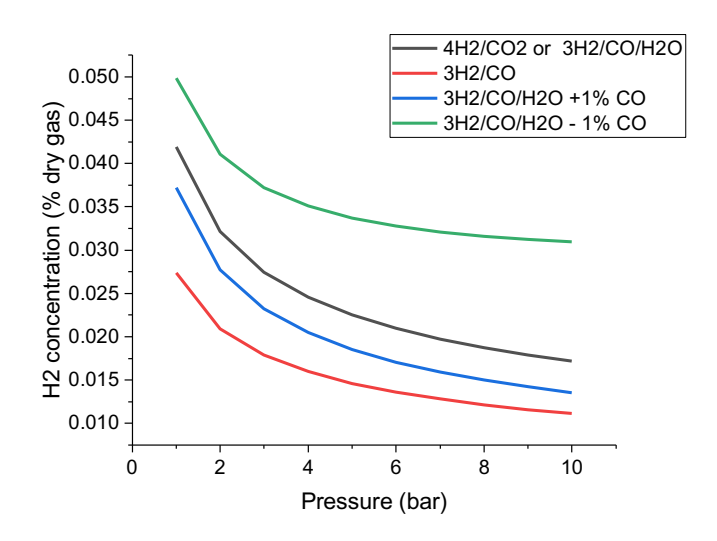


Figure 53: Equilibrium concentration at 200 °C as a function of pressure for CO methanation and CO₂ methanation (or CO with 1 H₂O/CO) in addition to 3 H₂/CO/H₂O +/- 1 % CO, reprinted with permission from [2].

4.2. WP2: Steam generation

4.2.1. Operation of the capillary steam generator at OST plant

The essential aspects of the operation of the steam generator based on capillary design can be seen in Figure 54. The steam flowrate (FT223) is shown, along with the pressure (PT240) and the temperature (TT240) in the superheating vessel V-24. The pressure at the outlet of V-24, i.e. the pressure that is 'seen' by the SOE module (PTC243) is shown with the scale on the right hand side. The data shown is the raw data, i.e. no interpolation. Note the very small units shown, 5 mbar between tick marks)



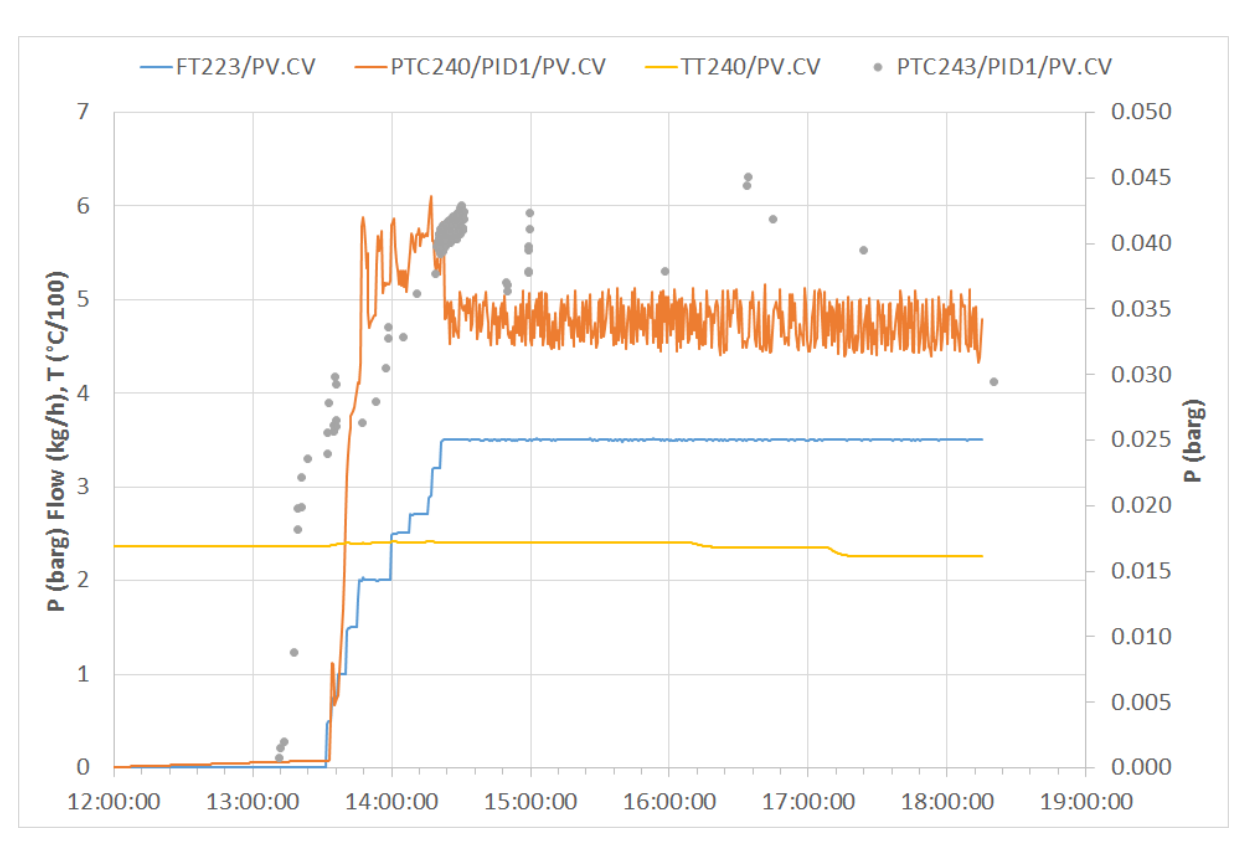


Figure 54: Operational data of the steam generation using the capillary steam generator.

In this experiment, the SOE module is simulated by sending the steam to a pipe with a constriction creating some backpressure. This backpressure built up after the steam flow was constant, raising from 25 mbar to 40 mbar. Very likely, this is due to the constriction narrowing as the material became hot and expanded between 14:30 and 15:00. From then on, the pressure towards the SOE remains within the range of 35 mbar to 45 mbar, i.e. a pressure fluctuation of about 10 mbar is observed.

During the experiment shown, 3.5 kg/h were evaporated and superheated to $240.6 \,^{\circ}\text{C}$, consuming $2.243 \, \text{kW}$ of heat. At the same time, the TO delivered $2.798 \, \text{kW}$ to this part of the system. At the time of writing of this report, no estimation had been made to evaluate whether the observed losses of $0.437 \, \text{kW}$ are plausible. The same considerations made previously for the reactor regarding the reliability of this calculation involving small differences applies.

The very small pressure fluctuations observed are on the other hand a very positive result of these initial experiments, and that at a much higher flowrate of 1 kg/h to 2 kg/h stipulated in the project proposal.

Control of the steam generation section involves setting the steam flowrate and the operating pressure of the pressure dampening vessel V-24 and, very importantly, the ramp-up and ramp-down of steam production for delivery to the SOE.

Flowrates are changed by adjusting the water flowrate that is admitted to the evaporator. A short time lag can be anticipated between change at the pump and change in the steam outflow, the pipe volume between the pump and the evaporator is estimated at 0.075 litres. Thus, ramping the steam flowrate up and down can be expected to be almost instantaneous. The evaporator was brought to full flowrate in about 45 minutes in the above experiment, but much

faster rates are achievable as this unit has shown to respond almost immediately to changes in operating conditions.

The steam temperature is above the expected minimal 150 °C required. We have thus far not tried to influence it. It is mainly given by the TO temperature. Further experiments will be conducted to test in what range this parameter can be set.

The above data also shows that the transition when the feed of steam to the SOE is started will have to be carefully tested and a protocol implemented for this transition, to avoid loading the SOE with too much pressure or sending moisture into the unit.

4.2.2. Stabilization of the steam production at EPFL laboratory

The assessment of the stability of the steam generation was performed on the methanation of CO₂. The following table presents the steam generation in terms of quantity and percentage of the required steam (assuming 85 % steam utilization in the SOE), the co-generation efficiency and heat exchanger efficiency.

\dot{V}_{H_2} [NL/min]	Steam Generation [g/min]	Steam Generation [%] (SU of 85%)	η _{Co} [%]	η _{Ex} [%]	
24	19.7* - 22.6**	87.0* - 105.7**	87.3 – 88.4	80.0 - 88.8	
36	32.1* - 36.3**	94.3* - 113.0**	88.17 - 89.0	86.6 – 91.1	
*Lowest values are the cases presented in the steam stability section which correspond to the runs with the					
lowest temperature at the inlet of the reactor.					
** Highest values occur with higher inlet temperatures due to the added enthalpy.					

Table 8: Steam generation and efficiencies, transcribed with permission from [1].

The quantity of steam generated is important, but the stability is also critical to limit the pressure pulsations and local steam starvation in the SOE. At low steam generation (low H_2 flow rates), the steam generation is stable. However, at higher flow rates, the generation can be unstable. The Figure 55 presents a case at low hydrogen flow rate with stable steam generation while the Figure 56 presents a higher hydrogen flow rate case and it was able to stabilise the steam generation through a higher recirculating water flow rate (lower vapor fraction at the outlet of the reactor) and through the use of a control valve at the inlet of the reactor which applies an important pressure drop. In both cases, the response is comparable to the ones from the commercial evaporator on Figure 17. Though, at certain operating points, and during transient operation, there can be instabilities that are not controllable using the present solutions.



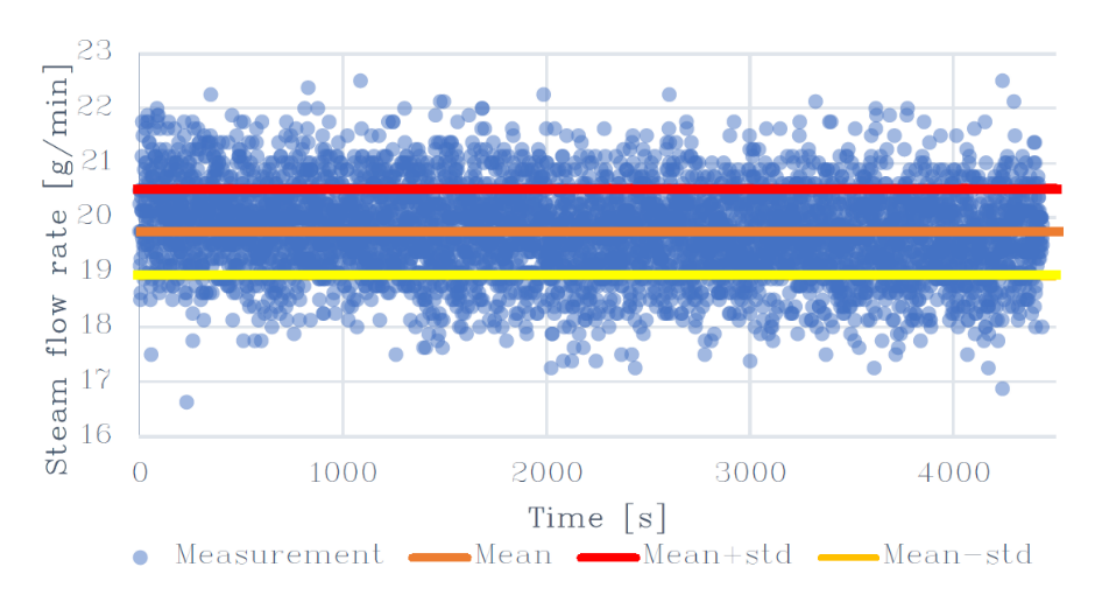


Figure 55: Steam generation from the methanation of 24 NL/min H₂: 6 NL/min CO₂, reprinted with permission from [11].

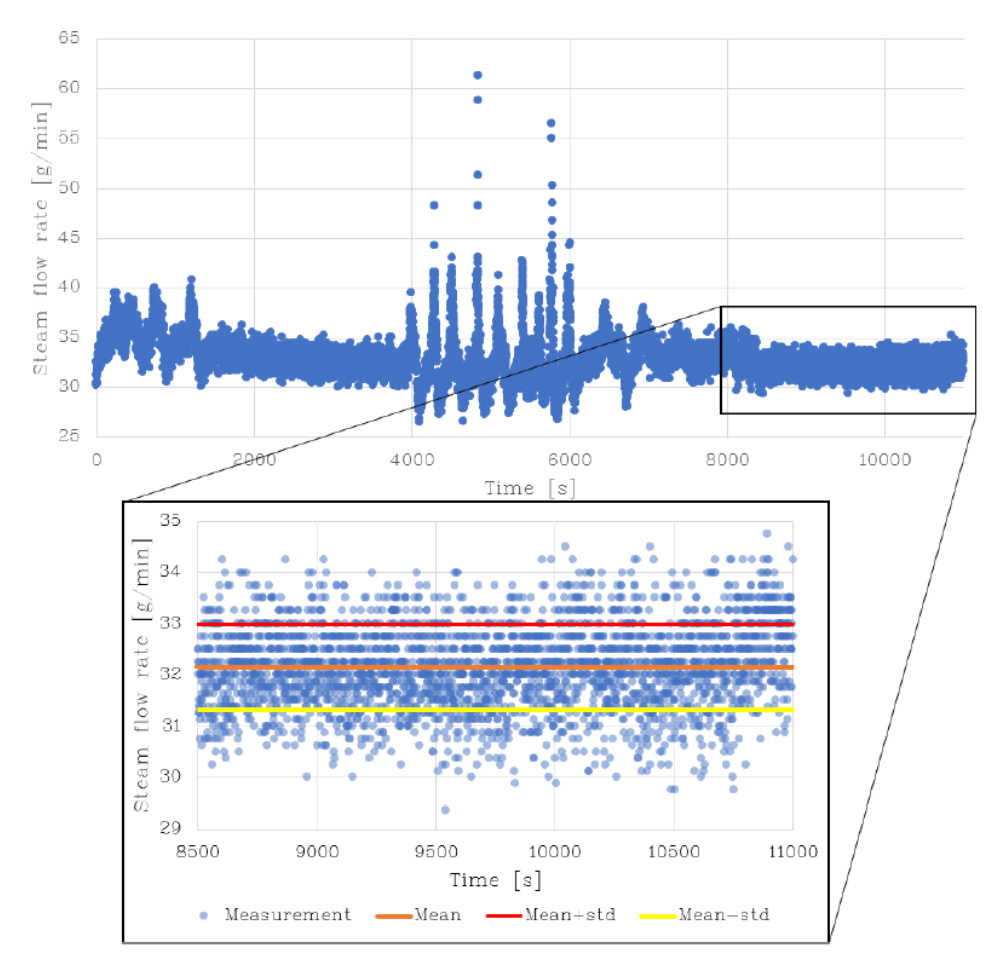


Figure 56: Steam generation from the methanation of 36 NL/min H_2 : 9 NL/min CO_2 , reprinted with permission from [1].

Consequently, a damping volume should be used before the SOE. This volume can also be used as mixing volume in the case of multiple evaporators. There are a few potential sources for the instabilities, possibly exacerbated by the combination of these sources: (1) the use of a manual back-pressure controller, (2) the evaporating process with unstable flow pattern(s), and (3) oscillations in the 3D temperature profile inside the bed which affects the reaction, and thus, the heat and steam generation.

A method to identify the damping volume is developed below. It has been applied for steam generated by the first methanation setup and still needs to be confirmed on the actual one. Figure 57 shows the relative pressure pulses at certain steam production as a function of time (left), and its Fourier transform (right).

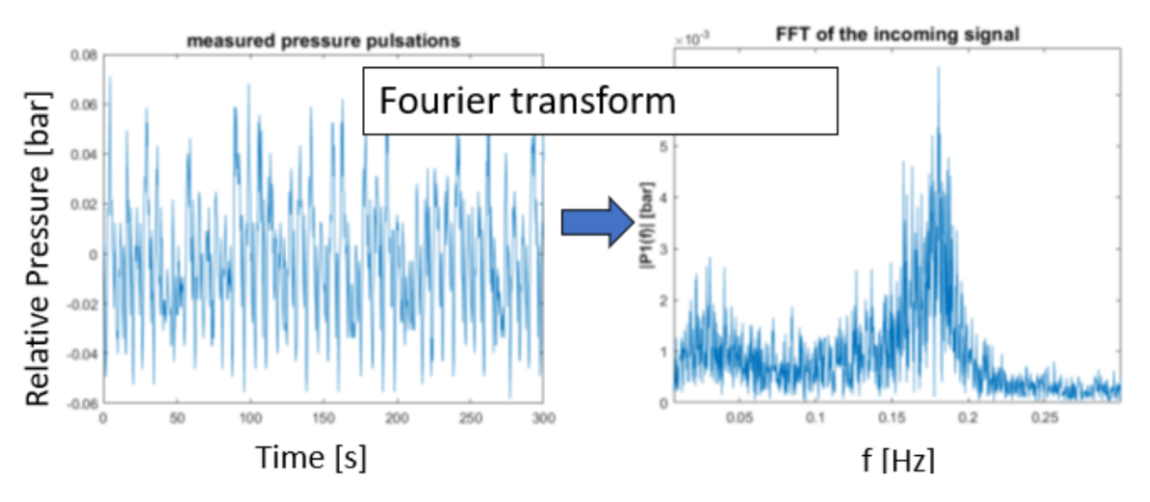


Figure 57: (Left) Relative steam pressure pulsation at a certain working point. (Right) Its Fourier Transform.

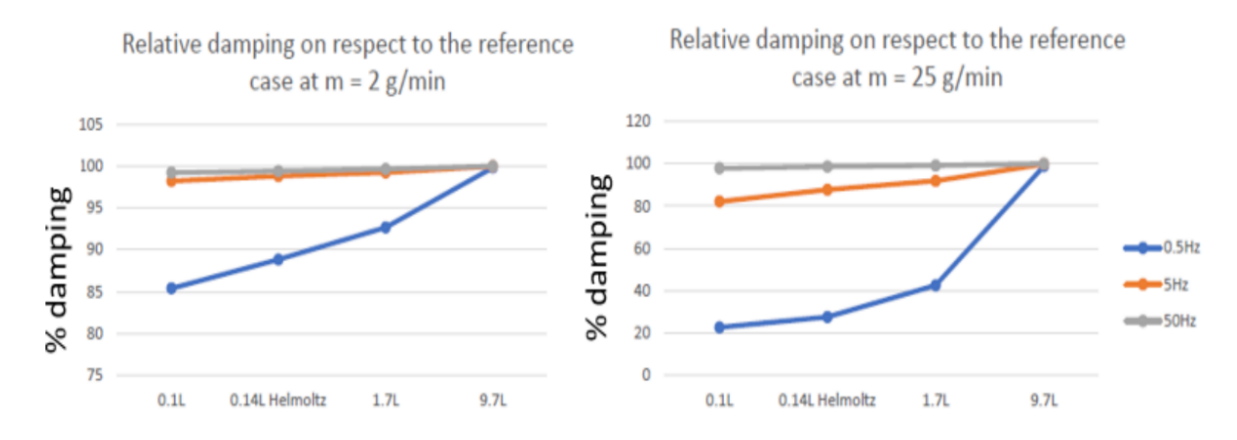


Figure 58:Effective dampening of steam pulsations by using various geometries, for the smaller and larger scale methanator (Left: initial version, Right: redesigned version with a scale factor of 10), and for 3 frequencies.

A range of frequency was found, but for computational reasons, the remainder of the analysis was performed for a larger range of frequencies. The aim was to develop a method, and thus the frequency used itself is less important. Various geometries were simulated in ANSYS Fluent to verify the effective pulse dampening, that results from introducing them. Cylindrical tanks of 0.1 litre, 1.7 litre and 9.7 litre, and a 0.17 litre Helmholtz resonator were the geometries in question, chosen to dampen the pulsations. Figure 58 presents the results of the simulation for three pulsation frequencies (0.5 Hz, 5 Hz and 50 Hz). The average water flow sent for this



smaller-scale system (10x smaller than the present reactor version) was \sim 2 g/min. The analysis was extended to the new, larger scale reactor, assuming a water flow of 25 g/min (1.5 kg/h, \sim 5 kW $_{\rm e}$ SOE). The results indicate that a fix tank of 10 litre can ensure the dampening of "high" frequency for both scales, but the analysis needs to be re-done for the exact frequencies of the new large scale setup, which could be lower.

4.2.3. Reactor cooling at EPFL laboratory

Effect of the evaporation pressure:

The operation of the system at multiple cooling water pressures is presented in Figure 59 (A). For each pressure level, the system was operated until a pseudo steady-state was reached. The water level in the steam separator was also maintained as constant as possible to ensure the change in effective column difference is only impacted by the evaporation process. A typical response in the recirculating water flow rate and produced vapor flow rate is presented in Figure 59(B).

Figure 59(C) presents the reaction temperature profile along the central axis of the reactor.

The comparison between passive and active operation of the cooling system is presented in Figure 59(D) with the average vapor flowrate and the standard deviation. The results indicate similar responses. The difference in average flow rate measured could be the result of a slight difference in certain operating variables that changes slightly the quantity of heat that can be extracted. One such variable is the temperature of the reactive gases sent to the reactor. As the system could still have some transient behaviour, the average steam flowrate at 15 bara was slightly lower than the other pressures.

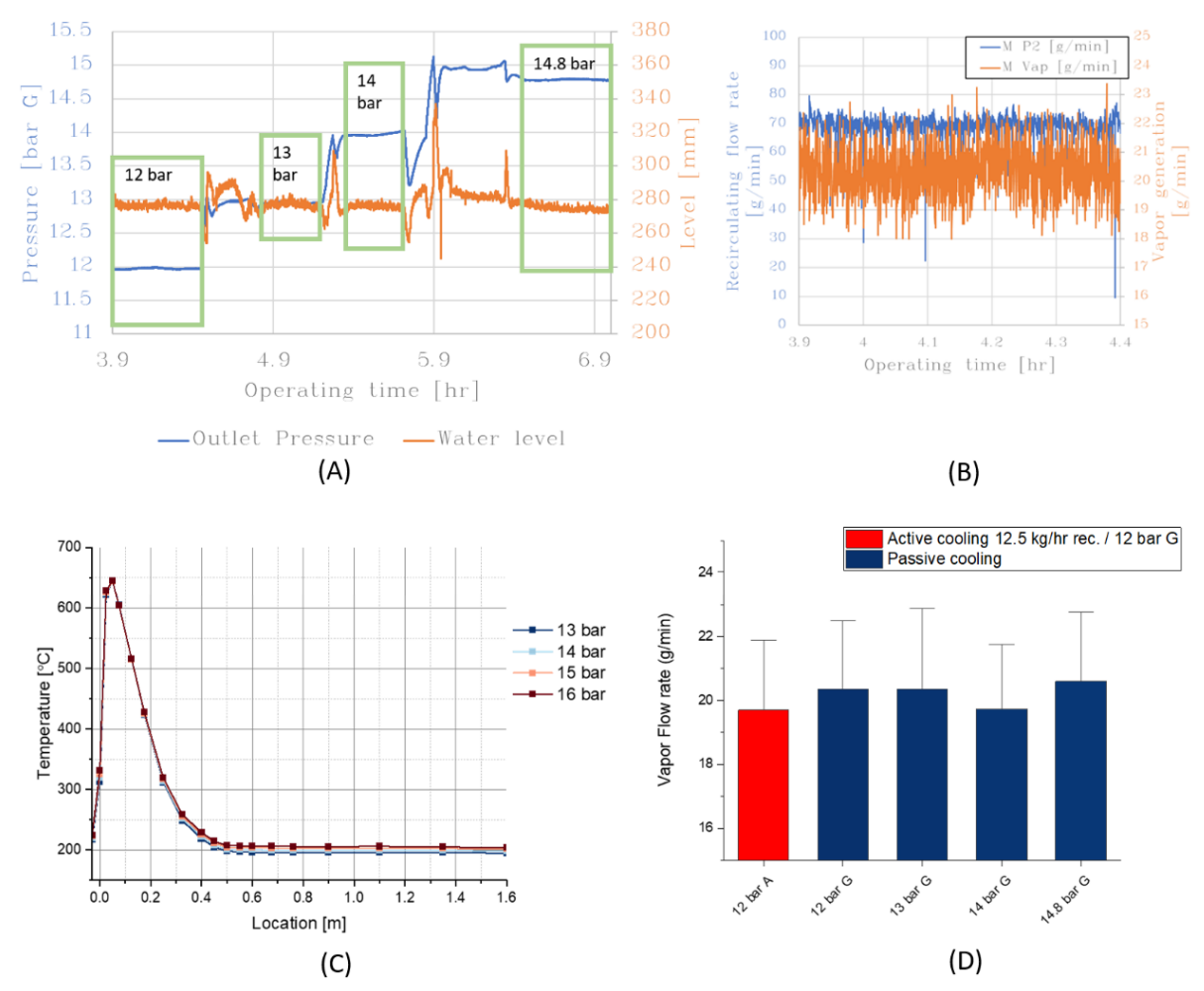
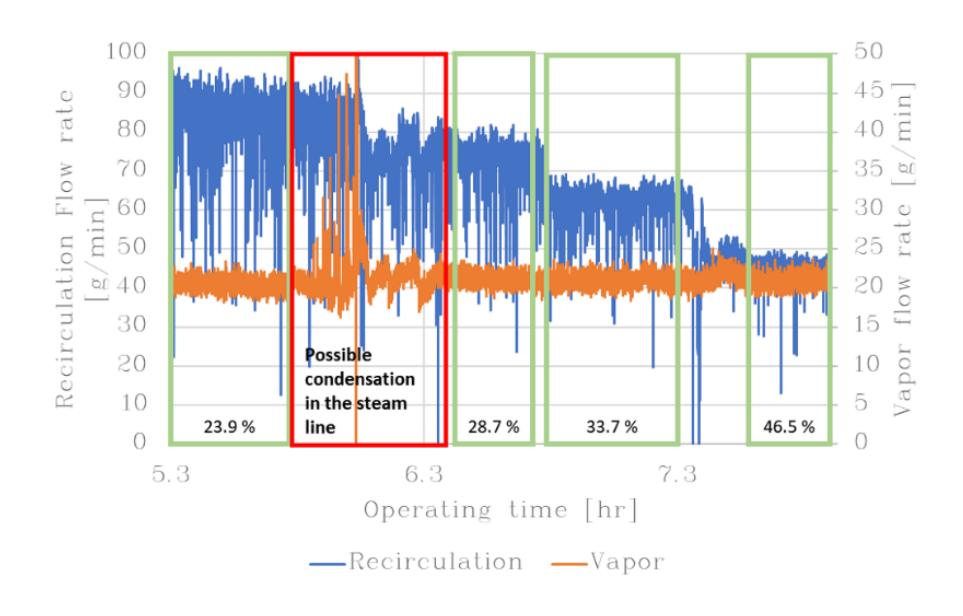


Figure 59: (A) Water level in the separator while changing the evaporation pressure, (B) the recirculation flow rate and produced vapor flow rate at 12 barg, (C) the temperature profile along the reactor's central axis, and (D) the comparison between the vapor measured during cooling and the vapor measured with varying saturation pressure.

Effect of the recirculating flowrate:

The valve located at the inlet of the evaporator can be used to add a restriction in the system to help stabilize the evaporation process. In this analysis, the valve is used to decrease the recirculation flow rate and increase the vapor fraction at the outlet of the evaporator. Figure 60(A) presents the recirculation flow rate and vapor flow rate, along with the corresponding vapor fraction at the outlet of the evaporator, assuming that negligible condensation/evaporation occurs in the separator. Heat tracing between the outlet of the separator and the back-pressure controller is performed manually and the dial was not increased when the temperature at the inlet of the back-pressure controller started to decrease. This potentially caused condensation in the line and the back-pressure controller is not designed to effectively control two-phase mixtures; the combination of both problems could have resulted in the behaviour at approximately 5.8 hours. Otherwise, the average vapor flow rate and standard deviation (Figure 60(B)) indicate comparable behaviours within the range of recirculation flow rate.





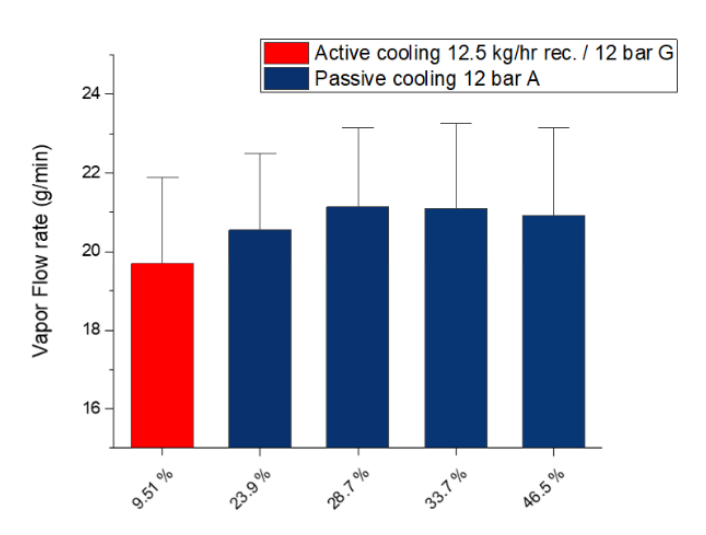


Figure 60: (A) Recirculation and vapor flow rates over time, and (B) the comparison between the vapor measured during cooling and the vapor measured with varying vapor fraction.

4.3. WP3, WP4 and WP5: Operation and control of the SOE

4.3.1. Pressurized single cell setup

Developing a thermo-mechanical-electrochemical system requires validating many components separately. A first series of the test on the oven alone were performed to make sure the material used could withstand the thermal shock.

An example of failed component was a cordierite support for the Kanthal heaters. It might be electrically insulating at room temperature but becomes electrically conductive at temperatures above 700 °C. Current would leak to the ground until the total current drawn from the outlet exceeds the breaker limit. This occurred at a temperature of approximately 870 °C. Consequently, the cordierite supports are now wrapped in mica to completely insulate them from the external casing.

The cell mounting was tested through a sintering cycle and measuring the OCV under dry gases (H_2/N_2 mixture in the fuel electrode). The temperature measured inside and outside the cell housing as well as the temperature used to control the oven are presented in Figure 61. The glass sintering cycle is know-how of SolydEra SA.

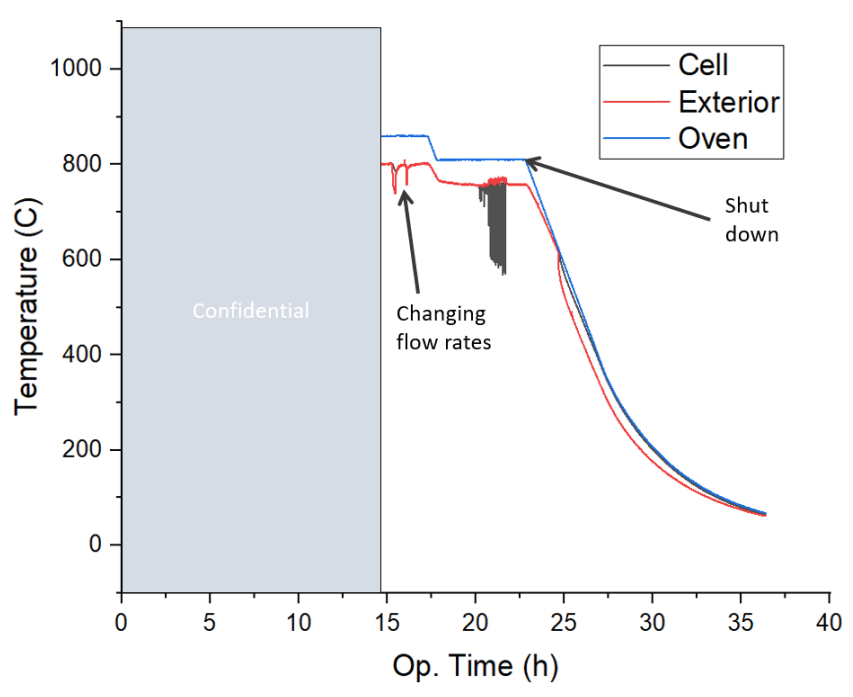


Figure 61: Cell temperatures and oven temperature during the test

During this test, a half cell (anode with electrolyte only) was used which allows the measurement of the OCV but not the measurement of performance under polarization. Due to either flow leaking across the cell through the glass seal or current leaks between the air electrode and the ground, the OCV measured was oscillating between 0.95 V and 1.17 V. At 1.17 V, a leak would have to be around 1 % steam in H_2 , but an OCV of 0.95 V is the result of a concentration between 45 % and 55 % of steam in H_2 . Such a leak is unlikely as the cell was still completely reduced after the cooling down using forming gas. If such a leak would occur with H_2 flow of 120 Nml/min, the 10 Nml/min of H_2 in H_2 during cooling down would not be enough to maintain the reduced state of the cell. Another observation against the cross-leak theory is the variation in pressure and flow rates (while maintaining the same concentration) in both lines did not remove the leak even in the case of an over pressure on the fuel side. The variations in pressure and flow rates throughout the test are presented in Figure 62.



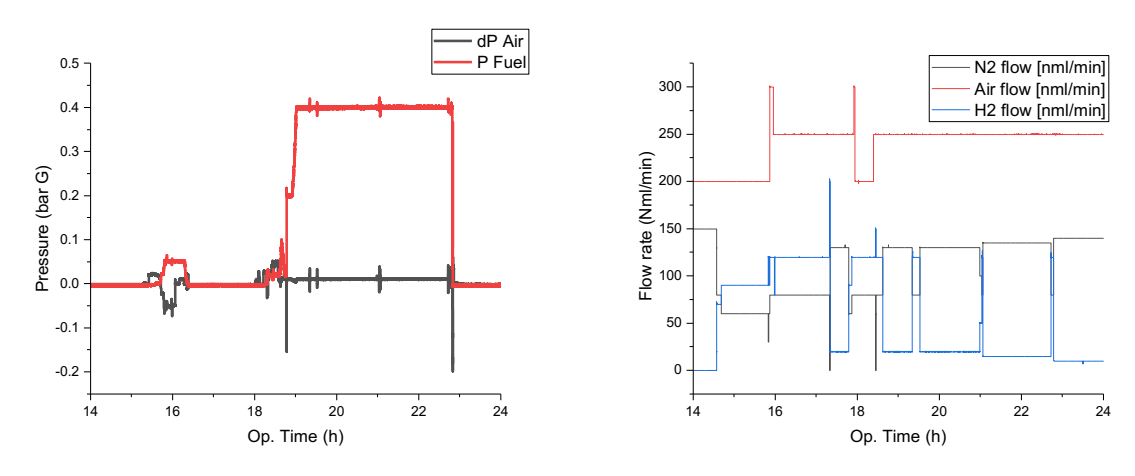


Figure 62 : (Left) Pressure in the fuel line, and differential pressure between the two lines. (Right) Flow rates of H₂, N₂ and Air.

More likely, the low OCV was due to a current leaking out of the setup. This possibility was identified while disconnecting certain grounds and the OCV would change abruptly. In addition, a half-cell does not have a cathode, and thus, any current leak of the order of uA could result in the observed drop in voltage.

Test bench improvement

A new version of the pressurized test bench is under development. As explained in the experimental section, the force applied on the cell casing allowing to guarantee a good sealing is currently not controlled. This results in a force variation during the experiment mostly due to the thermal expansion of the different parts. To maintain a constant force, a new setup was designed, as shown in the Figure 63 below. A bellows cylinder is used to control the force applied on the system by regulating the air pressure inside it. The advantage of such a cylinder is the compacity and the absence of stick-slip effect. Figure 64 shows the cylinder in its retracted and expanded position respectively. Four rods guided by plain bearings maintain the frame alignment.

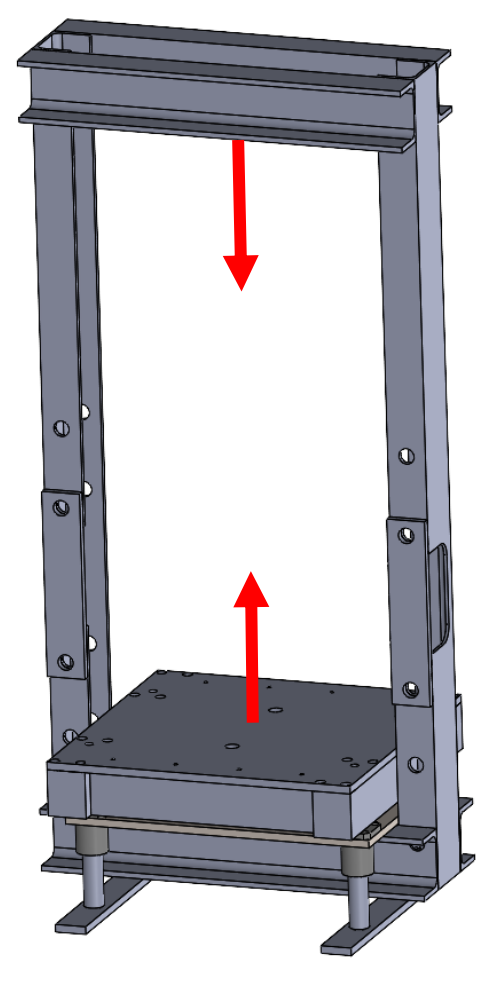


Figure 63: Pressurized test bench with cylinders from Figure 64

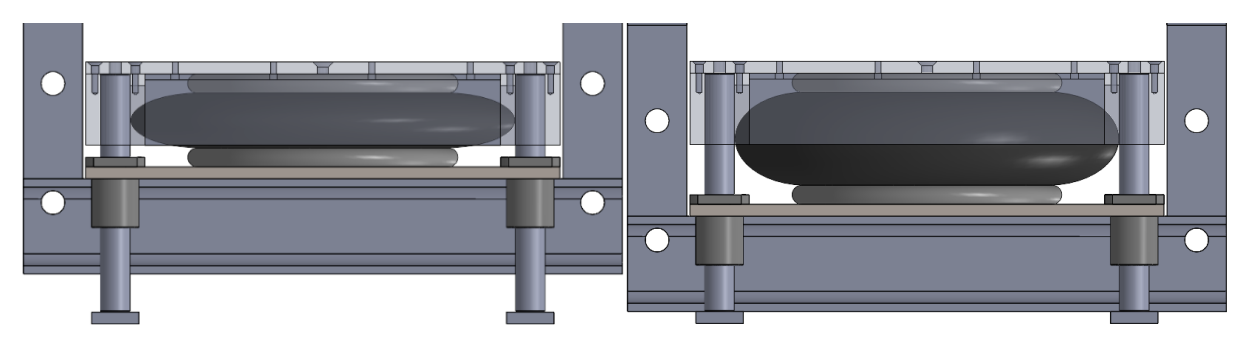


Figure 64: (Left) Retracted bellows cylinder, (Right) Expanded bellows cylinder.



4.3.2.SOE unit: Test with the bypass

The first test of the G-20 unit has been made with a bypass instead of a stack. The purpose of the test was to validate the entire BoP and characterize the temperature profiles of the SOE system, depending on the amount of natural gas and air sent to the burner. Also, by characterizing the burner behaviour, it permitted to build the code for flame detection inside the burner.

The Figure 65 shows the temperature evolution during the bypass test. It took approximately 10 hours to heat the burner to a temperature of 820 °C, leading to a temperature of the air at the entrance of the bypass ($T_{air\ in}$) equal to 730 °C. This is definitely acceptable for SolydEra stacks and the air-air heat exchanger as well as the burner are therefore validated. On the other hand, the fuel temperature ($T_{fuel\ in}$) is too low. The heating of the fuel inside the BoP is therefore not efficient enough, either because of the fuel-fuel heat exchanger, which is not working properly, or because the overall heat losses of the BoP are too high. It is very difficult to determine the main reason without testing the exchanger with additional thermocouples.

When the system reaches a temperature of 250 °C to 300 °C, DMW turned to steam has to be mixed with the natural gas that is sent to the burner. The steam presence avoids carbon deposition that occurs when the natural gas reaches high temperatures. The steam to carbon ratio must be at least equal to 2.2 to ensure no carbon deposition, otherwise the carbon deposit might block the gas path. Adding the steam is critical as it changes the mixture sent to the burner and might kill the flame. This is what happened after around 17 hours of test. By adding the steam, the flame was killed. A smoother way of adding the steam has been therefore implemented for future test with the stacks. It consists in automatically adapting the amount of steam to the amount of NG sent to the burner. This control is performed by the Labview software.

Based on the bypass test, the heating process of the SOE unit is validated. The flows have been fixed: the startup is done with 1 NL/min of natural gas mixed with 100 NL/min of air. When the burner starts, the air is increased to 180 NL/min and the natural gas is slowly increased with a ramp of 0.003 NL/min.

After 35 hours of test, steam was supplied to the SOE. The temperature of the steam at the entrance of the HotBox is around 200 °C to 250 °C, which is high enough and validates the steam-line on both OST and EPFL sides. The pressure at the fuel inlet is also acceptable when steam is delivered, as presented on Figure 66. It doesn't go higher than 45 mbar with a steam delivery of 3.5 kg/h. The maximum steam delivered for 5 kW $_{\rm e}$ electrolysis will be around 2 kg/h, therefore the pressure at fuel inlet should be below 45 mbar. The air pressure, which stays around 20 mbar, is also acceptable. However, those values must be confirmed with a real stack and a real hydrogen production as it will impact the overall fuel and air pressure.

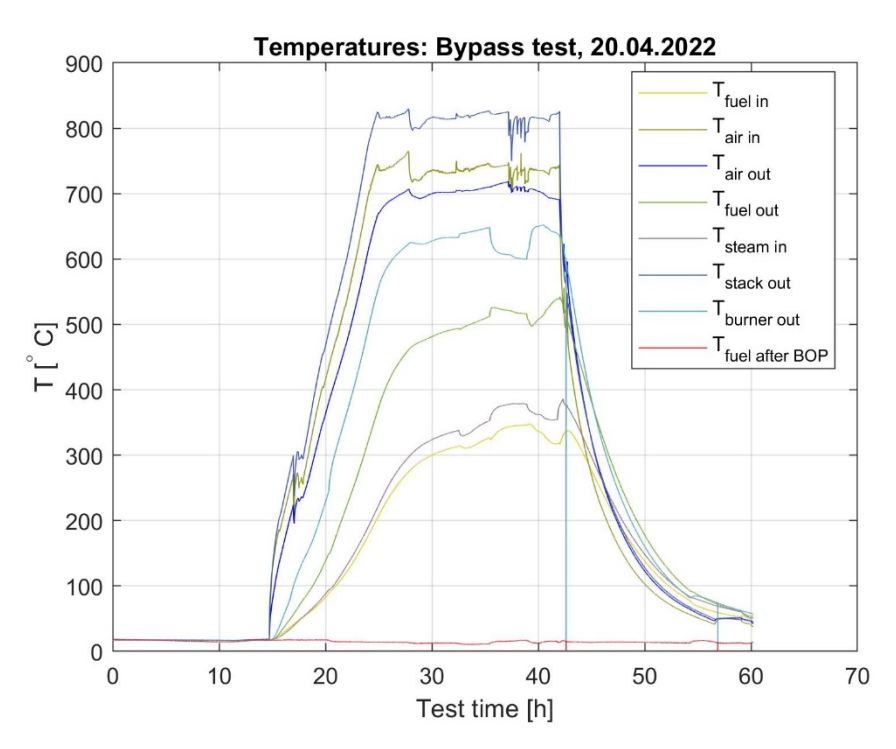


Figure 65: Temperature evolution during the bypass test in April 2022

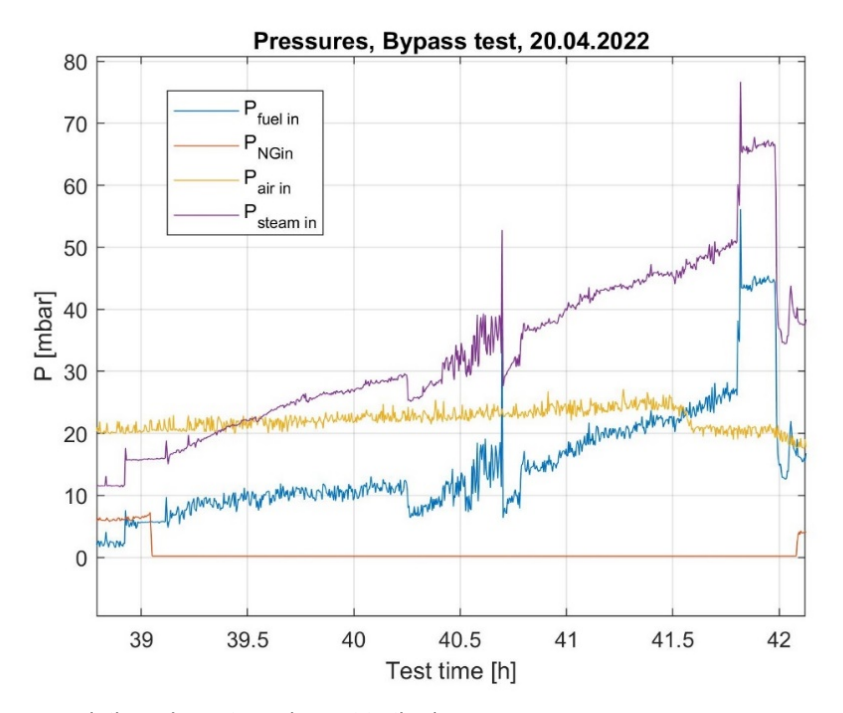


Figure 66: Pressure evolution when steam is sent to the bypass.

As presented in chapter 3.5 page 40, the temperature of the burner has been recorded and analysed in order to determine the threshold values that were showing a flame appearance/disappearance inside the burner. The analysed value is plotted on Figure 67. Several starts of



the burner have been performed during the bypass test, as well as several burner cut-offs through emergency shutdown. When the flame is created or killed, the value of the data goes above or under a threshold around 0.15 when the flame is created and -0.2 when the flame is killed. Those values are therefore used in the burner control code implemented in the PLC and will be confirmed through the first test with a stack. It is important to carefully choose those values to not miss any real flame disappearance but also not create multiple unnecessary emergency shutdowns due to unstable temperature in the burner, even if the flame is still existing.

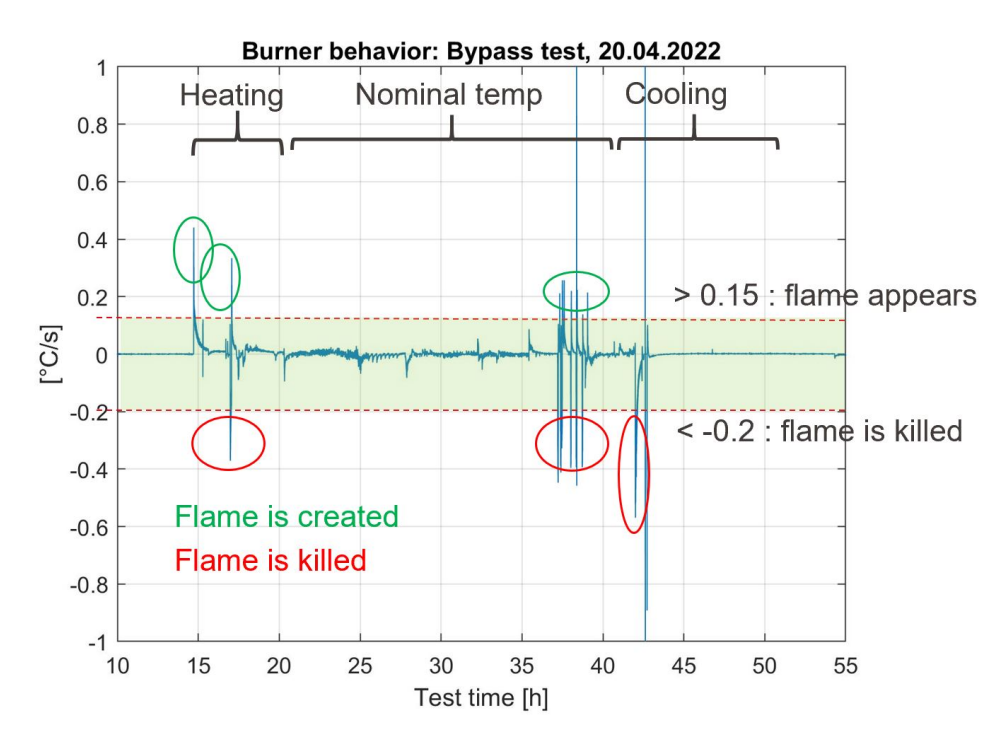


Figure 67: Data evolution in the burner during the bypass test in April 2022

4.3.3.SOE unit: Test with the stack #1801

The purpose of the test session in September 2022 was to validate the SOE unit with a real stack and to validate the coupling to the hydrogen compressor and the methanator, up to a power applied to the stack equal to 5 kW_e. An already used stack from SolydEra has therefore been used for this testing session. Here is a brief summary of the testing plan:

- Day 1 and 2: heating of the SOE-BoP
- Day 3: electrolysis at 3 kWe with coupling to the hydrogen compressor
- Day 4: electrolysis at 5 kW_e with coupling to the compressor and the methanator
- Day 5: cooling of the SOE-BoP

The heating of the SOE-BoP didn't show significant issues. The heating conditions validated during the bypass test were used and a mean heating ramp of 30 °C/h to 60 °C/h has been applied. The water injection into the burner, which was problematic during the bypass test because it creates a risk of flame-killing, didn't generate any disappearance of the flame as the amount of steam delivered has been increased very smoothly. This led to constant and smooth heating of the SOE unit. Nevertheless, an emergency shutdown occurred after twenty-

seven hours of heating. This was due to a problem with the plant infrastructure and not linked to the SOE unit.

During the heating, the stack is supplied by air and forming gas in order to keep a reductive atmosphere and avoid the oxidation of nickel at the fuel side. The heating with the stack took however much more time than with the bypass (approx. 30 hours instead of 10 hours). It can be explained by the high thermal inertia of the stack which cools down the air flow during heating.

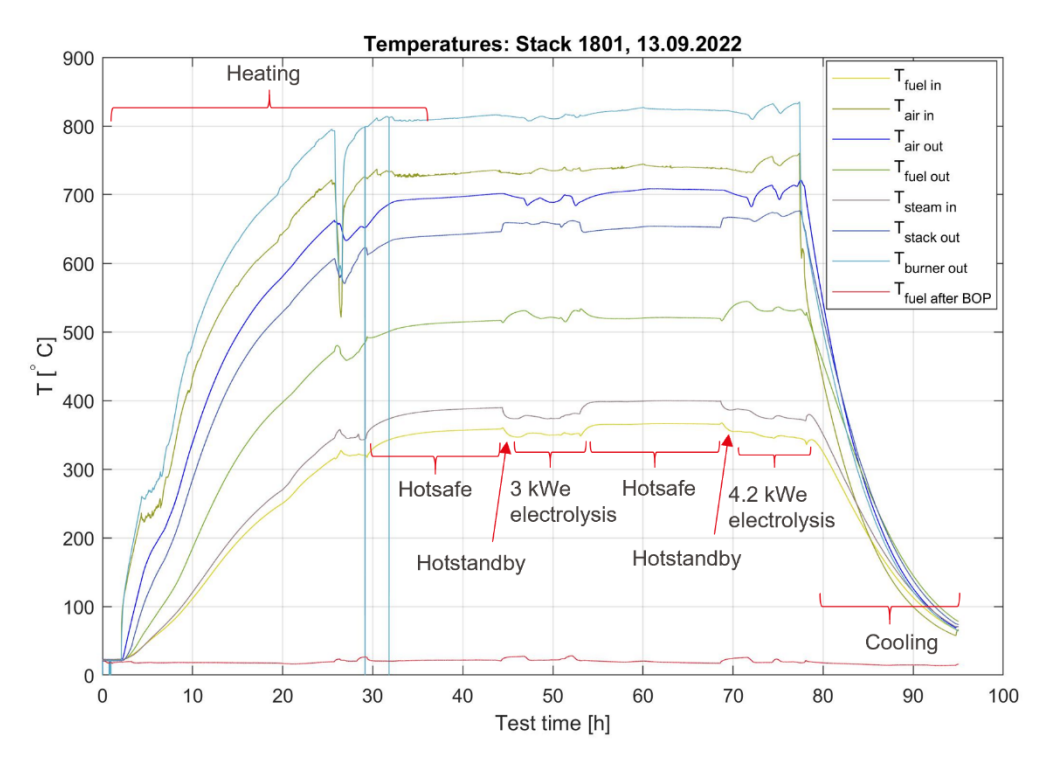


Figure 68: Temperatures during the testing week with the stack #1801 from SolydEra

The burner is the core heater of the BoP. It heats the air that travels through the BoP and the stack and brings the whole system to the requested temperature. The amount of methane consumed into the burner has been adjusted to reach a stabilized burner temperature around 820 °C. The corresponding stack temperature is 715 °C. This temperature will be increased to 740 °C in future tests, in order to improve the stack performance. This week of test has validated the air-air heat exchanger as well as the burner, which properly heats the rest of the system to the requested temperature, this time with a stack installed. Nevertheless, it has also shown that the fuel temperature is still dramatically low, as with the bypass ($T_{fuel\ in}$ and $T_{fuel\ out}$ in Figure 68).

Several reasons can explain that low temperature:

- The heat exchange between air and fuel in the stack is too low.
- The heat exchange in the fuel-fuel heat exchanger is too low.
- The heat losses of the SOE unit system are too high.
- The thermocouples are badly positioned and don't show the real temperature of the flow.



After discussion and comparison of the stack performance with SolydEra, that low temperature doesn't seem to impact the performance of the stack and might indicate that the thermocouples don't show the real temperature of the fuel flow. Another possible explanation is that, due to the high amount of air compared to the fuel flow, the impact of the fuel temperature on the mean stack temperature is negligible.

When the SOE-BoP reaches a steady-state temperature, the stack enters into HOTSAFE mode. A few minutes before entering ELECTROLYSIS mode, the stack is supplied by 0.9696 kg/h of steam and 2.42 NL/min of hydrogen and enters the HOTSTANDBY mode.

As shown on Figure 69, during the first electrolysis test, the current was slowly increased on the stack with a ramp of 1 A/min until reaching a voltage of 92.5 V at the power supply, corresponding to a stack voltage of 90.5 V when deleting the voltage losses inside the cables connecting the power supply to the stack. This voltage value corresponds to a mean cell voltage of approximately 1.29 V to 1.3 V per cell, which is the thermoneutral voltage.

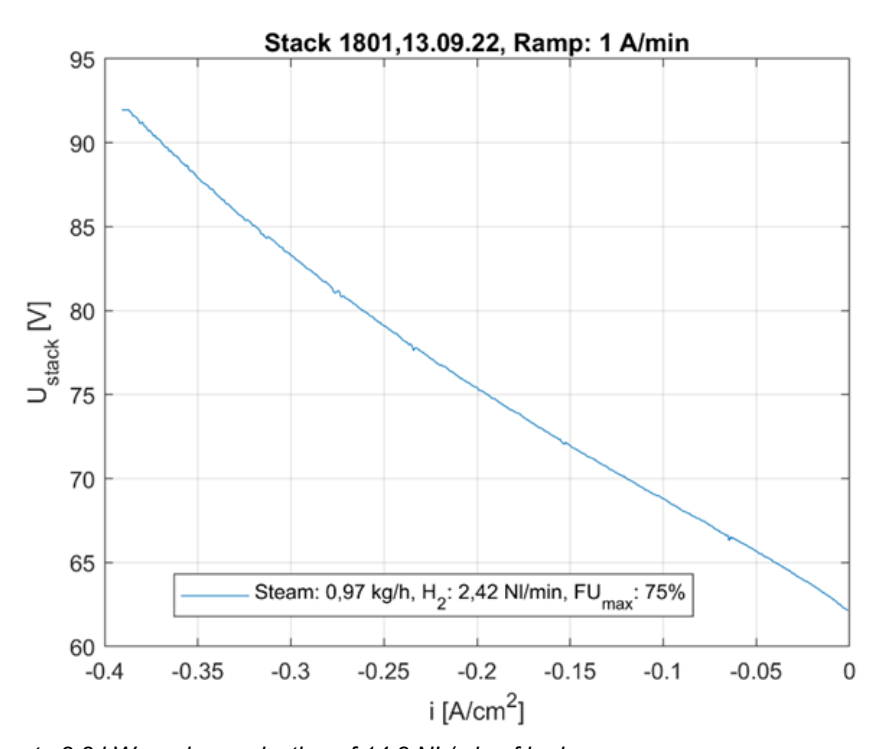


Figure 69: IV up to 2.8 kW $_{\rm e}$ and a production of 14.8 NL/min of hydrogen

After reaching the thermoneutral voltage, the current was maintained at a constant value of 30 A (0.375 A/cm²), corresponding to a production of hydrogen of 14.8 NL/min. During the IV, the hydrogen was fully sent to the vent. After two hours of temperature and voltage stabilization at 30 A, it was sent to the hydrogen compressor. The exchange of hydrogen between the SOE and the compressor is a critical point due to the pressure fluctuation generated on the stack. If the fluctuations are too high, the cells might break.

The Figure 70 shows significant pressure increase and fluctuations due to the exchange of hydrogen with the compressor. This is due to two main reasons: (1) the exchange methodology and (2) the control of the minimum pressure requirement at the entrance of the hydrogen compressor.

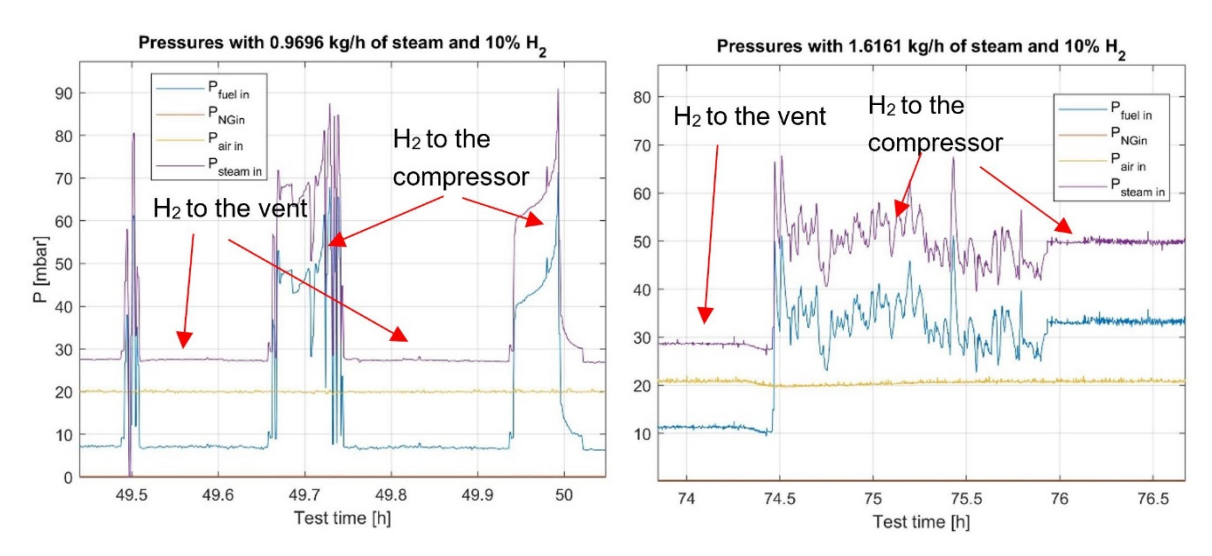


Figure 70: Pressure evolution when sending the produced hydrogen to the H₂ compressor (Left: old exchange methodology, Right: new exchange methodology).

Concerning the exchange methodology, it had been initially decided to send the hydrogen only when the stack power and the hydrogen production were stabilized. The results show that it is clearly problematic, as the compressor has to suddenly handle 100 % of the hydrogen produced, leading to a sudden increase of pressure. To delete this issue, it has been decided that the line connecting the stack to the compressor would be opened during the whole IV, leading to a smooth increase of hydrogen flow until reaching the maximum power.

Concerning the minimum pressure requirement at the entrance of the hydrogen compressor, more precision will be brought in another part of this project as it concerns the OST plant and not the SOE unit itself. Nevertheless, the combination of those two modifications (1) and (2) had a significant impact on pressure fluctuations, as it is shown on Figure 70 (right). After 76 hours, the fluctuations have been completely deleted. Therefore, the exchange of hydrogen with the compressor is validated. However, the pressure difference between the anode and cathode could still be decreased to diminish the risk of damaging the cells.

The validation of the hydrogen exchange allowed to run the stack at higher power and higher hydrogen production. For the second electrolysis test, a flow of 1.6161 kg/h of steam and 3.73 NL/min of hydrogen has been supplied to the stack. A current of 42.5 A has been applied with a ramp of 1 A/min. The current has been stabilized at 42.5 A, corresponding to a stack voltage of 96 V (around 1.37 V per cell), a power of 4 kWe to 4.2 kWe and a production of 20.5 NL/min of hydrogen. Here, the mean cell voltage is clearly above the thermoneutral value. This has been decided to generate enough heat via Joule effect inside the stack and replace the burner which was still used to maintain the BoP and stack temperature. Unfortunately, due to a lack of time, it was impossible to test the system without the burner. Nevertheless, the amount of natural gas has been decreased by half, leading to a constant temperature in the stack.

The second IV shown on Figure 71 presents an unstable behaviour when reaching high current density. This seems to be mainly due to pressure fluctuations, which are still not stabilized when this IV is run (it stabilizes around 76 hours of operation, see Figure 70) and might also be due to the stability of the steam delivery. To ensure that the steam delivery is stable and constant, a steam mass flow meter (MFM) will be installed on the steamline before the next test.



The two first IV presented on Figure 71 have been analysed and discussed with SolydEra. By comparing it with data from other stacks, it showed that this already-used stack had a good performance and was not impacted too much by previous use, low fuel temperature or damage during the stack installation. However, SolydEra advised to run the IV with a faster ramp, to avoid cooling down the stack during the endothermal part of the electrolysis and decrease its performance. Based on this remark, a new set of Ivs have been performed in November 2022. The third IV, in yellow, is part of this second week of test. It shows a better performance than the previous one, as the stack doesn't cool down during the electrolysis.

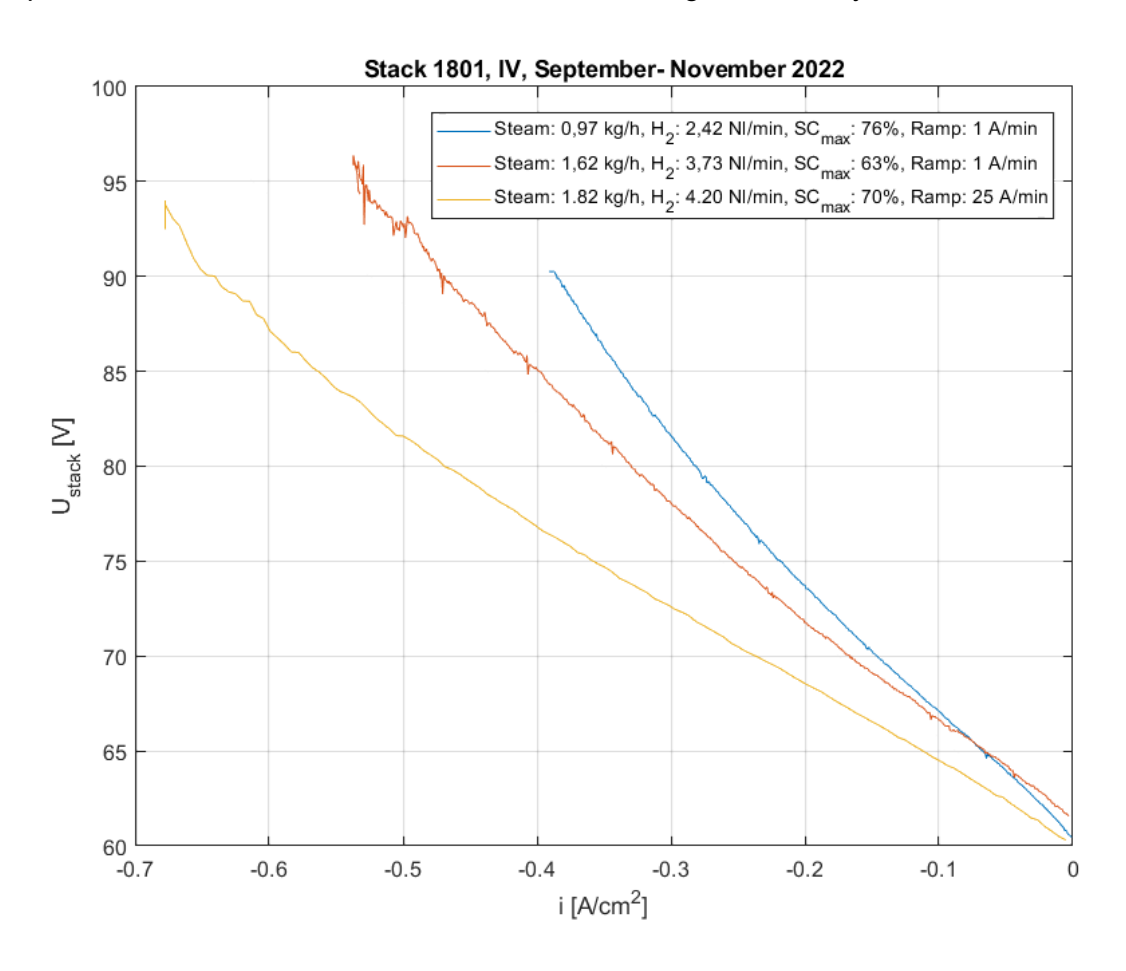


Figure 71: IV up to 4.2 kW_e and a production of 20.5 NL/min of hydrogen

The Figure 72 presents the stabilization of the voltage with a constant current of 42.5 A. By comparing this graphic with the pressure fluctuations, it is clearly visible that the fluctuation of pressure has a strong impact on the voltage of the stack. The stabilization of the pressure after 76 hours is therefore a significative achievement.

After waiting two hours for temperature and voltage stabilization, a first stack efficiency has been computed. Considering a stack voltage of 90.5 V, which corresponds to the power supply voltage (92.5 V) minus the voltage in the cables (2 V), a production of hydrogen equal to 20.5 NL/min, the stack efficiency is calculated as followed:

$$\eta_{stack} = \frac{P_{H_2}(\textit{LHV or HHV})}{P_{elec}}$$
Equation 4:29

The LHV and HHV stack efficiency are 96.1 % and 113.5 % respectively. Those results are preliminary as the tests described above have been performed to validate the installation and the exchange of steam and hydrogen with the compressor, the methanator and the evaporator, not to reach an optimal efficiency point. This will be performed in future tests on a new stack. Moreover, this efficiency takes only the stack into account, and not the additional energy necessary to maintain the SOE hot.

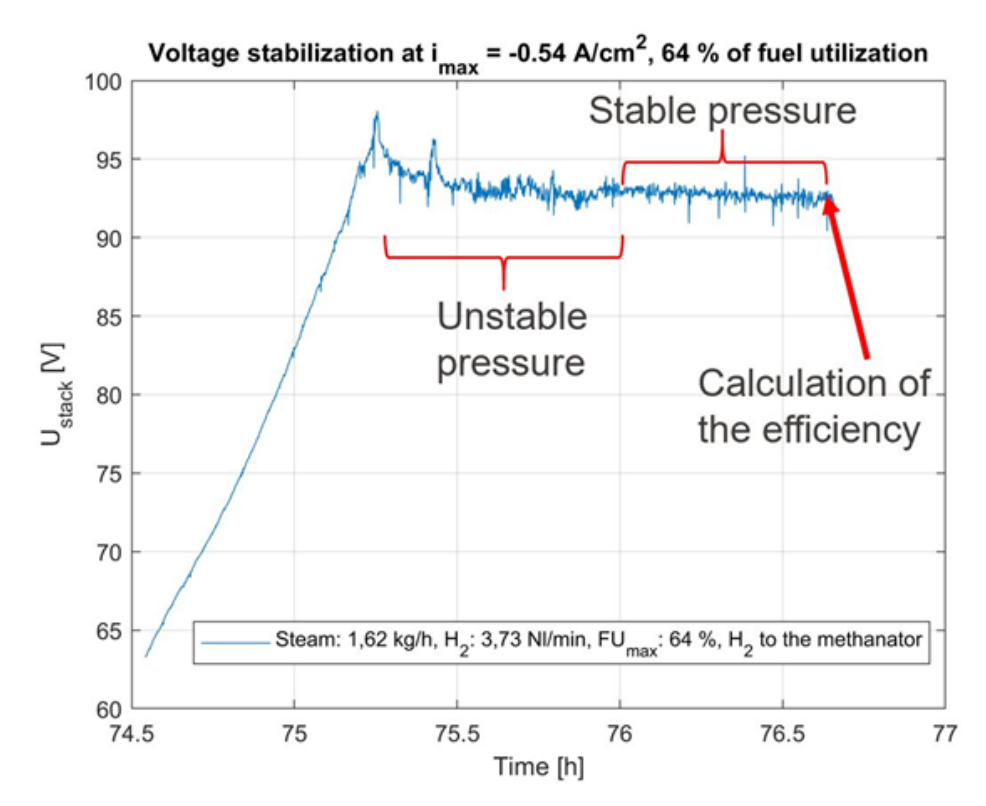


Figure 72: Stabilization of the voltage at current of 42.5 A (0.53 A/cm²) and a hydrogen production of 20.5 NL/min. The hydrogen produced is compressed and sent to the methanator.

The two tests performed with the bypass and the stack #1801 validated the majority of the SOE-BoP components:

- The humidity content of the hydrogen produced by the SOE has been measured and is acceptable for the hydrogen compressor. Therefore, the condenser specially designed at the outlet of the SOE is validated.
- The oxygen content in the hydrogen stream produced has been measured and is acceptable for safe hydrogen compression. This means that the leakages in the stack and the BoP are negligible and it validates the stack itself, the stack installation and the overall BoP.
- The burner is properly working, as well as the air-air heat exchanger. The burner control methodology is also validated.



 The overall SOE BoP is currently validated, as no issues occurred during a full week of tests in the different modes (HEATING, HOTSAFE, HOTSTANDBY, Production (ELECTROLY-SIS), COOLING)

On the other hand, the following issues must be solved before the next test:

- The condensate exhaust coming from the air line is not emptying properly. Manual draining had to be done during the tests to avoid a complete drowning of the air exhaust line. The line will be modified to allow the condensate to continuously leave the air line.
- The steam line supplying the SOE is placed between two chilling water (CHW) lines. The presence of the CHW line cools down the steam line, risking some condensation of the steam. Furthermore, condensate water on the CHW line might drop on the heating chord which maintains the steam line hot. This can create a short-circuit and stop the entire installation. The CHW line will be moved to a smarter position.
- Additional thermocouples must be installed to obtain useful data about the efficiency of the fuel-fuel heat exchanger and the overall heat losses of the BoP.
- The amount of steam received by the SOE-BoP is currently not measured anywhere. To ensure that the steam delivery is stable, a steam mass flow meter will be installed on the steam supply line.

4.3.4.SOE unit: Test with the stack #1803

Improvement of the SOE unit

At the beginning of 2023, the stack #1801 has been removed from the SOE unit and replaced by the new stack #1803. Moreover, the SOE unit has been modified based on the issues discovered during the tests with the stack #1801. Four main modifications have been performed:

- The cooling circuit has been modified and separated from the steam line. There is therefore less heat loss on the steam line and less risk of droplets of water going around the steam line and generate a short-circuit.
- A steam mass-flow-meter (MFM) has been mounted on the steam line, at the entrance of the SOE unit. This MFM is used to validate the flow of steam that the stack receives and to monitor the stability of the steam delivery.
- The exhaust of the condensate in the air line has been moved to a better location to ensure that the condensate would automatically be taken out of the unit without any manual intervention.
- Thermocouples have been added at the exhaust of the air and fuel line to get a rough estimation of the fuel-fuel heat exchanger performance. Furthermore, two voltage measurements have been added to measure the stack voltage closer to the stack, without taking into account the whole voltage drop on the cables leading to the power supply.

Characterization of the stack #1803

The stack #1803 has been characterized through three IV with different composition of inlet flows. The current has been increased with a ramp of 50 A/min until reaching a stack voltage equal to 91 V, which corresponds to a mean cell voltage of 1.3 V (thermoneutral). The three IV clearly show a steep voltage increase when reaching a steam consumption higher than 45 % to 50 %. This is not representative of normal stack performance and indicates a steam starvation (leak) at low steam consumption. The comparison with the stack #1801 presented

on Figure 74 confirms that both stacks show the same performance at low steam consumption but diverge when reaching higher steam consumption.

After the end of the testing week, the SOE unit has been cooled down and investigated. A leakage has been discovered at the interface between the stack and the hot BoP. The steam was therefore leaking at that position and the stack was not properly supplied with steam. Nevertheless, the stack performance was "fair" enough to be coupled with the methanation system and used for efficiency calculation.

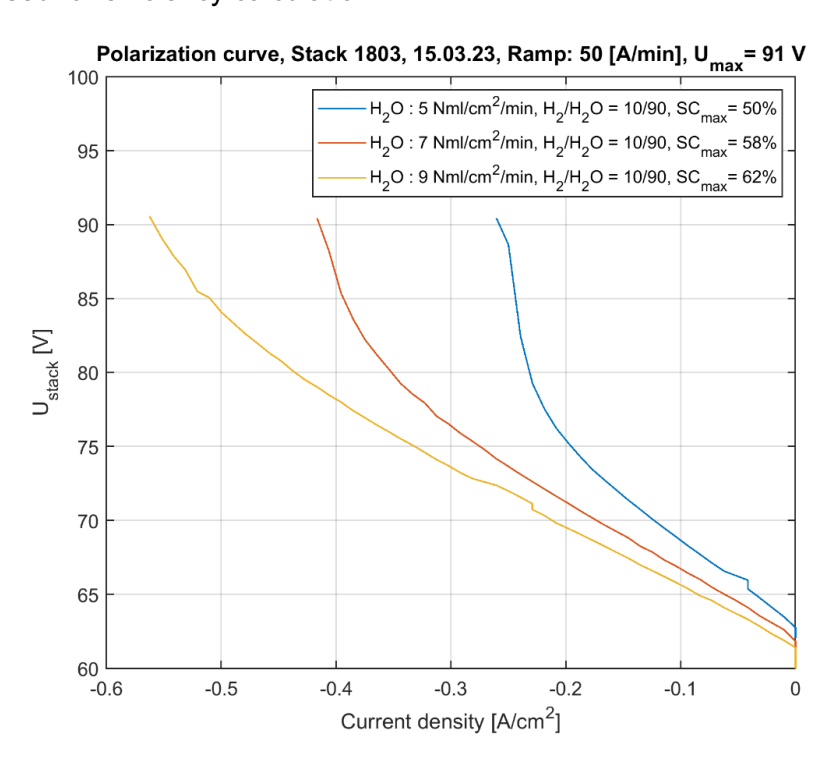


Figure 73: Characterisation of the stack #1803



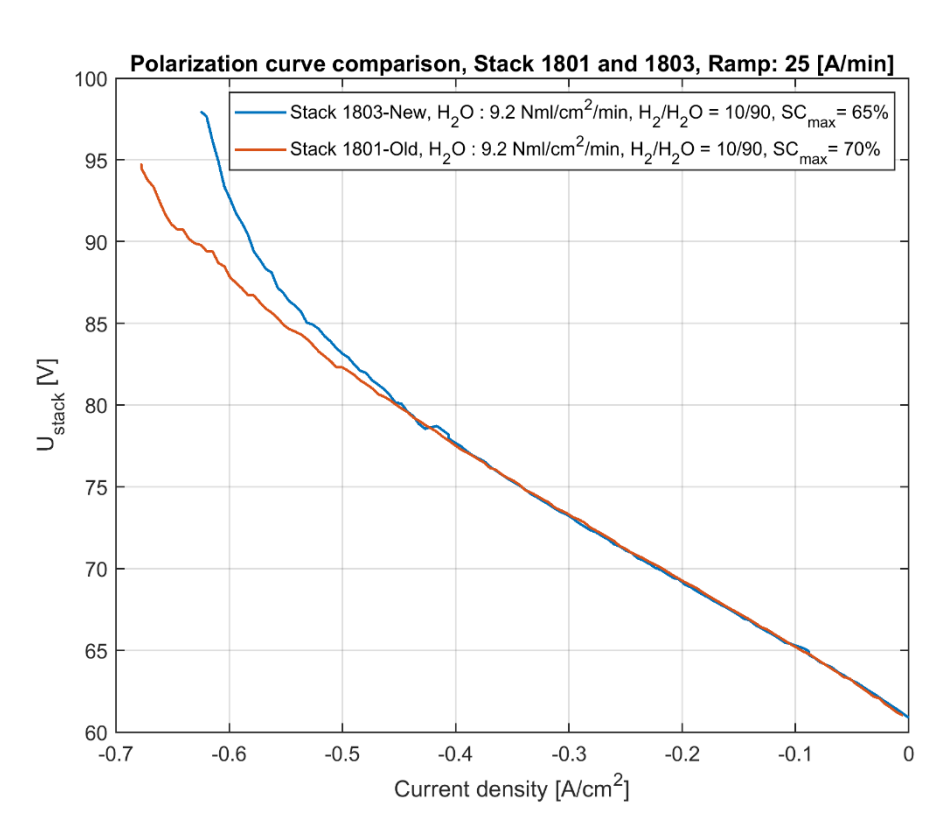


Figure 74: Comparison of the stack #1801 and #1803.

Stack and burner efficiencies

When a solid oxide stack is running in ELECTROLYSIS mode, it will consume heat for the reaction to happen, but it will also generate heat through its internal heat losses. The balance between the need of heat and the production of heat leads to three different working conditions: endothermal, thermoneutral and exothermal. When the cell voltage is below 1.29 V to 1.3 V, the stack is working under endothermal conditions, which means that it consumes more heat than it actually produces, the stack temperature therefore decreases. At 1.29 V to 1.3 V, the stack is at the thermoneutral point, meaning that all the heat needed by the electrolysis is supplied by the internal heat generation of the stack and the temperature of the stack stabilizes. When the stack absorbs power above the thermoneutral voltage, the heat generated by the stack is higher than the heat needed by the electrolysis, therefore the stack enters the exothermal mode and its temperature increases. The working conditions of the stack highly impact on the efficiencies η presented on Figure 75 and Figure 76. It is calculated according to the following equations:

$$\eta_{stack} = \frac{P_{H_2}(LHV \ or \ HHV)}{P_{elec}}$$

Equation 4:30 - Stack efficiency

$$\eta_{stack+burner} = \frac{P_{H_2}(LHV \ or \ HHV)}{P_{elec} + P_{CH4}(LHV \ or \ HHV)}$$

Equation 4:31 – Efficiency of stack and burner

where P_{H2} and P_{CH4} are the equivalent heating power of the produced hydrogen or methane and P_{elec} is the electrical power consumed by the stack.

On 15.03.23, the stack was running under thermoneutral conditions. The stack voltage was equal to 91 V which corresponds to a mean cell voltage of 1.3 V, a current of 50 A (0.625 A/cm^2) was applied for a total power of 4.55 kW_e. The LHV and HHV stack DC efficiencies were 95 % and 112 % respectively. Adding the natural gas consumed by the burner into the equation to maintain thermal balance, the efficiencies drop to 76.4 % LHV and 88.7 % HHV leading to an efficiency decrease of around 20 %. It is significant as the burner is consuming 2 NL/min of CH₄ to maintain the system on temperature.

On 17.03.23, the stack was running under exothermal conditions. The stack voltage was equal to 96 V which corresponds to a mean cell voltage of 1.371 V, a current of 60 A (0.75 A/cm²) and a power of ~5.72 kW_e. The LHV and HHV stack efficiencies were 91 % and 107.5 % respectively. Considering the burner into the equation, which consumed approximately 0.6 NL/min of methane, the efficiencies dropped to 86 % LHV and 101.5 % HHV. The efficiency decrease is therefore only around 5 % to 6 %. Comparing the two data sets, it is clear that running the stack in exothermal conditions decrease stack efficiency. In this case the decrease is 4 %. Nevertheless, under exothermal conditions most of the heat generated by the NG burner can be replaced by the heat losses of the stack, therefore the reduction of fuel consumption in the burner highly impacts the stack and burner efficiency, leading to a better overall efficiency compared to the thermoneutral conditions. It is therefore more efficient to run the stack under slightly exothermal conditions if there is no available "free" heat to maintain the SOE unit hot.

The stack #1803 has also been coupled to the hydrogen compressor and the methanation system. Based on the experiment made with the stack #1801, the coupling methodology has been further improved and validated with the stack #1803. More details about the coupling and the overall SOE-methanation system efficiency are presented in chapter 4.4.



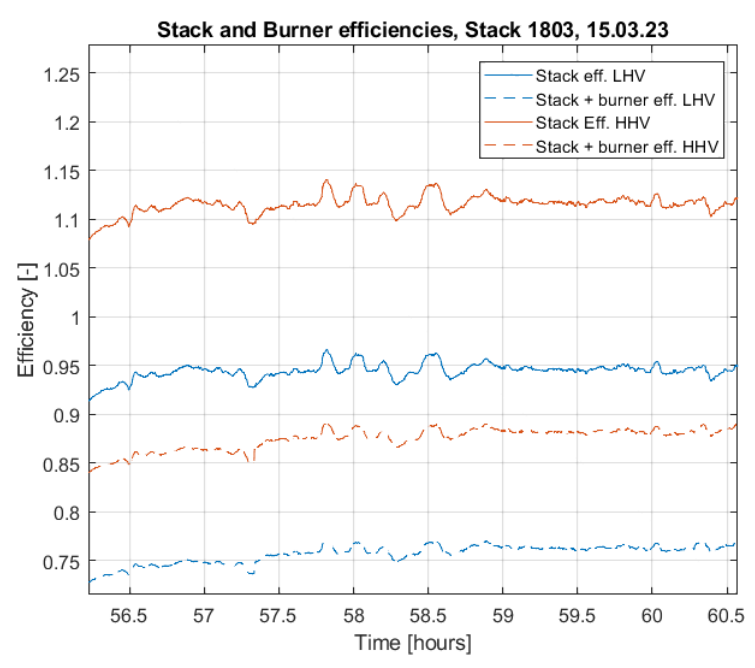


Figure 76: Stack #1803 and burner efficiency on 15.03.23. The efficiency is calculated with the power consumed by the stack only. Working conditions: 91.5 V, 50 A (0.625 A/cm²), 4.575 kW_e.

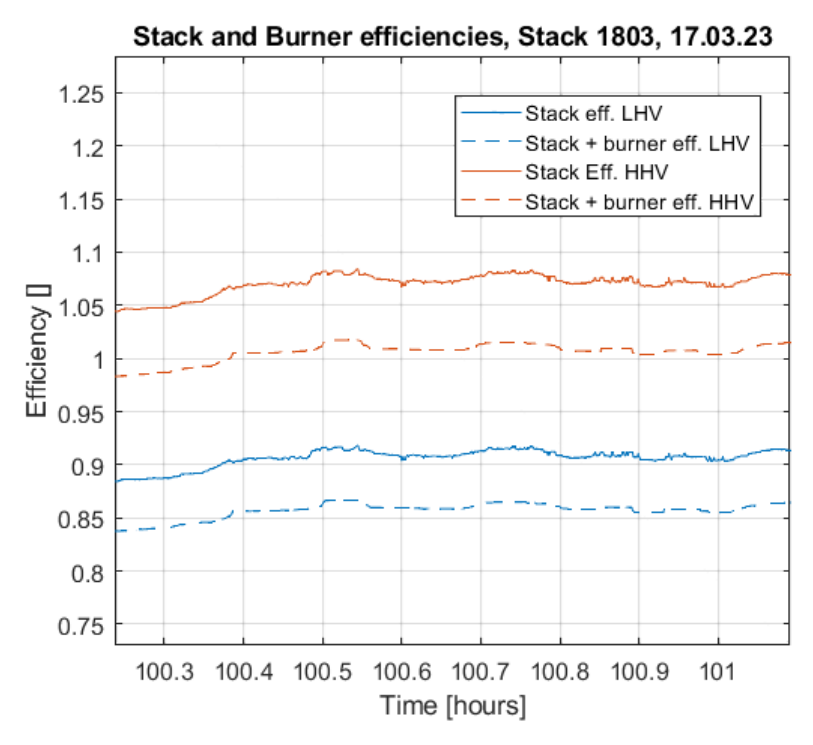


Figure 75: Stack #1803 and burner efficiency on 17.03.23. The efficiency is calculated with the power consumed by the stack only. Working conditions: 96 V, 60 A (0.625 A/cm²), 5.75 kW_e.

4.4. SOE-Methanation Coupling: Results

The pressures of the gases inside the SOE stack must be carefully monitored during operation. The ceramic cells are fragile and a too elevated pressure difference between the anode and the cathode might damage it, as well as too elevated pressure fluctuations on both sides. When the SOE is coupled to the methanation, the produced hydrogen that initially goes to the VENT line is sent to the compressor. The fuel line pressure is therefore increased by the pressure of the compressor's inlet. For this reason, the coupling is a critical moment and must be carefully handled.

4.4.1.Coupling procedures

First procedure

The coupling procedure between the methanation reactor and the SOEC is an essential part of the standard operation for both systems to work together. Before the coupling procedure, the SOE is already producing hydrogen, which is vented and the methanation uses hydrogen produced by the PEM electrolysis. When both systems are ready and stable, the following procedure can begin: First, the C-41 compressor needs to be started and needs to run smoothly. Second, the power uptake of the SOE is reduced to half, from 6 kWe to 3 kWe. Then, an internal switch is executed in order to send the produced hydrogen to the compressor instead of the vent, and the power of the PEM electrolysis is reduced to the minimum. The latter is kept on hot stand-by with its pressure lower than the pressure coming from the compressor, keeping it ready to kick in in case of problem or lack of hydrogen in the system. Lastly, the pressure in the hydrogen low-pressure line between SOEC and compressor via storage tank should be reduced by closing the XV-444C valve which forms a bypass between high- and low-pressure lines.

Unfortunately, the last step did not quite work as well as expected as the hydrogen pressure in the low pressure tank remained unstable. Besides, a pressure drop was observed when the hydrogen was sent to the compressor because the line was empty before the tests.

During the first test, the pressure in the low-pressure tank was slightly too high (appr. 25 mbar) due to the hydrogen flowing through the pressure reducer PCV-444A, which was set at 25 mbar. To improve this and reach lower pressure levels, it was tempted to close the direct link between the high pressure and the low-pressure tank (XV-444C). This resulted in a drop in the low-pressure (LP) line (PI-203) which triggered the automatic closing of the SOE outlet. Both outlets of the SOE being then closed, the pressure inside rose quite quickly and reached dangerous levels (90 mbar and higher). A likely explanation is that the compressor sucked too much from the low-pressure tank which had one of its inlets closed, leading to the drop in pressure.

For the second test, PV-440 was again open fully and the pressure in the low-pressure line was again stable but still slightly too high (25 mbar). This time, PV-440 was closed to 70 % of aperture and later to 50 % shortly after having closed XV-444C in an attempt to limit the flow going out of the compressor and therefore the pressure drop in the low-pressure storage tank. This unfortunately did not have the expected effect and a quick pressure increase was observed in the low-pressure line. This is because by closing slowly PV-440 with the intention to avoid sucking too much with the compressor, the opposite effect was achieved, and the pressure peaked too high. A third test was carried out to try a different method of managing the regulation of PV-440 but was not conclusive either.



Second procedure

The second procedure is similar to the first one, but the pressure control valve (PCV-444A) between high- and low-pressure lines is set to 7 mbar instead of 25 mbar. This way, less or no flow at all is expected to go from the high-pressure lines to the low-pressure lines directly, solving the problem of a too high pressure in the low-pressure line. The neighboring valve (XV-44C) also does not need to be closed anymore, greatly simplifying the coupling process. After coupling the systems the same way it was done before, by reducing the SOE output power and switching the H₂ output before increasing the output power again, the pressure in the low-pressure line was in fact reduced and stabilized around 5 mbar. After this success, the system was left running for a few minutes and showed a great stability.

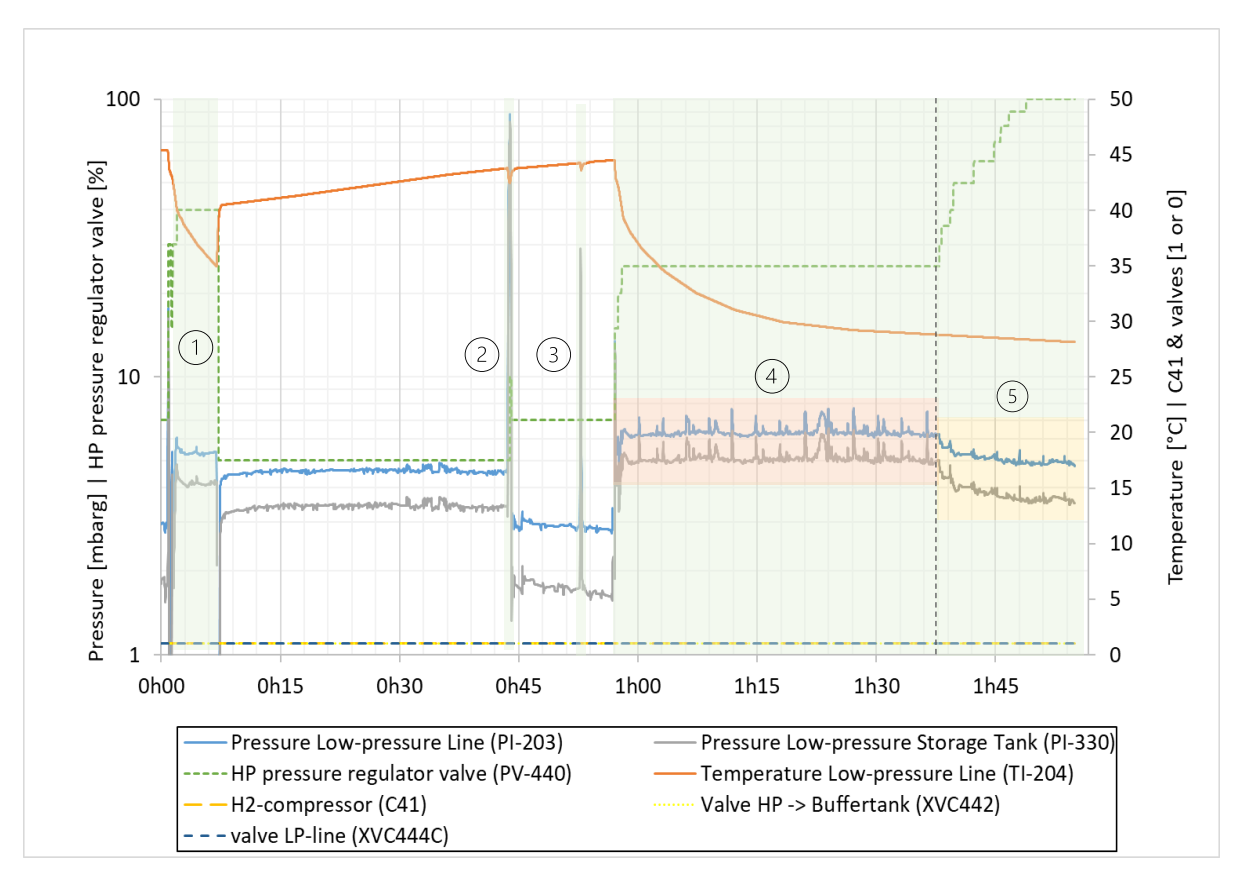


Figure 77: Graphs of the H₂-takeover experiments from SOE to the Methanation plant.

Figure 77 shows the pressure in the low-pressure line during the following prolonged experiment. It is important to note that the two systems, SOE and methanation reactor, where not continually coupled. The moments they were coupled can be recognized by a drop in the temperature and is shown in the graph with numbers from 1 to 5. At point 1, the systems were coupled for a few minutes, at point 4 and 5 for one hour and more, and only for a few seconds at point 2 and 3. During the experiments, the pressure in the low-pressure line remained constant between 3.5 mbarg and 5 mbarg for the most part of it, and the pressure in the corresponding low-pressure storage tank (V33) followed the trend closely with a permanent offset of around 1.2 mbar. The pressure decrease between zones 4 and 5 can be related to the

opening of the PV-440 valve which allowed the compressor C-41 to reduce its work and therefore reach lower pressures on the inlet side. Various positions of that valve between fully closed and fully open were manually tested and it was observed that its position barely influences the pressure in the low-pressure line. The pressure only fell by a few mbar and stabilized, which is positive for the SOE. One could therefore even imagine removing the valve and its control completely in a future system, provided it is not used in another operational state of the system.

The peaks observed in zones 2 and 3 can be attributed to tests of the safety system of the SOE. A safety system had indeed been integrated after the pressure reached a dangerously high level during the first procedure tests, and this new system is supposed to automatically switch the hydrogen outlet to the vent in case the pressure reaches a threshold of 60 mbarg. In the first case (2), the safety did not activate and had to be triggered manually. In the mean-time, the pressure had reached very high level again, up to 90 mbarg. The second time, the safety triggered at 60 mbarg like it was supposed to, limiting the pressure peak to around 30 mbar in reality.

The pressure drop into negative values right after zone 1 can be attributed to a uncontrolled decoupling of the SOE and the methanation reactor. When the hydrogen outlet of the SOE is suddenly switched from reactor back to vent, the low-pressure line empties and the pressure drops quickly as the compressor continues to suck in. In the next seconds, the PV-440 is manually closed, preventing hydrogen flowing into the high-pressure tank. Instead, the hydrogen flows through PRV-332 back into the low-pressure tank, stabilizing the pressure in the low-pressure line again around 4 mbarg.

Stack pressure during the coupling

The coupling methodology presented above has definitely decreased the pressure stress on the stack during the coupling. As shown on Figure 78, the first coupling methodology used with the stack #1803 generated strong pressure peaks up to 90 mbar when the VENT valve is closed and the hydrogen goes to the compressor. The second picture shows the pressure when the new coupling methodology is used. In this case, there is no more pressure peak when hydrogen is sent to the compressor. Furthermore, the pressure at fuel side ($P_{fuel\ in}$) during stable operation is limited to 25 mbar compared to the 40 mbar with the initial methodology. This is crucial as it decreases the pressure difference between fuel side and air side. The pressure increase is therefore acceptable with the new methodology and the coupling can be achieved without damage. For safety reasons, a monitoring of the stack pressure has been added in the control of the system. If this pressure goes above 60 mbar, the VENT valve is opened to flush all the fuel out of the system and automatically decrease the pressure.

Nevertheless, after the coupling the fuel and steam pressures still show peaks every 2 to 3 minutes. Those peaks are generated by sudden increase of steam delivery, as shown in Figure 77. The reason of this increase of steam is still not clear. The effects of the steam increase are clearly visible on the stack voltage, as shown on Figure 79. The voltage suddenly drops every 2 to 3 minutes as the stack receives more steam, leading to a variation of the voltage value of approximately 5 %. However, between 80.5 hour and 82.5 hours of test the voltage is perfectly stable, even if the pressure peaks are still present. It starts to fluctuate again after 82.5 hours of test, even if no action has been performed on the SOE or the methanation system at that moment. Additional tests are therefore needed to obtain a better understanding of the causes of those peaks and to decrease it to a minimum.



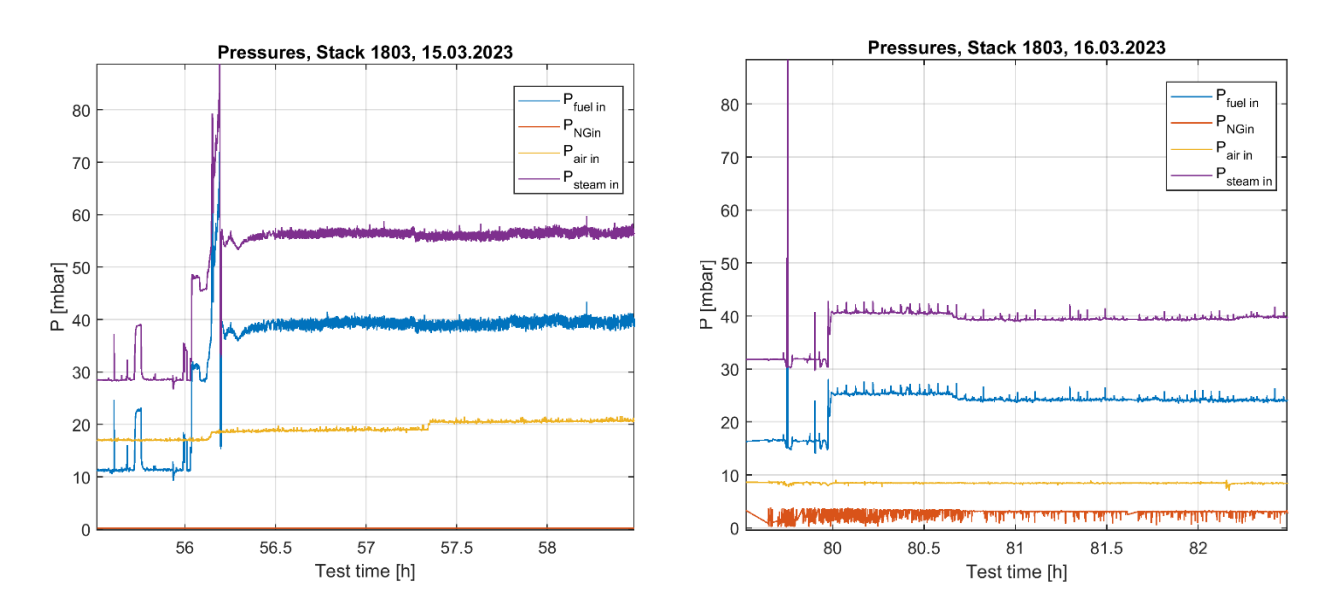


Figure 78: Pressures of the SOE unit using two different coupling methodologies.

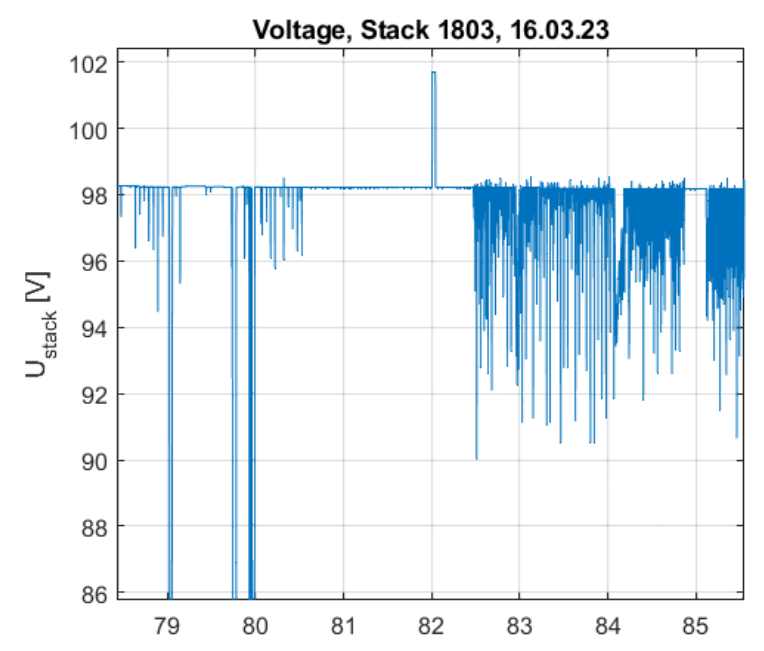


Figure 79 : Stack voltage when the SOE unit is coupled to the hydrogen compressor.

4.4.2. Results of the SOE-Methanation system

The description of the multi-loop eSankey in Figure 81 (on page 99) starts at the SOE-unit placed on the left side of the figure. 0.154 kg/h of hydrogen (6.05 kW_{HHV}) are produced for which an electrical power of 7.02 kW_e (of which 5.72 kW_e are used by the stack itself) was needed. The value for the power to heat the SOE (0.026 kg/h NG or roughly 0.4 kW_{HHV}) corresponds to the exothermal tests performed the days ahead (15^{th} to 17^{th} of March 2023, described in chapter 4.3.4). The H_2 at ambient pressure is later compressed to 12.5 barg and

then sent to the methanation section. The hydrogen is then mixed with 33 % of the CO₂ and preheated by a heat recovery heat exchanger through the product outlet (0.10 kW). To reach sufficient temperature, the feed is heated up in a second heat exchanger, where 0.12 kW of thermal power are added from the thermal oil management. In the two-stage fix-bed catalytic reactor methane is formed with an energy conversion efficiency of 67.4 %.

Through the thermal heat management, 0.80 kW exothermal heat at 250 °C could be transferred to the steam production unit. The water-feed to the steam generator is preheated by the SNG-product (and vice versa to cooldown the SNG-product), 0.28 kW useful heat could be transferred into the water. To produce steam at 240 °C, a total amount 1.63 kW of thermal heat had to be supplied to the water. 1.08 kW (or 66.3 %) were supplied by the methane reaction. In the SOE, the steam utilisation rate was 70.6 %.

In the separation module the raw SNG is upgraded to a level of 96.9 vol-% of methane, 1.3 vol-% of H_2 and 1.0 vol-% of CO_2 (0.8 vol-% residual substances and background noise of the measuring signal). 0.267 kg/h (4.02 kW_{HHV}) of this mixture, the retentate, could be sent to the grid. 0.296 kg/h, the permeate stream, was compressed and sent back to the inlet of the reactor system.

Figure 80 on the right shows the energy required for the production of 1 kg hydrogen from the SOE including compression to 12.5 barg. The efforts for the BoP, the cooling and the compression are labelled "inefficient". Due to the very small scale of the experimental plant all contributions labelled "inefficient" are substantial in comparison to the total effort of 75.84 kWh/kg. The preheating and evaporation energy is necessary, but is considered free, if this thermal energy, e.g. from a waste heat process, is available for freely availaboe for the power-to-methane process.

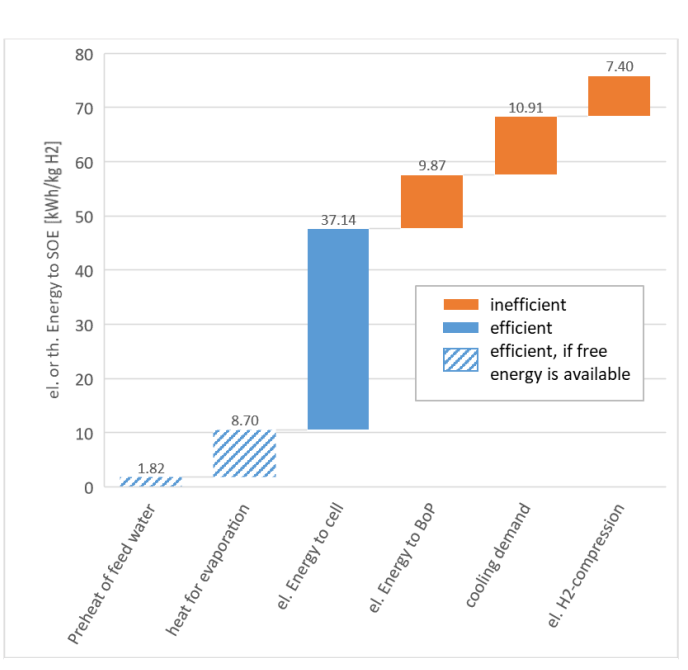


Figure 80: Waterfall-Diagram for different energy demand to produce 1 kg of hydrogen at 12.5 barg from the SOE. Total amount is 75.84 kWh.

4.4.3. Results of the PEM-Methanation system

The eSankey for the Methanation combined with a PEM-Electrolyser (Figure 82, page 100) shows that during the test from September 2022 0.126 kg/h useable hydrogen (4.96 kWhHV) is produced. For that, an electrical effort of 10.37 kW was observed. Approx 11.3% of the produced H_2 is consumed by the PEM itself for desorbing the dryer column at the H_2 outlet in the system. The H_2 is already pressurized at 28.5 barg, which is more than necessary. The theoretical energy demand for H_2 compressing from 12.5 barg to 28.5 barg has been substracted from the electricity demand of the PEM.



CO2 Source steam: 0.0 kg/h H2: 0.0 kg/h CO2: 0.502 kg/h CO2: 0.001 kg/h VENT CO2: 0.255 kg/h HHV H2: 0 kW SNG: 0.005 kg/h PEM, conv. wet H2 Electrolyser H2: 0.0 kg/h water: 0.0 kg/h PEM internal: 0 % 0.0 kg/h PEM external: 0 % 0 kW H2: 0.003 kg/h SNG: 0.505 kg/h CO2: 0.055 kg/h SNG: 0.237 kg/h SNG: 0.259 kg/h O2: 0.0 kg/h H2: 0.003 kg/h SNG: 0.505 kg/h CO2: 0.31 kg/h H2: 0.0 kg/h CO2: 0.055 kg/h 0 kW water: 0.601 kg/h H2: 0.157 kg/h CO2: 0.008 kg/h AC/DC steam: 0.0 kg/h Methanation: Enthalpy (water): 0.41 SNG output HHV H2: 6.2 kW HHV H2: 0.02 kW Supply Mixing & Distribution HHV H2: 0.1 kW Fixed Bed HHV H2: 0.1 kW HHV CH4: 4 kW P el aux: 1.52 kW Reactor fuelling station O2: 1.253 kg/h H2: 0.1 1.14 kW grid injection ON NOBBET 6.05 kW etc.) 1.999 kg/h Meth_eff: 67.4% Aux|Stack 1.63 kW water: 1.999 kg/h SOE Steam WRG E52 0.1 kW Generator el + NG Eff: 81.4 water: 0.601 kg/h Stack: 107.59 H2-Compressor Stack&Burner:101.5% 1.14 kW 0.12 kW loss H2 Recirculation steam: 0.0 kg/h Legend H2: 0.025 kg/h SNG: 0.237 kg/h **WRG E53** HHV H2: 0.98 kW NG: 0.026 kg/h P_el_main [kW] H2: 0.004 kg/h 0.28 kW Recycle-Compressor HHV CH4: 0.4 kW water: 0.579 kg/h CO2: 0.055 kg/h Enthalpy (water) [kW] Steam-conv: 0.706 steam: 0.0 kg/h HHV CH4 [kW] HHV CH4: 3.65 kW 1.34 kW -0.8 kW HHV H2: 0.15 kW HHV H2 [kW] P_el_main: 2.5 kW SNG [kg/h] Heat Management, Oil temp [°C] = 270 CO2 [kg/h] H2 [kg/h] heat loss: Scale 1.87 kW 1.68 kW 0 kW 0.23 kW steam [kg/h] Overall efficencies: water [kg/h] **Energy Fluxes** P_el_main: 1.38 kW Chilled water, 3 - 5 °C 8 kW 0.4 kW 2 kW P Stack to SNG out: 70.2 % P el aux: 2.9 kW 02 [kg/h] P in ideal -> SNG out: 50.3 % ideal: Kompression, no therm. NG [kg/h] Verluste, P in real -> SNG out: 24.4 % Mass Flow 2 kg/h 0.4 kg/h 0.1 kg/h P_el_aux [kW]

17.03.2023 - SOE (2nd Stack) & Methanation (half load), Oil = 270 °C

Figure 81: eSankey with Energy- and Mass flows of a SteadyState. H₂ from SOE coupled with downstream methanation. Measured 17th March of 2023 10h55m at the Research Platform Power-to-X at OST in Rapperswil. NG Input of 0.026 kg/h to the SOE is composed from a test during 16th of March, where thermoneutral point could achieved.

heat loss: unknown

15.09.2022 - PEM & Methanation (LF 0.4), Oil = 250 °C CO2 Source steam: 0.001 kg/h CO2: 0.01 kg/h CO2: 0.475 kg/h VENT H2: 0.016 kg/h CO2: 0.224 kg/h SNG: 0.057 kg/h HHV H2: 0.62 kW PEM. conv. H2: 0.002 kg/h Electrolyser water: 1.266 kg/h PEM internal: 54.3 % 0.126 k H2: 0.005 kg/h PEM external: 48.3 % 4.96 kV CO2: 0.027 kg/h SNG: 0.445 kg/h SNG: 0.445 kg/h H2: 0.005 kg/h SNG: 0.187 kg/h SNG: 0.173 kg/h water: 0.58 kg/h CO2: 0.027 kg/h O2: 1.124 kg/h CO2: 0.26 kg/h H2: 0.001 kg/h Enthalpy (water): 0.39 kW steam: 0.001 kg/h H2: 0.133 kg/h 10.37 kW HHV H2: 0 19 kW CO2: 0.004 kg/h AC/DC HHV H2: 5.26 kW HHV H2: 0.19 kW Methanation SNG output HHV H2: 0.02 kW Supply HHV CH4: 6.86 kW HHV CH4: 6.86 kW P el main: 0 kW Mixing & Distribution HHV CH4: 2.88,kV Fixed Bed HHV CH4: 2.67 kW P el aux: 0 kW Reactor fuelling station O2: 0.0 kg/h H2: 0.0 kg/h grid injection, HHV H2: 0 kW 0 kW % 0.0 kg/h Meth eff: 78.1% Aux|Stack 0 kW water: 0.0 kg/h SOE WRG E52 0.07 kW Steam Generator P el + NG Eff: 0% water: 0.579 kg/h Stack: H2-Compressor Stack&Burner 1.14 kW 0.09 kW loss H2 Recirculation steam: 0.0 kg/h Legend H2: 0.0 kg/h SNG: 0.187 kg/h WRG E53 NG: 0.0 kg/h HHV CH4: 0 kW HHV H2: 0 kW P_el_main [kW] H2: 0.008 kg/h 0 kW Recycle-Compressor water: 0.0 kg/h CO2: 0.036 kg/h Enthalpy (water) [kW] Steam-conv steam: 0.0 kg/h HHV CH4 [kW] HHV CH4: 2.88 kW 0.73 kW 0 kW HHV H2: 0.29 kW HHV H2 [kW] P el main: 1.35 kW Heat Management, Oil temp [°C] = 250 SNG [kg/h] CO2 [kg/h] H2 [kg/h] heat loss: Scale 2.37 kW 0 kW 3.87 kW 0.28 kW steam [kg/h] Overall efficencies: water [kg/h] P_el_main: 2.54 kW Chilled water, 3 - 5 °C **Energy Fluxes** P el aux: 2.9 kW P Stack to SNG out: O2 [kg/h] P in ideal -> SNG out: 27.2 % ideal: Kompression, no therm. NG [kg/h] 2 kW 0.5 kW 20 kW P in real -> SNG out: 14.8 % Verluste, P_el_aux [kW] heat loss: unknown Mass Flow

2 kg/h

0.3 kg/h

0.06 kg/h

Figure 82: eSankey with Energy- and Mass flows of a SteadyState. H₂ (0.126 kg/h) from PEM coupled with the downstream methanation. Measured 15th of September 2022 17h30m at the Research Platform Power-to-X at OST in Rapperswil. Due to non-functional data storage in the mass spectrometry system, the methane composition values from preliminary experiments were used, in which the same methanation parameters were used.



In the catalytic reactor methane is formed with an energy conversion efficiency of 78.1 %, which is slightly over the maximum possible number of 77.9 %. The reason for that number is non perfect measurement and the fact, that at this time the mass spectrometry had an internal data storage error. It was not possible to store the measured values, therefore the data in this evaluation was composed by data from a former testing campaign. Through the thermal heat management, 0.78 kW exothermal heat at 250 °C were extracted from the methanation. Unfortunately, in this configuration the heat could not be used for another process, so it had to be dissipated and is lost. Therefore, the cooling demand in this configuration is higher than in combination with an SOE (+0.05 kW). But the big difference in cooling demand is the heat dissipation of the PEM. With its lower efficiency, it has a significant increase on the cooling load (+2.2 kW)

In the separation module, the raw SNG is upgraded up to level of 96.7 vol-% of Methane, 2.4 vol-% of H_2 and 0.9 vol-% of CO_2 . 0.178 kg/h (2.70 kW_{HHV}) of this mixture could be sent to the grid/NG-refueling station. 0.231 kg/h, the permeate stream was compressed and sent back to the inlet of reactor system.

4.4.4. Overall efficiency and comparison of the Methanation Plant

Figure 102 shows several efficiency comparisons considering to several system boundaries. If we consider only the electrical input to the electrolysers and 2.85 kW_{HHV} of SNG output to the grid, the SOE is almost twice as efficient than the PEM (+ 93 %). The second line shows the comparison if the compression of H_2 for the methanation system is ideal and no additional inputs is required to produce the steam (+ 85 %). But neither comparison is fair from the PEM perspective. The third line takes the real compression and the SNG used to maintain the heat of the SOE into account. For the PEM, the total electrical input power was considered (= no reductions due to overpressure or H_2 losses for the internal drying column). Here we can see that the SOE efficiency was 42.4 % compared to 27.5 %, representing +54% in efficiency for the power-to-methane system with the SOE.

Lines number four and five consider more and more the real situation measured at the Research Platform. The fourth line also takes the additional energy input from the thermal oil circuit (= heat losses) into account, while the last line also takes the expenditures for the chiller and the production of instrument air into account. Some minor things are still not included in the calculation, such as methanation PLC, safety systems and room ventilation, lights, and some heating chords. All comparisons show major differences in the overall efficiency of the systems.

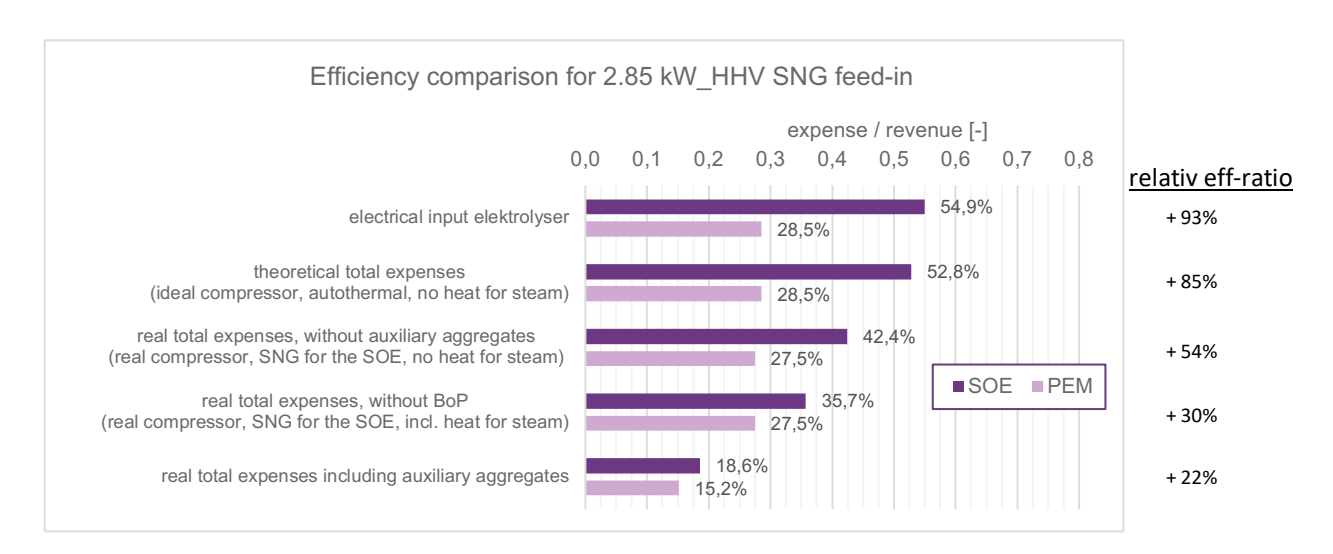


Figure 83: Comparison of different system boundaries of the power-to-methane system with SOE and PEM.-

4.4.5. Fields for Further Improvements

The experiments performed during the full period of the project allowed to identify several points to improve the quality and the quantity of the data obtained, as well as raising the overall efficiency of the power-to-methane system with an SOE.

The control and the safety routines of the SOE system should be modified to be able to run the electrolyser remotely. Currently for safety reasons, the system has been designed to be only used with at least one person from EPFL onsite 24h/24h. It means that three EPFL employees have to do eight hours shift during all of the tests, limiting the duration of the experiments to a maximum of one week. This has been a main drawback as it limited the number of tests that have been performed and the amount of data recorded. Long-duration tests were therefore impossible. Moreover, the fact that Rapperswil is four hours away from the GEM laboratory in Sion made the experiments rather expensive, due to travel and accomodation costs.

Modifying the control and safety routines of the SOE would allow EPFL to run the SOE from Sion, as well as leaving the SOE running by itself overnight. This must be done through a complete review of the safety routines as well as an improvement of the control of the SOE. Thanks to this improvement, long-term tests could be performed with the system, as well as Real Time Optimisation (RTO) of the SOE which would permit to achieve better efficiency.

Longer tests would also allow EPFL and OST to optimize the entire power-to-methane system with the SOE. First, by finding the optimum between the amount of steam generated by the methanator and the steam utilization factor in the SOE. Secondly, optimizing the hydrogen compression circuit to decrease the compressor's power and improve the stability of the pressure in the line. Finally, a deeper optimization of the methanation section itself would be possible, for example by finding the optimized tradeoff between maximization of SNG output regarding the limits of regulation (> 96 % of methane and < 2 % of H₂), the pressure difference over the separation membrane and the amount of mass flow have both influence on the compression work for the reinjection through the recycling section.

The performance of the fuel-fuel heat exchanger in the SOE should be carefully monitored and analyzed. As shown previously, the fuel temperature entering the electrolyser is far too low.



As it was difficult to know where the problem came from without dismantling the whole Hot-BoP, this problem was put aside during the end of the project. But it should be solved in the near future. Having a hotter fuel temperature at the entrance of the stack would allow to decrease even more the need for the burner and therefore increase the overall efficiency of the system.

Additional improvements could be made to the entire system such as the installation of an advanced hydrogen (and/or CO₂) separation system like an electrochemical hydrogen separation. Following information from a supplier, such an equipment is able to separate H₂ from methane while at the same time, compressing the H₂ to a higher level than its origin combined in a single unit.

Another research topic could be the tactic to raise the hydrogen limit in the SNG output up to 10 vol-% or even 20 vol-%. Obviously, this would influence different parts of the plant in different ways. The influence on overall efficiency is positive, not only because less hydrogen is converted, which reduces the heat dissipation, also because of a reduced demand of CO₂. Second, the methanator can be built smaller or, if it stays on the same size, can achieve a higher conversion performance due to a reduced gas hourly space velocity. Fourth, no separation membrane and therefore also no recycling line has to be used, which reduces the efforts in CAPEX and OPEX. On the other hand, the negatives on this strategy are:

- Less conversion also means less heat can be used by the steam generator. This missing heat has to be satisfied from another source.
- The installed NG-refilling stations can no longer be fed by SNG from the plant due to the maximum allowable amount of hydrogen being 2 vol-% in a NG-refilling station.
- For the low pressure gasgrid, a study about its ability to receive higher hydrogen levels than
 the 2 vol% according to the old standard, has to be performed. It's not only about the grid
 where the gas is injected, it's further also the consumers respectively their usage in different
 types of equipment, which has to be investigated.

Moreover, the recirculation of the forming gas (FG) in the SOE should be tested. It would highly decrease the consumption of FG while being in STARTUP, SHUTDOWN or HOT STANDBY mode and therefore also reduce the costs on gases. Of course, this would make some more equipment necessary, like a gas recirculation pump, pressure and flow sensors to monitor the flow of the forming gas.

Concerning the pressurization of SOE, the experiments have shown that pressurization is very challenging, therefore more time and resources must be dedicated to that topic in near future to obtain satisfying results.

Co-electrolysis experiments could be performed within the plant. Replacing part of the steam with CO_2 would first decrease the energy need for steam generation. Secondly, the SOE would produce a mixture of H_2 and CO, directly feeding the methanator. As the methanation of CO generates more heat than CO_2 (–217 kJ/mol versus –177 kJ/mol), a better overall efficiency would be attained with co-electrolysis.

Finally, at the time this report is written, a new SOE-methanator system has been mounted and operated successfully in the GEM laboratory in Sion for a parallel project. Using a methanator with direct water cooling and thermosyphon, which decreases the heat losses and power needs, the methanator delivered stable steam and the overall system showed satisfying efficiency results. The knowledge acquired on both systems, in Rapperswil and Sion, should therefore be used to scale-up, optimize and build the future P2G plants.

5. Dissemination and Outlook

5.1. Dissemination

The results of project "HotCat4Steam" have been published and presented on the following occasions so far (in chronological order):

	[29] Wang, Ligang; Chen, Ming; Küngas, R; Lin, Tzu-En; Diethelm, Stefan; Maréchal,
	François; Van herle, Jan: "Power-to-fuels via solid-oxide electrolyzer: Operating window
	and techno-economics", Renewable and Sustainable Energy Reviews 110, 174-187
	(2019)
	[33] Hanfei Zhang, Ligang Wang, Jan Van herle, François Maréchal, Umberto Desid-
	eri:"Techno-Economic Optimization of CO ₂ -to-Methanol with Solid-Oxide Electrolyzer, <i>En-</i>
	ergies, 12(19), 3742; https://doi.org/10.3390/en12193742 (2019)
	[30] Wang, Ligang; Rao, Megha; Diethelm, Stefan; Lin, Tzu-En; Zhang, Hanfei; Hagen,
	Anke; Maréchal, François; Van herle, Jan: "Power-to-methane via co-electrolysis of H ₂ O
	and CO ₂ : The effects of pressurized operation and internal methanation", <i>Applied Energy</i>
	250, 1432-1445 (2019)
	[25] Sun, Y., Wang, L., Xu, C., Van herle, J., Maréchal, F. and Yang Y.: "Enhancing the
	operational flexibility of thermal power plants by coupling high-temperature P2G", Applied
	Energy 263, 114608 (2020)
	[34] Yumeng Zhang, Ningling Wang, Xiaofeng Tong, Liqiang Duan, Tzu-En Lin, François
	Maréchal, Jan Van herle, Ligang Wang, Yongping Yang: "Reversible solid-oxide cell stack
	based power-to-x-to-power systems: economic potential evaluated via plant capital-cost
	target", Applied Energy (2021), 290, 116700
	[22] Schmidlin, L., presentation at Expertinnen- und Expertengespräche Power-to-X, Rap-
	perswil-Jona, 23 rd of September 2021
	[23] Schmidlin, L., Ruoss, F. and Friedl, M.: "Effiziente Methansynthese", <i>Bulletin.ch, Ver-</i>
	band Schweizer Elektrizitätsunternehmen, December 2021
	[1] Aubin, P., Wang, L., Van herle, J.: "Evaporating water-cooled methanation reactor for
	solid-oxide stack-based power-to-methane systems: Design, experiment and modeling",
_	Chemical Engineering Journal 456, 140256 (2022)
	[10] Friedl, M., Schmidlin, L., Steiner, Ch. and Ruoss, F., "Forschungsplattform für Power-
_	to-Gas", Aqua and Gas, No. 3, 1 st March 2022
	[2] Aubin, P.; Wang, L. and Van herle, J.: "Power-to-methane via co-electrolysis of H2O
	and CO2: Reactor operation and system simulation" Energy Conversion and Management
	294, 117520 (2023)
	[16] Moussaoui, H.; Subotić, V.; Van herle, J.; Wang, L.; Wei, X. and Yu H.: "Stack/Sys-
	tem Development for High-Temperature Electrolysis", High Temperature Electrolysis, 383-
	407 (2023)
	[24] Schmidlin, L., van Herle, J. and Steiner, C., presentation at "Expertengespräche
	Power-to-X", Rapperswil-Jona, 20 th of June 2023
	[11] Friedl, M., Kunz, B., Wuillemin, Z. and Van herle, J. "L'électrolyse à haute tempé-
	rature", Aqua and Gas, No. 11, 1st November 2023

Since the HTE from EPFL was installed at the demo site in Rapperswil, it was shown to 2'000 interested visitors in guided tours. The visits had to be interrupted due to the corona pandemic. Further publications on national and international level are planned. The project partners will make use of the results in future projects.



5.2. Outlook

This section shows how the two project partners OST and EPFL plan to scale up the technology developed in project HotCat4Steam. It also lists the attempts the two partners have made in the past and which were not yet successful. While HotCat4Steam includes activities in the scales of 0.5 kW_e to 5 kW_e, the project partners OST and EPFL keep attempting to start a project at a scale of 50 kW_e. The results from HotCat4Steam will allow both partners together or separately to co-operate with industry and to contribute in consortia for European projects.

- 0.5 kW_e: Project HotCat4Steam, EPFL, direct steam generation
- 5 kWe: Project HotCat4Steam, OST, heat transfer via thermal oil

Project Power2Methane, EPFL, direct steam generation from methanator sent to 5 kW_e SOE, achieved in 2023, including with wind and PV input profiles.

50 kW_e: follow-up P&D. Due to their experience in HotCat4Steam, OST and EPFL are attractive partners for future research projects:

This work was part of the SWEET proposal REFERENT in October 2020, which was not successful.

- A P&D proposal was submitted in July 2021 to SFOE for a 30 kW $_{\rm e}$ SOE (in fact a reversible SOC). After several exchanges with BfE, the latest in March and April 2021, it will be resubmitted in the near future.
- EPFL applied for HORIZON-JTI-CLEANH2-2022-01-01 and 02: Development and validation of high temperature steam electrolysis stacks (Solid Oxide Electrolysis / Proton Conducting Electrolysis). The project was accepted and started in September 2023.
- OST and EPFL each have joint separate consortia applying for the call "HORI-ZON-JTI-CLEANH2-2022-04-03: Reversible SOC system development, operation and energy system (grid) integration" submitted May 2022. The consortium "24/7 ZEN" with OST as member is financed by the European commission and started in spring 2023.
- A new Innosuisse Flagship GreenHub at the waste incineration plant in Horgen is funded and due to start in February 2024. An SOE with a downstream synthesis of methanol and a thermal management system using thermal oil is built and tested.
- EPFL submitted a proposal dedicated to upscaling SOE (HORIZON-JTI-CLEANH2-2022-01-09: Scaling-up technologies for SOEL), together with Solydera Switzerland. The proposal was refused.
- EPFL/SolydEra applied for HORIZON-JTI-CLEANH2-2023-01-02: Innovative stacks for Solid Oxide Electrolysis / Proton Conducting Electrolysis. The project was accepted and starts in February 2024.
- 500 kWe, real scale P&D. A potential demo project with Gaznat in the scale of 200 kWe

The applicants aim at bringing the know-how acquired during HotCat4Steam into future research and demonstration projects on national and European level.

The "Forschungsplattform Power-to-X" at OST is serving for other projects, e.g. Innosuisse project "Swiss Low-Cost Hydrogen Refuelling Station". It also can serve as experimental site in future projects. It will continue to be available for tours, discussions and other projects.

6. Conclusions

The purpose of the HotCat4Steam project was to validate the coupling between a high temperature solid oxide electrolyzer (SOE) and a methanation system as well as improving the knowledge on both technologies and their coupling.

The coupling has been successfully validated through three weeks of continuous testing in Rapperswil with two different 5 kW $_{\rm e}$ stacks delivered by SolydEra. A maximum of 0.154 kg/h of hydrogen (6.04 kW HHV) has been produced by the SOE and turned into 4 kW of methane (HHV) for an overall efficiency of 70.2 %. The efficiency of SOE coupled to the methanator compared to a PEM coupled with the methanator is increased by 93 %, regarding the total electrical consumption of the electrolyser. It clearly shows the advantage of using high temperature electrolysis (HTE) and the gains in efficiency possible with this technology. The goal of project HotCat4Steam could be reached.

The technical challenges to experimentally couple SOE and methanation were larger than anticipated and required more resources. An important part of the project was the development of a coupling methodology ensuring the safe exchange of hydrogen and steam between the electrolyser and the methanator. This methodology can be used on large-scale installations. Nevertheless, additional long-term experiments should first be performed to understand the behaviour of the installation over longer periods. Additionally fields of improvement have been identified like a fully automated SOE module enabling long-term tests and a further development of the system.

The knowledge on the methanation technology has been deepened through multiple tests at OST and at EPFL. Efforts have been made to stabilize and optimize steam generation by testing a methanator cooled by thermo-oil and a methanator directly cooled by water. Both technologies showed stable steam production as well as satisfying heat recovery from the reaction. Moreover, the used catalysts presented no degradation during the duration of the experiments.

Due to the complexity of the setup and the fragility of the cells, the experiments on pressurized solid oxide cells have not yet generated satisfying results but allowed to understand the different challenges and prepare the ground for new experiments that will be run in a near future.

The results of the HotCat4Steam project are therefore promising and should be used as a steppingstone, first to design and build larger scale Power-to-X systems incorporating an SOE and a downstream catalytic fuel synthesis in research or industry and secondly to pressurize solid oxide cells and stacks. Follow-up projects are already running and will be started early 2024.



Appendix

A.1 Literature

- [1] Aubin, P.; Wang, L. and Van herle, J.: "Evaporating water-cooled methanation reactor for solid-oxide stack- based power-to-methane systems: design, experiment and modeling," *Chemical Engineering Journal 456*, 140256 (2022).
- [2] Aubin, P.; Wang, L. and Van herle, J.: "Power-to-methane via co-electrolysis of H2O and CO2: Reactor operation and system simulation" *Energy Conversion and Management* 294, 117520 (2023)
- [3] Bauer, R.: "Effective radial thermal conductivity of gas-permeated packed beds containing particles of different shape and size distribution," *VDI Forschungsheft*, vol. 39, no. 582, 1977.
- [4] Chen, J. C.: "Correlation for Boiling Heat Transfer to Saturated Fluids in Convective Flow," *Ind. Eng. Chem. Process Des. Dev.*, vol. 5, no. 3, pp. 322–329, Jul. 1966, doi:10.1021/i260019a023.
- [5] Dengler, C. E. and Addoms, J. N.: "Heat transfer mechanism for vaporization of water in a vertical tube," *Chem. Eng. Prog. Symp. Ser.*, no. 18, 1956.
- [6] Dixon, A. G.: "An improved equation for the overall heat transfer coefficient in packed beds," *Chem. Eng. Process. Process Intensif.*, vol. 35, no. 5, pp. 323–331, Oct. 1996, doi: 10.1016/0255-2701(96)80012-2.
- [7] Eisfeld, B. and Schnitzlein, K.: "The influence of confining walls on the pressure drop in packed beds," *Chem. Eng. Sci.*, vol. 56, no. 14, pp. 4321–4329, 2001, doi: https://doi.org/10.1016/S0009-2509(00)00533-9.
- [8] Ergun, S.: "Fluid flow through packed columns," *Fluid Flow Packed Columns*, vol. 48, pp. 89–94, 1952.
- [9] Freund, A., Friedrich, G., Merten, C. and Eigenberger, G.: "Pulsationsarmer Laborver-dampfer für kleine Flüssigkeitsströme," *Chemie Ingenieur Technik*, vol. 78, no. 5, pp. 577-580, 2006
- [10] Friedl, M., Schmidlin, L., Steiner, Ch. and Ruoss, F., "Forschungsplattform für Powerto-Gas", *Aqua and Gas*, No. 3, 1st March 2022
- [11] Friedl, M., Kunz, B., Wuillemin, Z. and Van herle, J. "L'électrolyse à haute température", *Agua and Gas*, No. 11, 1st November 2023
- [12] Fuller, E. N.; Schettler, P. D. and J. Calvin. Giddings: "New Method for Prediction of Binary Gas-Phase Diffusion Coefficients," *Ind. Eng. Chem.*, vol. 58, no. 5, pp. 18–27, May 1966, doi: 10.1021/ie50677a007.
- [13] S. G. Kandlikar and P. Balasubramanian, "An Extension of the Flow Boiling Correlation to Transition, Laminar, and Deep Laminar Flows in Minichannels and Microchannels," *Heat Transf. Eng.*, vol. 25, no. 3, pp. 86–93, 2004, doi: 10.1080/01457630490280425.
- [14] Kiewidt L. and Thoming, J., "Predicting optimal temperature profiles in single-stage fixed-bed reactors for CO2-methanation," *Chem. Eng. Sci.*, vol. 132, pp. 59–71, 2015.
- [15] Koschany, F.; Schlereth, D. and Hinrichsen, O.: "On the kinetics of the methanation of carbon dioxide on coprecipitated NiAl(O)x," *Appl. Catal. B Environ.*, vol. 181, pp. 504–516, Feb. 2016, doi: 10.1016/j.apcatb.2015.07.026.
- [16] Moussaoui, H.; Subotić, V.; Van herle, J.; Wang, L.; Wei, X. and Yu H.: "Stack/System Development for High-Temperature Electrolysis", *High Temperature Electrolysis*, 383-407 (2023)

- [17] D. Nemec and J. Levec, "Flow through packed bed reactors: 1. Single-phase flow," Chem. Eng. Sci., vol. 60, no. 24, pp. 6947–6957, 2005, doi: https://doi.org/10.1016/j.ces.2005.05.068.
- [18] R. K. Niven, "Physical insight into the Ergun and Wen & Yu equations for fluid flow in packed and fluidised beds," *Chem. Eng. Sci.*, vol. 57, no. 3, pp. 527–534, 2002, doi: https://doi.org/10.1016/S0009-2509(01)00371-2.
- [19] Schefold, J.; Brisse, A. and Poepke, H.: "Long-term Steam Electrolysis with Electrolyte-Supported Solid Oxide Cells," Electrochimica Acta, vol. 179, pp. 161-168, 2015
- [20] Schlereth, D.: "Kinetic and reactor modeling for the methanation of carbon dioxide", Dissertation, Technische Universität München, 2015
- [21] Schlereth D. and Hinrichsen, O.: "A fixed-bed reactor modeling study on the methanation of CO2," *ECCE9 9th Eur. Congr. Chem. Eng.*, vol. 92, no. 4, pp. 702–712, Apr. 2014, doi: 10.1016/j.cherd.2013.11.014.
- [22] Schmidlin, L.: presentation at *Expertinnen- und Expertengespräche Power-to-X*, Rapperswil-Jona, 23rd of September 2021
- [23] Schmidlin, L.; Ruoss, F. and Friedl, M.: "Effiziente Methansynthese", *Bulletin.ch, Verband Schweizer Elektrizitätsunternehmen*, December 2021
- [24] Schmidlin, L.; van Herle, J. and Steiner, C., presentation at "Expertengespräche Power-to-X", Rapperswil-Jona, 20th of June 2023
- [25] Sun, Y.; Wang, L.; Xu, C.; Van herle, J.; Maréchal, F. and Yang, Y.: "Enhancing the operational flexibility of thermal power plants by coupling high-temperature P2G", *Applied Energy* 263, 114608 (2020)
- [26] Tsotsas, E. "Wärmeleitung und Dispersion in durchströmten Schüttungen," in VDI-Wärmeatlas: Fachlicher Träger VDI-Gesellschaft Verfahrenstechnik und Chemieingenieurwesen, P. Stephan, D. Mewes, S. Kabelac, M. Kind, K. Schaber, and T. Wetzel, Eds., Berlin, Heidelberg: Springer Berlin Heidelberg, 2018, pp. 1–20. doi: 10.1007/978-3-662-52991-1 102-1.
- [27] Tsotsas, E. "Wärmeleitfähigkeit von Schüttschichten," in *VDI-Wärmeatlas: Fachlicher Träger VDI-Gesellschaft Verfahrenstechnik und Chemieingenieurwesen*, P. Stephan, S. Kabelac, M. Kind, D. Mewes, K. Schaber, and T. Wetzel, Eds., Berlin, Heidelberg: Springer Berlin Heidelberg, 2019, pp. 1831–1843. doi: 10.1007/978-3-662-52989-8 30.
- [28] Universität Stuttgart "Verdampfertechnologie / Laborverdampfer", [Online]. Available: https://www.icvt.uni-stuttgart.de/forschung/verdampfer/ . [Accessed 11 02 2019]
- [29] Wang, L.; Chen, M.; Küngas, R.; Lin, T.-E.; Diethelm, S.; Maréchal, F. and Van herle, J.: "Power-to-fuels via solid-oxide electrolyzer: Operating window and techno-economics", *Renewable and Sustainable Energy Reviews* 110, 174-187 (2019)
- [30] Wang, L.; Rao, M.; Diethelm, S.; Lin, T.-E.; Zhang, H.; Hagen, A.; Maréchal, F. and Van herle, J.: "Power-to-methane via co-electrolysis of H₂O and CO₂: The effects of pressurized operation and internal methanation", *Applied Energy* 250, 1432-1445 (2019)
- [31] Winterberg M. and Tsotsas, E., "Impact of tube-to-particle-diameter ratio on pressure drop in packed beds," *AIChE J.*, vol. 46, no. 5, pp. 1084–1088, 2000, doi: https://doi.org/10.1002/aic.690460519.
- [32] Yagi, S. and Kunii, D.: "Studies on effective thermal conductivities in packed beds," *AIChE J.*, vol. 3, no. 3, pp. 373–381, 1957, doi: https://doi.org/10.1002/aic.690030317.
- [33] Zhang, H.; Wang, L.; Van herle, J.; Maréchal, F. and Desideri, U.: "Techno-Economic Optimization of CO₂-to-Methanol with Solid-Oxide Electrolyzer", *Energies*, *12*(19), 3742; https://doi.org/10.3390/en12193742 (2019)



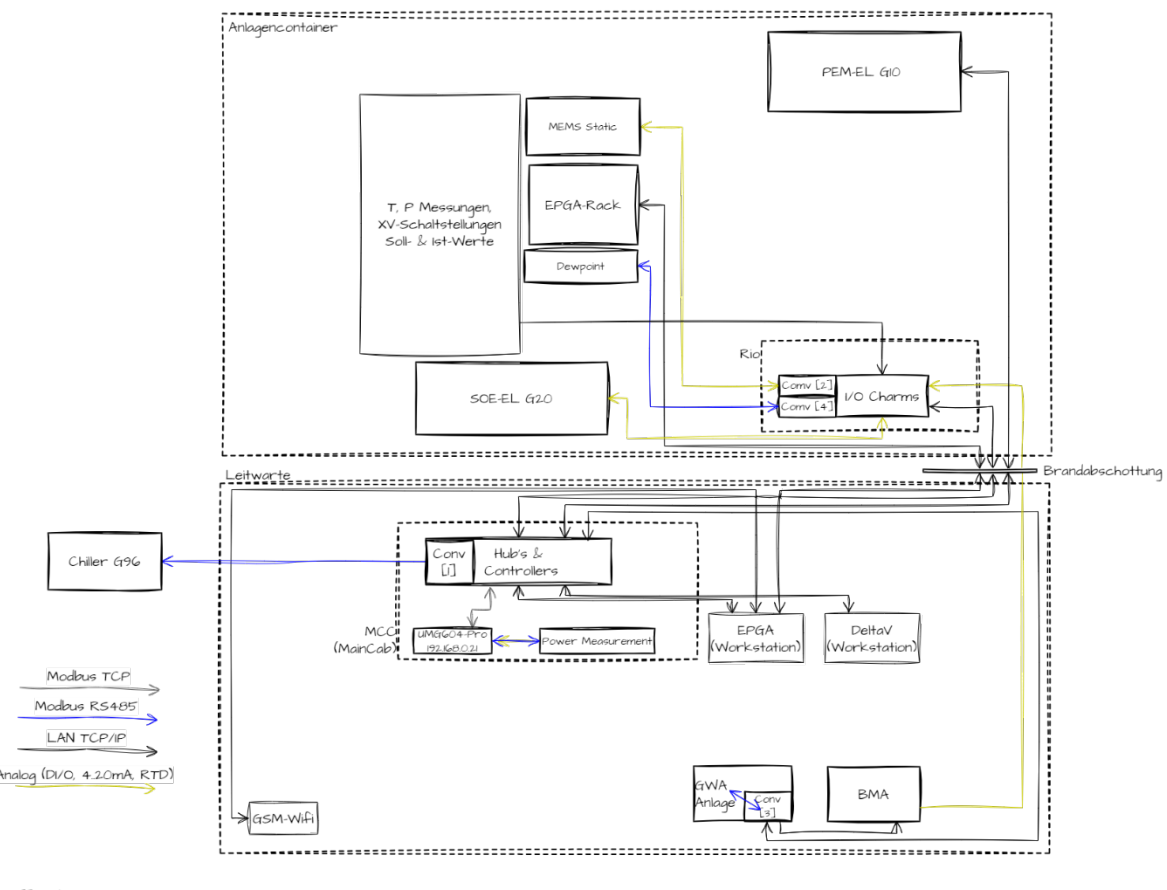
[34] Zhang, Y.; Wang, N.; Tong, X.; Duan, L.; Lin, T.-E.; Maréchal, F.; Van herle, J.; Wang, L. and Yang, Y.: "Reversible solid-oxide cell stack based power-to-x-to-power systems: economic potential evaluated via plant capital-cost target", *Applied Energy* (2021), 290, 116700

A.2 Members of IG-PtX:

The Interessengemeinschaft Power-to-X (IG-PtX) has decided to co-finance this extension. It is an association founded by OST and the following energy providers (electricity, gas, district heat) from the eastern part of Switzerland (in alphabetic order):

Elektrizitätswerk Jona Rapperswil AG	Stadt Gossau Stadtwerke
Energie Zürichsee Linth AG	Technische Betriebe Flawil
Gravag Energie AG	Technische Betriebe Goldach
Liechtensteinische Gasversorgung	Technische Betriebe Glarus
OST – Ostschweizer Fachhochschule	Technische Betriebe Weinfelden AG
SN Energie AG	Technische Betriebe Wil
SGSW, St.Galler Stadtwerke	Technische Betriebe Uzwil

A.3 Schematic Communication Flow of the Research Platform's PLC "DeltaV"



- [j] Modbus TCP <-> RTU Converter 192,168.0.18, Phoenix Contact
- [2] CAN <> Modbus TCP Converter 192,168.012, HMS Anybus
- [3] Modbus TCP <>> RTU Converter 192168.0.19, Anybus
- [4] Modbus TCP -> RTU Converter 1921/68.0.71, Phoenix Contact